QUANTITATIVE BEHAVIOR OF NON-INTEGRABLE SYSTEMS (III)

J. BECK, W.W.L. CHEN, AND Y. YANG

ABSTRACT. The main purpose of part (III) is to give explicit geodesics and billiard orbits in polysquares and polycubes that exhibit time-quantitative density.

In many instances of the 2-dimensional case concerning finite polysquares and related systems, we can even establish a best possible form of time-quantitative density called *superdensity*.

In the more complicated 3-dimensional case concerning finite polycubes and related systems, we get very close to this best possible form, missing only by an arbitrarily small margin.

We also study infinite flat dynamical systems, both periodic and aperiodic, which include billiards in infinite polysquares and polycubes. In particular, we can prove time-quantitative density even for aperiodic systems. In terms of optics the billiard case is equivalent to the result that an explicit single ray of light can essentially illuminate a whole infinite polysquare or polycube with reflecting boundary acting as "mirrors". In fact, we show that the same initial direction can work for an uncountable family of such infinite systems.

Some of these infinite systems belong to the class of Ehrenfest wind-tree models, introduced by physicists about 100 years ago. Thus we obtain, for the first time, explicit density results about the time evolution of these infinite aperiodic billiard models in physics. What makes our positive density results in the case of the periodic Ehrenfest wind-tree models particularly interesting is the recent discovery by Fraczek and Ulcigrai [8] about these models that for almost every initial direction, the billiard orbit is *not* dense.

To prove density of explicit orbits, we use a non-ergodic method, which is a novel "eigenvalue-free" version of the shortline method. The original "eigenvalue-based" version of the shortline method, introduced and developed in [2, 3], enables us to prove time-quantitative equidistribution of orbits. The reader does not need to be familiar with those long papers. Here we make a serious effort to keep this paper self-contained.

6. TIME-QUANTITATIVE DENSITY

6.1. **From density to superdensity.** Our goal in part (III) is to prove time-quantitative density of explicit orbits, and, in many cases, even its best possible form called *superdensity*.

The concept of *time-quantitative* density is simply a means to describing how long it takes for a particle moving with unit speed on an explicit geodesic or a point-billiard to enter a given small target set.

Perhaps the reader is wondering: why should we care about "density" when we already know many "uniformity" results, for instance, the collection of uniformity results in Section 2.1 in [2] that are proved by ergodic methods. Well, it is true that uniformity implies density, but uniformity does not imply any form of time-quantitative density, not to mention superdensity. Note that in general even superuniformity (meaning extremely small poly-logarithmic error term) is not strong enough to imply superdensity.

2010 *Mathematics Subject Classification.* 11K38, 37E35.

Key words and phrases. geodesics, billiards, time-quantitative density.

Time-quantitative uniformity and time-quantitative density represent two (in general incomparable) complementary viewpoints to describing the "evenness" of an infinite orbit in the undelying space.

Our tool is a new *eigenvalue-free* version of the surplus shortline method, which, for the convenience of the reader, will be developed here from scratch. A great advantage of this new version is that, unlike the old eigenvalue-based version used in [2, 3], it is flexible enough to work in higher dimensions to prove, for example, the density of 3-*dimensional billiards* in cube-tiled solids ("polycubes"), as well as to prove the density of orbits on *infinite aperiodic* polysquare surfaces.

We know very, very little about 3-dimensional "flat" dynamical systems, where "flat" refers to locally Euclidean 3-space, and similarly, we know very, very little about the density of orbits on infinite aperiodic polysquare surfaces. So one may say that the most interesting results of part (III) are our density results for 3-dimensional systems and for infinite aperiodic polysquare surfaces. Nevertheless, we start the detailed discussion in the natural/historic order, meaning the case of lower dimensions and compact underlying space.

First we study *superdensity*, a best possible form of time-quantitative density. Superdensity has already been mentioned in [2]; see Section 1.1 and Theorem 3.4.1 there. For the convenience of the reader we repeat the formal definition. The first place to see it is Property A below, which is a special case.

We begin the discussion with the one-dimensional case, and very briefly recall some basic facts about the density and uniformity of the irrational rotation sequence $\{k\alpha\}$, $k = 1, 2, 3, \ldots$, in the unit interval $[0, 1)$. Here α is irrational and $0 \leqslant \{x\} < 1$ denotes the fractional part of a real number x.

The density of the irrational rotation sequence has been known since the early nineteenth century, through the work of Dirichlet, Chebyshev and Kronecker, *etc.*, and extended to uniform distribution in the first years of the twentieth century by Bohl, Sierpinski and Weyl. We can clearly assume that $0 < \alpha < 1$, which has an infinite continued fraction expansion of the form

$$\alpha = [a_1, a_2, a_3, \ldots] = \frac{1}{a_1 + \frac{1}{a_2 + \frac{1}{a_3 + \cdots}}}, \tag{6.1.1}$$

with digits, or partial quotients, $a_i \geqslant 1$. The works of Hardy and Littlewood [9, 10], Ostrowski [22], Weyl [25], *etc.* around 1920 helps to clarify the key role of the continued fraction digits a_i in the quantitative aspects of the distribution of the irrational rotation sequence. A main result of this classical work is that the sequence $\{k\alpha\}$, $k = 1, 2, 3, \ldots$, is *most* uniformly distributed in the precise sense that it exhibits logarithmic error, which is the minimum order of magnitude, if and only if the average size of the digits is bounded, formally, if

$$\limsup_{n \to \infty} \frac{1}{n} \sum_{i=1}^{n} a_i < \infty. \tag{6.1.2}$$

An irrational number $\alpha \in [0, 1)$ is *badly approximable* if and only if the continued fraction digits are bounded, *i.e.*, there is a constant $C = C(\alpha)$ such that $a_i \leqslant C$ for every digit a_i in (6.1.1). For badly approximable numbers the average size of the digits is trivially bounded, *i.e.*, (6.1.2) holds. Note that every quadratic irrational is badly approximable, since the continued fraction is eventually periodic, a result that goes back to Euler and Lagrange.

Superdensity is closely related to this classical work about uniform distribution. Indeed, the irrational rotation sequence exhibits superdensity if and only if α is

badly approximable. It means precisely that Property A and Property B below are equivalent.

Property A. *There is an absolute constant $C_1 = C_1(\alpha)$ such that for every integer $n \geqslant 1$ and subinterval $I \subset [0,1)$ of length $1/n$, there exists $1 \leqslant j \leqslant C_1 n$ such that $\{j\alpha\} \in I$.*

Property B. *The number α is badly approximable, i.e., there exists a constant $C = C(\alpha)$ such that $a_i \leqslant C$ for every digit a_i in* (6.1.1).

It is Property A that we consider the definition of *superdensity* in the special case of the irrational rotation sequence.

Lemma 6.1.1. *Property A and Property B are equivalent.*

A proof of this can be found in, for instance, Khinchin [19]; see Theorem 26 there. For the sake of completeness we include here our shorter proof, which has the extra benefit that the reader can compare it to the more complicated proof of Lemma 6.1.2.

Proof of Lemma 6.1.1. The proof is an easy exercise by using the theory of continued fractions. Let $k \geqslant 1$ be any integer. The initial segment

$$[a_1, a_2, \ldots, a_k] = \frac{p_k}{q_k}$$

of (6.1.1) is a rational number, called the k-th convergent of the irrational number α. Here the numerators $p_k = p_k(\alpha)$ and the denominators $q_k = q_k(\alpha)$ of the convergents of α satisfy the recurrence relations

$$p_k = a_k p_{k-1} + p_{k-2}, \quad q_k = a_k q_{k-1} + q_{k-2}, \quad p_k q_{k-1} - q_k p_{k-1} = (-1)^k, \quad k \geqslant 2, \tag{6.1.3}$$

with the initial conditions $p_0 = 0$, $q_0 = 1$, $p_1 = 1$ and $q_1 = a_1$. The k-th convergent p_k/q_k gives an excellent rational approximation of α, in the form

$$\left| \alpha - \frac{p_k}{q_k} \right| < \frac{1}{q_k q_{k+1}}. \tag{6.1.4}$$

The proof of Lemma 6.1.1 is based on (6.1.3) and (6.1.4), which are well known facts in the theory of continued fractions; see any book on number theory that has a chapter on continued fractions.

First we derive Property A from Property B. For any arbitrary integer $n \geqslant 1$, let $k = k(\alpha; n)$ be the smallest integer such that

$$q_k = q_k(\alpha) > 3n. \tag{6.1.5}$$

Let $I \subset [0,1)$ be of length $1/n$. By (6.1.5) there exists an integer $1 \leqslant \ell \leqslant q_k$ such that I contains both $(\ell - 1)/q_k$ and $(\ell + 1)/q_k$, with the convention that $(q_k + 1)/q_k$ denotes $1/q_k$. Multiplying (6.1.4) by a nonzero integer $1 \leqslant j \leqslant q_k$ we have

$$\left| j\alpha - \frac{jp_k}{q_k} \right| < \frac{j}{q_k q_{k+1}} < \frac{1}{q_k}. \tag{6.1.6}$$

From the last equation in (6.1.3), we see that p_k and q_k are relatively prime, so there exists an integer $1 \leqslant j_0 \leqslant q_k$ such that

$$\left\{ \frac{j_0 p_k}{q_k} \right\} = \frac{\ell}{q_k}. \tag{6.1.7}$$

Using (6.1.6) with $j = j_0$, and combining it with (6.1.7), we obtain that $\{j_0\alpha\} \in I$ for some $1 \leqslant j_0 \leqslant C_1 n$, which proves Property A. Indeed, it follows from (6.1.5) and (6.1.3) that

$$q_{k-1} \leqslant 3n \quad \text{and} \quad q_k \leqslant (a_k + 1) q_{k-1},$$

which imply that $j_0 \leqslant q_k \leqslant 3(C+1)n$, so that $j_0 \leqslant C_1 n$ if we take $C_1 = 3(C+1)$.

Next we derive Property B from Property A. For any positive integer k, consider the interval

$$I = \left[\frac{1}{3q_k}, \frac{2}{3q_k}\right]. \tag{6.1.8}$$

Multiplying (6.1.4) by a nonzero integer $1 \leqslant j \leqslant q_{k+1}/3$ we have

$$\left|j\alpha - \frac{jp_k}{q_k}\right| < \frac{j}{q_k q_{k+1}} < \frac{1}{3q_k}.$$

This implies that

$$-\frac{1}{3q_k} < j\alpha - \frac{jp_k}{q_k} < \frac{1}{3q_k}, \quad \text{or} \quad \frac{3jp_k - 1}{3q_k} < j\alpha < \frac{3jp_k + 1}{3q_k}.$$

Write $x = jp_k - [j\alpha]q_k$. Then clearly

$$\frac{3x-1}{3q_k} < \{j\alpha\} < \frac{3x+1}{3q_k}.$$

Naturally we must have $3x + 1 > 0$, and so x is a non-negative integer. If $x = 0$, then $\{j\alpha\} < 1/3q_k$. If $x \geqslant 1$, then $\{j\alpha\} > 2/3q_k$. Thus it follows that

$$\{j\alpha\} \notin I \quad \text{for every } 1 \leqslant j < \frac{q_{k+1}}{3}. \tag{6.1.9}$$

Note from (6.1.8) that $|I| = 1/n$ with $n = 3q_k$. If Property A holds, then there exists a $1 \leqslant j_0 \leqslant C_1 n$ such that $\{j_0\alpha\} \in I$. Combining this with (6.1.9), we have

$$\frac{q_{k+1}}{3} \leqslant j_0 \leqslant C_1 n = 3C_1 q_k,$$

and since $a_{k+1}q_k < q_{k+1}$, we obtain

$$\frac{a_{k+1}q_k}{3} < \frac{q_{k+1}}{3} \leqslant j_0 \leqslant 3C_1 q_k,$$

which implies $a_{k+1} < 9C_1$. This proves Property B with the choice $C = 9C_1$. □

Superdensity of the *discrete* irrational rotation sequence with badly approximable α immediately implies superdensity of the *continuous* torus lines with slope α in a square. The standard trick is *discretization*. Discretization simply means we look at the points where the torus line hits the sides of the square. This reduces the problem of uniformity in the 2-dimensional case to the 1-dimensional case.

More precisely, discrete superdensity implies via discretization that an infinite torus half-line of badly approximable slope α in the unit square $[0,1)^2$ has the following remarkable property. There is an absolute constant $C_2 = C_2(\alpha)$ such that for every integer $n \geqslant 1$ and for every point $P \in [0,1)^2$ in the unit square, the initial segment of length $C_2 n$ of this torus half-line gets $1/n$-close to P. This is what we call the *superdensity of the torus line* in the unit square.

In higher dimensions we have Kronecker's classical theorem concerning the density of the torus line flow in the unit cube $[0,1)^d$, where $d \geqslant 2$ is arbitrary. Let $\mathbf{v} = (v_1, \ldots, v_d) \in \mathbb{R}^d$ be a vector such that its coordinates are linearly independent over the rational numbers. Then by Kronecker's theorem any infinite torus half-line of direction $\mathbf{v}$ is dense in the unit cube $[0,1)^d$. And we also have the converse, that density implies linear independence of the coordinates of the direction vector.

It is straightforward to define superdensity of the torus line in a cube of any dimension. An infinite torus half-line of direction vector $\mathbf{v} \in \mathbb{R}^d$ is *superdense* in the unit cube $[0,1)^d$, if there is an absolute constant $C_3 = C_3(\mathbf{v})$ such that for every integer $n \geqslant 1$ and for every point $P \in [0,1)^d$ in the unit cube, the initial segment of length $C_3 n^{d-1}$ of this torus half-line gets $1/n$-close to P.

Superdensity represents a best possible quantitative form of density in both the discrete and the continuous case. For simplicity we just show it in the continuous case. We prove that the polynomial order of magnitude of the length n^{d-1} in the variable n is necessary to get $1/n$-close to every point. For simplicity we choose an integer $n \geqslant 3$ which is divisible by 3, and consider the usual decomposition of the unit cube $[0,1)^d$ into n^d congruent subcubes. Next we decompose each one of these subcubes with side length $1/n$ into 3^d congruent smaller cubes, and refer to the particular cube of side length $1/3n$ in the middle as a *center cube*. The distance between any two center cubes is at least $2/3n$. If a continuous curve $\mathcal{C}$ gets $1/6n$-close to every point, then it must visit every center cube. Since there are n^d center cubes, $\mathcal{C}$ must have length at least

$$(n^d - 1)\frac{2}{3n} = \frac{2}{3}n^{d-1} - o(1),$$

which gives the desired polynomial order of magnitude n^{d-1}.

Superdensity of a torus line in a square $[0,1)^2$ is completely understood. The necessary and sufficient condition of superdensity is that the slope is badly approximable.

Badly approximable slopes are not typical, as they form a set of zero Lebesgue measure. But we cannot call this set "totally negligible" either, since it has positive Hausdorff measure.

For almost every slope α the torus line exhibits "almost" superdensity. Then the linear bound $C_3 n$ above is replaced by the slightly larger order of magnitude $n(\log n)^{1+\varepsilon}$, where, as usual, $\varepsilon > 0$ can be arbitrarily small but fixed, assuming that n is large enough. This follows from a classical result of Khinchin [18] in diophantine approximation.

The problem of superdensity of a torus line in a cube $[0,1)^d$ with $d \geqslant 3$ is harder. One reason is that the theory of continued fractions does not seem to extend to higher dimensions, and one has to find an alternative approach. What works here is the geometry of numbers, which provides some "transference theorems"; see Chapter 5 in Cassels [4]. Combining a couple of transference theorems it is not difficult to prove the following result, which is basically a weaker form of Lemma 6.1.1 in higher dimensions. Lemma 6.1.2 below is a one-sided result. It is a sufficient condition for superdensity in higher dimensions. It gives infinitely many explicit superdense directions. It is well possible that it has already been published somewhere, but we have not been able find it.

To understand Lemma 6.1.2 the reader needs to be familiar with at least the simplest basic concepts of algebraic number fields.

Lemma 6.1.2 ("possibly folklore"). *Let $m \geqslant 1$ be an integer, and let $\alpha_1, \ldots, \alpha_m$ be any m numbers in a real algebraic number field of degree $m+1$ such that $1, \alpha_1, \ldots, \alpha_m$ are linearly independent over the rationals. Write*

$$\mathbf{v} = (1, \alpha_1, \ldots, \alpha_m) \in \mathbb{R}^{m+1}.$$

Then any torus half-line with direction $\mathbf{v}$ is superdense in the unit cube $[0,1)^{m+1}$.

Proof. Let $\|x\|$ denote the distance of a real number x from the nearest integer.

The first step of the proof is to show that there exists a constant $C_4 > 0$, depending at most on m and $\alpha_1, \ldots, \alpha_m$, such that

$$\left\| \sum_{i=1}^{m} n_i \alpha_i \right\| \geqslant \frac{C_4}{(\max_{1 \leqslant i \leqslant m} |n_i|)^m} \tag{6.1.10}$$

for all nonzero integral vectors $\mathbf{n} = (n_1, \ldots, n_m) \in \mathbb{Z}^m$ with $\mathbf{n} \neq \mathbf{0}$. The assertion (6.1.10) will follow from using the concept of *norm* in an algebraic number field.

Since every algebraic number is the ratio of an algebraic integer and a nonzero rational integer, it is enough to prove (6.1.10) when α_i, $1 \leqslant i \leqslant m$, are algebraic integers. Let n_0 be the nearest integer to the sum $\sum_{i=1}^m n_i\alpha_i$. The norm of the algebraic integer $n_0 - \sum_{i=1}^m n_i\alpha_i$ is the product

$$\prod_{j=0}^m \left(n_0 - \sum_{i=1}^m n_i \alpha_i^{(j)} \right),$$

where $\alpha_i^{(0)} = \alpha_i$ and $\alpha_i^{(j)}$, $1 \leqslant j \leqslant m$, are the m other algebraic conjugates of α_i. Since the norm of an algebraic integer is a nonzero rational integer, and so has absolute value at least 1, we deduce that

$$\left\| \sum_{i=1}^m n_i\alpha_i \right\| = \left| n_0 - \sum_{i=1}^m n_i\alpha_i \right| \geqslant \frac{1}{\prod_{j=1}^m |n_0 - \sum_{i=1}^m n_i\alpha_i^{(j)}|} \geqslant \frac{C_5}{(\max_{1\leqslant i\leqslant m} |n_i|)^m}$$

where the constant $C_5 > 0$ depends at most on m and $\alpha_1, \ldots, \alpha_m$. The assertion (6.1.10) follows.

The second step of the proof is to use Mahler's transference theorem in the relevant special case; see Mahler [20] or Theorem 2 in Chapter 5 of Cassels [4].

Theorem A. *A necessary and sufficient condition that there exists a constant $C' > 0$ such that*

$$\left\| \sum_{i=1}^m n_i\alpha_i \right\| \left(\max_{1\leqslant i\leqslant m} |n_i| \right)^m \geqslant C'$$

for every $\mathbf{n} = (n_1, \ldots, n_m) \in \mathbb{Z}^m$ with $\mathbf{n} \neq \mathbf{0}$, is that there exists another constant $C'' > 0$ such that

$$\left(\max_{1\leqslant j\leqslant m} \|n\alpha_j\| \right)^m |n| \geqslant C''$$

for every $n \in \mathbb{Z}$ with $n \neq 0$.

The third step of the proof is to apply the following transference result, which is a special case of a theorem of Hlawka [12] about general linear forms; see also Theorem 6 in Chapter 5 of Cassels [4].

Theorem B. *Let $\alpha_1, \ldots, \alpha_m$ be $m \geqslant 1$ real numbers such that for all $N \geqslant 1$,*

$$\max_{1\leqslant j\leqslant m} \|n\alpha_j\| \geqslant C_0 N^{-1/m}$$

for every integer $1 \leqslant n \leqslant N$, where $C_0 = C_0(\alpha_1, \ldots, \alpha_m) > 0$ is a constant independent of N. Then for any set of m real numbers $0 < \beta_i < 1$, $1 \leqslant i \leqslant m$, there exists an integer $1 \leqslant \ell_0 \leqslant C^*N$ such that

$$\|\ell_0\alpha_i - \beta_i\| \leqslant C^* N^{-1/m}$$

for every $1 \leqslant i \leqslant m$, where the constant $C^* = C^*(C_0)$ depends only on the value of C_0.

Lemma 6.1.2 now follows from a combination of the inequality (6.1.10) together with Theorem A and Theorem B. □

By Lemma 6.1.1 a torus line in a square is superdense if and only if the slope is a badly approximable number. The torus line flow in a square, the quintessential integrable flat system, is very "user-friendly" in the sense that it exhibits remarkable stability and predictability. Indeed, two particles moving on two close parallel torus lines with the same speed remain close forever, and they preserve their distance. This raises a natural question: When can we guarantee superdensity in the much

harder case of non-integrable flat systems, where parallel orbits split and the long-term behavior becomes unpredictable?

The good news is that it is possible to guarantee infinitely many superdense geodesics for *every* polysquare surface. It is based on a new version of the shortline method. We illustrate the basic idea of the proof on the simplest flat polysquare surface, the so-called *L-surface*.

The L-surface is a compact closed flat polysquare surface with 3 unit square faces forming letter L ("L-shape"). It is obtained by identifying the two horizontal edges h_1, the two horizontal edges h_2, the two vertical edges v_1, and the two vertical edges v_2; see Figure 6.1.1.

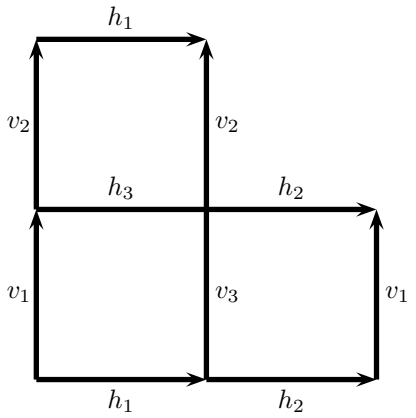

Figure 6.1.1: net of the L-surface with edge identification

Unlike the cube surface, the L-surface is not the surface of a 3-dimensional solid, so one may call it "exotic". Nevertheless, it is a perfectly legitimate surface with genus 2.

A geodesic on the L-surface is basically a generalized torus line on the L-shape, as illustrated in Figure 6.1.2.

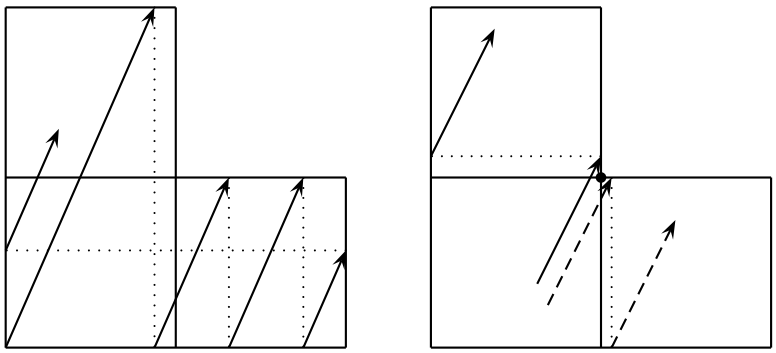

Figure 6.1.2: geodesics on the L-surface and a split singularity

The L-surface is non-integrable, since it has a split singularity, as demonstrated in the picture on the right in Figure 6.1.2. Two geodesics close together behave rather differently after getting close to this singularity.

In Section 6.2 we shall prove the following result.

Theorem 6.1.1. *Let $\alpha > 1$ be any badly approximable number with the extra restriction in the continued fraction*

$$\alpha = a_0 + \cfrac{1}{a_1 + \cfrac{1}{a_2 + \cfrac{1}{a_3 + \cdots}}}$$

that every digit $a_i \geqslant 2$, $i \geqslant 0$, is ***even****. Then any half-infinite 1-directional geodesic with slope α exhibits superdensity on the L-surface.*

Remark. We should explain here part of the reasoning for restricting the continued fraction digits a_i to even integers. Here we consider a geodesic of slope $\alpha = [a_0; a_1, a_2, a_3, \ldots]$. Since $a_0 \geqslant 2$, we clearly have $\alpha > 1$. We shall call this geodesic "almost vertical". The idea is to replace part of this geodesic by part of another geodesic which is "almost horizontal", meaning that its slope has absolute value less than 1. We elaborate on this below.

Consider the digit a_0. Clearly $\alpha = a_0 + \{\alpha\}$, where $\{\alpha\} = [a_1, a_2, a_3, \ldots]$ is the fractional part of α.

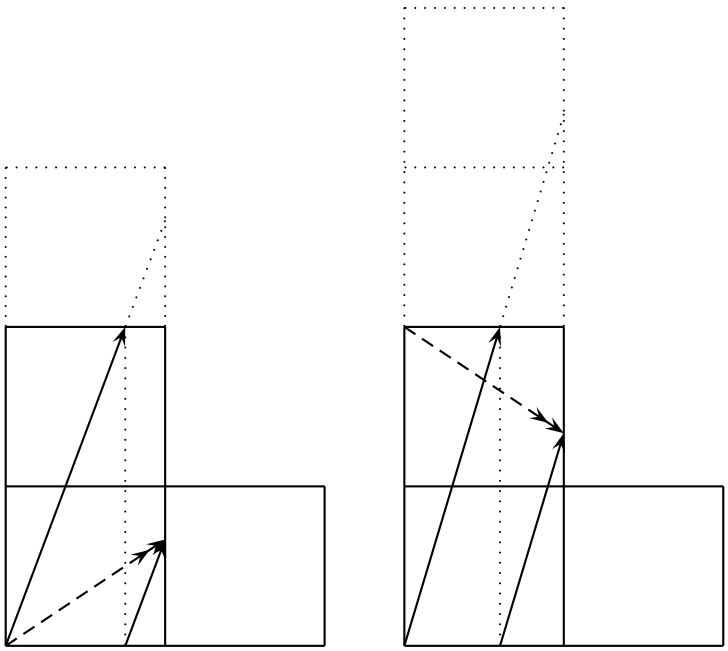

Figure 6.1.3: the cases $a_0 = 2$ and $a_0 = 3$

Suppose that $a_0 = 2$, or in general, a_0 is even. It is clear from the picture on the left in Figure 6.1.3 that a geodesic of slope α that starts from the origin, represented by the solid line in the picture, cuts the edge v_3 at the point $(1, \{\alpha\})$. For the part of the geodesic of slope α from the origin to this point, a "shortcut" can be obtained by the geodesic of slope $\{\alpha\} < 1$ from the origin to this point, represented by the dashed line in the picture, and the slope of this "shortcut" is positive.

Suppose that $a_0 = 3$, or in general, a_0 is odd. It is clear from the picture on the right in Figure 6.1.3 that a geodesic of slope α that starts from the origin, represented by the solid line in the picture, cuts the edge v_2 at the point $(1, 1 + \{\alpha\})$. For the part of the geodesic of slope α from the origin to this point, a "shortcut" can be obtained by the geodesic of slope with absolute value less than 1 from the top left vertex, which is identified with the origin, to this point, represented by the dashed line in the picture, and the slope of this "shortcut" is negative.

In our initial discussion, we want to avoid geodesics with negative slopes. As will be clear later, this can be achieved by ensuring that all the continued fraction digits a_i are even.

The reader who has read [3] is probably wondering why we consider the L-surface here, when Theorem 5.3.1 there already establishes the superdensity of L-lines for all quadratic irrational slopes. Well, the proof of Theorem 5.3.1 comes to more than 100 pages, and the proof of Theorem 6.1.1 in Section 6.2 is considerably shorter. This difference clearly shows that the new eigenvalue-free version of the shortline method here is simpler than the eigenvalue-based shortline method developed in [2, 3]. We shall see later that this new approach is also much more flexible.

Theorem 6.1.1 provides an infinite set of "good slopes" such that the corresponding geodesics are superdense on the L-surface. From the viewpoint of set theory this set is "large", since it is uncountable. From the viewpoint of topology this set is "small", since it is *nowhere dense* on the unit circle. In Section 6.4 we shall show how we can extend this set to a larger set of "good slopes", which is *dense* on the unit circle. There we shall also generalize Theorem 6.1.1 to all polysquare surfaces.

Next we move to the 3-space; in particular to the class of cube-tiled solids, both finite and infinite. This is quite interesting because, as far as we know, there is no known density result for non-integrable systems of dimension greater than 2. We elaborate on this.

The first non-trivial result for 2-dimensional non-integrable flat systems is a result of Katok and Zemlyakov [17] in 1975; see Theorem 2.1.1 in [2]. It concerns the density of any infinite geodesic on a *rational surface*, *i.e.*, a surface where every angle on every polygonal face is a rational multiple of π. The proof is a clever application of Poincare's recurrence theorem, but it does not say anything definite about how long it takes for a geodesic to first enter a given test set such as a small circle on a face with radius $1/n$.

For comparison note that Theorem 6.1.1 is a superdensity result, a strongest form of time-quantitative density, and it *does* tell us how long it takes for a geodesic to enter first a given test set such as a small circle on a face with radius $1/n$.

To illustrate how little is known about the density of flat dynamical systems in general, we mention the following humiliatingly long-standing open problem.

Open Problem 1. *Let $\mathcal{T}$ be an arbitrary right triangle, and consider billiards in $\mathcal{T}$.*

(a) *Does there exist a half-infinite billiard orbit that is dense in $\mathcal{T}$?*

(b) *Does there exist an explicit half-infinite billiard orbit that is dense in $\mathcal{T}$? Here "explicit" means that we can express the starting point and the initial slope of the orbit in terms of the given data of the triangle $\mathcal{T}$.*

(c) *Does there exist a slope such that every half-infinite billiard orbit with this initial slope is dense in $\mathcal{T}$?*

(d) *Is it true that for almost every real number α, every half-infinite billiard orbit with initial slope α is dense in $\mathcal{T}$?*

What Open Problem 1 really illustrates is the lack of results or methods for handling geodesic flow on *infinite* flat surfaces. Indeed, if the acute angle of the right triangle $\mathcal{T}$ is an irrational multiple of π, then iterated *unfolding* reduces billiard flow in $\mathcal{T}$ to geodesic flow on an infinite flat surface; see, *e.g.*, Section 1.3 in [2]. Unfortunately we know much, much less about the case of infinite flat surfaces than about finite flat surfaces. Starting in Section 6.5 we are going to prove several results for infinite polysquare surfaces but, unfortunately, we cannot make any progress with Open Problem 1.

We also recall Theorem 2.1.3 in [2], which extends density to uniformity for every rational surface and for almost every slope. Unfortunately, the elegant Theorems 2.1.3, like Theorem 2.1.1, is a "time-qualitative" result that does not say anything definite about the "necessary time range", due to the fact that Birkhoff's ergodic theorem and Poincare's recurrence theorem, the underlying thrust of the proof, do not have an explicit error term.

All of the results mentioned up to this point in [2, 3] are about some 2-dimensional systems; namely, geodesic flow on flat polygonal surfaces. The existing ergodic methods do not seem to work for flat systems in higher dimensions.

Luckily the new version of the shortline method happens to work in higher dimensions. It can provide time-quantitative density in infinitely many 3-dimensional

non-integrable systems. Corresponding to Theorem 6.1.1, we start with the simplest non-trivial case, the *L-solid*, the simplest example of a polycube, *i.e.*, cube-tiled solid. It is the 3-dimensional analog of the L-surface, and is an L-shaped solid formed from 3 unit cubes; see Figure 6.1.4. The L-solid has volume 3, and the 3 unit cubes are called accordingly the *top-cube*, the *middle-cube* and the *right-cube*.

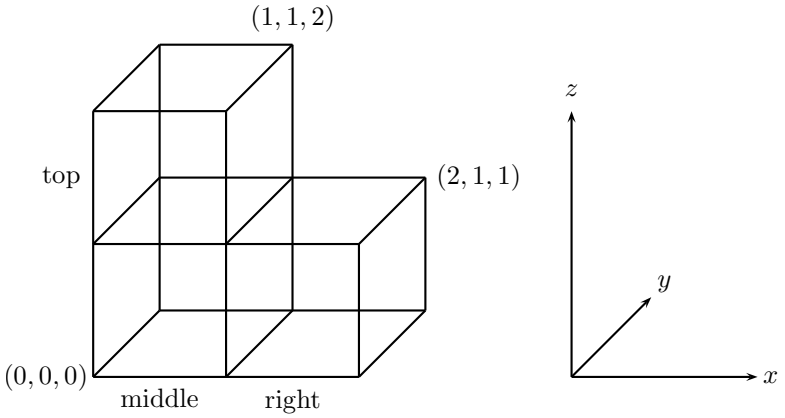

Figure 6.1.4: the L-solid

We may say, with some exaggeration, that the L-surface basically represents the whole difficulty of polysquares. Similarly, the L-solid basically represents the whole difficulty of polycubes.

We study the density of "generalized torus lines" in the L-solid, an analog of geodesics on the L-surface. An ordinary torus line in a cube means a straight line in 3-space reduced to the inside of the unit cube by taking the fractional parts of the coordinates, *i.e.*, "modulo one". Taking "modulo one" in 3-space is equivalent to the identification of the opposite faces of the unit cube surface.

Similarly, a "generalized torus line" in the L-solid is a straight line reduced to the inside of the L-solid by an analogous boundary identification of the faces. It goes as follows. Given a square face on the surface of the L-solid, we take its normal which will hit the surface in another square face that we call the *opposite face* of the original square face. Given a point P in the L-solid and a nonzero 3-dimensional direction vector $\mathbf{v}$, consider the half-line starting from P in the given direction $\mathbf{v}$. When this half-line hits a face at a point, we move to the corresponding point on the opposite face, and from that point we start a second half-line in the same given direction $\mathbf{v}$. When this second half-line hits another face at another point, we move to the corresponding point on the opposite face, and from that point we start a third half-line in the same given direction $\mathbf{v}$. And so on. The union of these parallel line segments defines a "generalized torus line" in the L-solid. For simplicity we call it an *s-L-line*, where the letter "s" refers to "solid".

Let $\mathcal{L}$ be an s-L-line, and let $\mathcal{L}(\mathbf{v}; t)$ denote its arc-length parametrization, where $\mathbf{v}$ is the direction vector of $\mathcal{L}$, and t denotes time. Note that the arc-length parametrization represents dynamics: a particle moving on the s-L-line $\mathcal{L}$ with constant unit speed. The particle starts at the point $\mathcal{L}(\mathbf{v}; 0)$, and we study the time evolution of the motion on the infinite half-line $\mathcal{L}(\mathbf{v}; t)$, $t \geqslant 0$, *i.e.*, we focus on the long-term behavior as $t \to \infty$.

The edge between the top-cube and the right-cube is a *split-singularity* of this motion. It means the ambiguity that when the particle hits this edge, there are *two* natural ways to continue the s-L-line, *i.e.*, there is no unique extension of the motion.

Note that a typical s-L-line is infinite, since it never hits an edge of the L-solid.

We study the following question.

Question 1. *Find an explicit direction vector* $\mathbf{v}$ *such that every half-infinite* 1*-directional geodesic* $\mathcal{L}(\mathbf{v};t)$*,* $t \geqslant 0$*, with direction* $\mathbf{v}$ *exhibits density in the L-solid. In fact, we are interested in time-quantitative density.*

Superdensity is an optimal form of time-quantitative density, which leads to another natural question.

Question 2. *Does there exist a half-infinite* 1*-directional geodesic that exhibits superdensity?*

In the 3-dimensional case we cannot prove superdensity.

In Section 6.3, we prove the following 3-dimensional time-quantitative density result for the L-solid.

Theorem 6.1.2. *For any fixed constant* $\varepsilon > 0$*, there exist infinitely many explicit* 3*-dimensional vectors* $\mathbf{v}_0$ *such that every half-infinite* 1*-directional geodesic* $\mathcal{L}(\mathbf{v}_0;t)$*,* $t \geqslant 0$*, with direction vector* $\mathbf{v}_0$ *and arc-length parametrization, exhibits time-quantitative density in the L-solid in the following precise sense. There is an effectively computable threshold constant* $C_0 = C_0(\varepsilon;\mathbf{v}_0)$ *such that for every integer* $n \geqslant C_0$ *and every point* Q *in the L-solid, the initial segment* $\mathcal{L}(\mathbf{v}_0;t)$*,* $0 < t < n^{2+\varepsilon}$*, gets* $1/n$*-close to* Q*.*

Later in Section 6.4, we discuss a generalization of Theorem 6.1.1 to a large class of polysquares, as well as a generalization of Theorem 6.1.2 to a large class of polycubes.

6.2. **Size-magnification version of the shortline method.**

Proof of Theorem 6.1.1. We refer to geodesics on the L-surface as L-lines; see Figure 6.2.1. We start with the concept of surplus *shortline* of an L-line, and then discuss the concept of *exponentially fast zigzagging to a street corner*, which has a crucial role in the new version of the shortline process. In the rest we refer to this new eigenvalue-free version of the process as the "size-magnification" version. The term "size-magnification" will be justified by the arguments below.

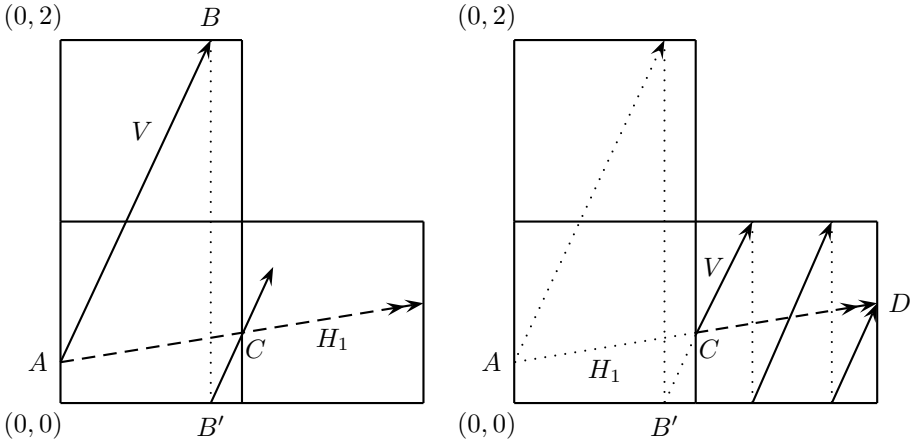

Figure 6.2.1: (left) H_1 is the shortline of V; (right) second detour street crossing of V, the part of V from C to D, with the part of the shortline H_1 from C to D

In Figure 6.2.1 we consider an "almost vertical" L-line V. Assume that V is infinite in both directions, and let $\alpha > 1$ denote the slope of V. Note that we use the term "almost vertical" (or "almost horizontal") in the very broad sense that the slope is greater than 1 (or it is between 0 and 1). Formally, let $\pi/4 < \theta < \pi/2$ be the angle between V and the horizontal side of the L-shape. Then $\alpha = \tan\theta$; see the

picture on the left in Figure 6.2.1. Here AB and $B'C$ are consecutive line segments of V, and together they exhibit a left to right detour crossing of the vertical "street" with corners $(0,0)$, $(1,0)$, $(1,2)$ and $(0,2)$, whereas the line segment AC represents a shortcut street crossing of the same street. (This street is in fact a cylinder. Owing to the intuitive meaning of street-crossing, we prefer to use the term *street*.) Now AC is a line segment of the almost horizontal L-line H_1. We call H_1 the *shortline* of V. Let $\pi/4 < \theta_1 < \pi/2$ be the angle between H_1 and the vertical side of the L-shape. Then the slope of H_1 is α_1^{-1}, where $\alpha_1 = \tan\theta_1$.

By hypothesis the continued fraction of the given badly approximable slope satisfies

$$\text{slope of } V = \alpha = a_0 + \frac{1}{a_1 + \frac{1}{a_2 + \frac{1}{a_3 + \cdots}}} = [a_0; a_1, a_2, a_3, \ldots], \tag{6.2.1}$$

and has the *even digit* property, *i.e.*, $a_i \geqslant 2$ is even for every $i \geqslant 0$. Note that since α is irrational, (6.2.1) has infinitely many digits. The geometric fact that AC is a shortcut of $AB + B'C$ gives rise to an algebraic relation between the slopes of V and H_1. In view of the even digit condition, the slope of H_1 is $\alpha - a_0$. More precisely, we have

$$\text{slope of } H_1 = \alpha_1^{-1} = \left(a_1 + \frac{1}{a_2 + \frac{1}{a_3 + \frac{1}{a_4 + \cdots}}} \right)^{-1} = [a_1; a_2, a_3, a_4, \ldots]^{-1}. \tag{6.2.2}$$

In other words, the continued fraction of the slope of H_1, the shortline of V, is obtained from the continued fraction of the slope of V by a shift followed by taking inverse.

The three consecutive line segments of V between C and D in the picture on the right in Figure 6.2.1 together exhibit a left to right detour crossing of the vertical street with corners $(1,0)$, $(2,0)$, $(2,1)$ and $(1,1)$, whereas the line segment CD represents a shortcut street crossing of the same street. Now CD is a line segment of the almost horizontal L-line H_1, the shortline of V.

Figure 6.2.1 also illustrates the crucial geometric property that any almost vertical L-line V and its shortline H_1 have precisely the same edge-cutting points on the vertical sides of vertical streets. We refer to this as the *vertical same edge cutting property* of the shortline process.

We can iterate this shortline process. To find the shortline of H_1, we simply repeat the argument above by switching the roles of horizontal and vertical. Let V_2 denote the shortline of H_1, and let $\alpha_2 > 1$ denote the slope of the almost vertical L-line V_2. Again, in view of the even digit condition, we have an analog of (6.2.1) and (6.2.2), in the form

$$\text{slope of } V_2 = \alpha_2 = a_2 + \frac{1}{a_3 + \frac{1}{a_4 + \frac{1}{a_5 + \cdots}}} = [a_2; a_3, a_4, a_5, \ldots].$$

In other words, the continued fraction of the slope of V_2, the shortline of H_1, is obtained from the continued fraction of the slope of H_1 by taking inverse followed by a shift.

We also have the analogous *horizontal same edge cutting property* of the shortline process, that an almost horizontal L-line H_1 and its shortline V_2 have precisely the same edge-cutting points on the horizontal sides of horizontal streets.

Of course we can define in a similar way the shortline of V_2, and so on. Thus we obtain an infinite sequence

$$V \to H_1 \to V_2 \to H_3 \to V_4 \to H_5 \to \cdots, \tag{6.2.3}$$

where, for every $i \geqslant 0$,

$$H_{2i+1} \text{ is the shortline of } V_{2i} \quad \text{and} \quad V_{2i+2} \text{ is the shortline of } H_{2i+1}, \tag{6.2.4}$$

$$V_{2i} \text{ and } H_{2i+1} \text{ satisfy the vertical same edge cutting property,} \tag{6.2.5}$$

and

$$H_{2i+1} \text{ and } V_{2i+2} \text{ satisfy the horizontal same edge cutting property.} \tag{6.2.6}$$

Combining (6.2.3)–(6.2.6) we obtain an *exponentially fast zigzagging* to a street corner; see Figure 6.2.2.

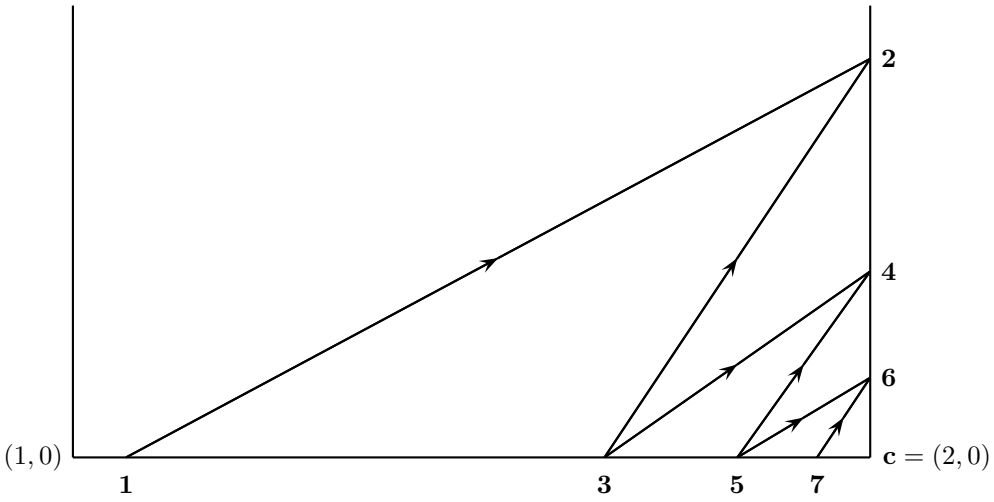

Figure 6.2.2: exponentially fast zigzagging to a street corner

Assume, for example, that the line segment **12** in Figure 6.2.2 belongs to an almost horizontal L-line H_{2i+5}, say, in (6.2.3). The term *exponentially fast zigzagging* means the following. By (6.2.5) the line segment **23** in Figure 6.2.2 belongs to the almost vertical L-line V_{2i+4} in (6.2.3). By (6.2.6) the line segment **34** belongs to the almost horizontal L-line H_{2i+3}. By (6.2.5) the line segment **45** belongs to the almost vertical L-line V_{2i+2}. By (6.2.6) the line segment **56** belongs to the almost horizontal L-line H_{2i+1}. Finally, by (6.2.5) the line segment **67** belongs to the almost vertical L-line V_{2i}.

The zigzagging in Figure 6.2.2 represents an exponentially fast convergence to the street corner $\mathbf{c} = (2, 0)$. More precisely, since the slope of H_{2i+5} is α_{2i+5}^{-1}, we have

$$\frac{\text{length}(\mathbf{1c})}{\text{length}(\mathbf{2c})} = \alpha_{2i+5}. \tag{6.2.7}$$

Similarly,

$$\begin{gathered} \frac{\text{length}(\mathbf{2c})}{\text{length}(\mathbf{3c})} = \alpha_{2i+4}, \quad \frac{\text{length}(\mathbf{3c})}{\text{length}(\mathbf{4c})} = \alpha_{2i+3}, \quad \frac{\text{length}(\mathbf{4c})}{\text{length}(\mathbf{5c})} = \alpha_{2i+2}, \\ \frac{\text{length}(\mathbf{5c})}{\text{length}(\mathbf{6c})} = \alpha_{2i+1}, \quad \frac{\text{length}(\mathbf{6c})}{\text{length}(\mathbf{7c})} = \alpha_{2i}. \end{gathered} \tag{6.2.8}$$

We can also write (6.2.7)–(6.2.8) in the equivalent form

$$\text{length}(\mathbf{2c}) = \frac{\text{length}(\mathbf{1c})}{\alpha_{2i+5}}, \quad \text{length}(\mathbf{3c}) = \frac{\text{length}(\mathbf{1c})}{\alpha_{2i+5}\alpha_{2i+4}},$$
$$\text{length}(\mathbf{4c}) = \frac{\text{length}(\mathbf{1c})}{\alpha_{2i+5}\alpha_{2i+4}\alpha_{2i+3}}, \quad \text{length}(\mathbf{5c}) = \frac{\text{length}(\mathbf{1c})}{\alpha_{2i+5}\alpha_{2i+4}\alpha_{2i+3}\alpha_{2i+2}},$$
$$\text{length}(\mathbf{6c}) = \frac{\text{length}(\mathbf{1c})}{\alpha_{2i+5}\alpha_{2i+4}\alpha_{2i+3}\alpha_{2i+2}\alpha_{2i+1}},$$
$$\text{length}(\mathbf{7c}) = \frac{\text{length}(\mathbf{1c})}{\alpha_{2i+5}\alpha_{2i+4}\alpha_{2i+3}\alpha_{2i+2}\alpha_{2i+1}\alpha_{2i}}.$$

We return to the chain (6.2.3). Let V^* be a finite initial segment of this almost vertical L-line V with slope $\alpha > 1$, and assume that V^* is "long". It is clear that V^* consists of a number of *whole* detour crossings and a *fractional* detour crossing at the end. Clearly the length of V^* is some multiple of $(1+\alpha^2)^{1/2}$, the common length of detour crossings of slope α of vertical streets. In other words,

$$\text{length}(V^*) = m_0(1+\alpha^2)^{1/2} \quad \text{for some large positive real number } m_0. \tag{6.2.9}$$

Each whole detour crossing in V^* has a shortcut, which is part of the almost horizontal shortline H_1 of V. The fractional detour crossing at the end in V^*, if extended to a full detour crossing, also has a shortcut, which is also part of the almost horizontal shortline H_1 of V. For this fractional detour crossing, we shorten its shortcut by the same fraction and at the appropriate end to obtain a fractional shortcut. We then take the union of these shortcuts and this fractional shortcut. This union is a segment of H_1 that we denote by H_1^*. Clearly the length of H_1^* is some multiple of $(1+\alpha_1^2)^{1/2}$, the common length of detour crossings of slope α_1^{-1} of horizontal streets. In other words,

$$\text{length}(H_1^*) = m_1(1+\alpha_1^2)^{1/2} \quad \text{for some real number } m_1.$$

We keep iterating this. Let

$$\text{length}(V_2^*) = m_2(1+\alpha_2^2)^{1/2} \quad \text{for some real number } m_2,$$
$$\text{length}(H_3^*) = m_3(1+\alpha_3^2)^{1/2} \quad \text{for some real number } m_3,$$

and so on. Consider the decreasing sequence

$$m_0 \geqslant m_1 \geqslant m_2 \geqslant m_3 \geqslant \cdots. \tag{6.2.10}$$

At this point, we make the *assumption* that the continued fraction digits a_i, $i = 0, 1, 2, 3, \ldots$, have a common upper bound $a_i < U$, where U is an integer. In other words, the number α is badly approximable. This implies, in particular, that for every $i = 0, 1, 2, 3, \ldots$, we have the bound

$$\alpha_i < U. \tag{6.2.11}$$

It is almost trivial to note that

$$\alpha_1 m_1 = m_0. \tag{6.2.12}$$

Indeed, we have the general form that for every $j \geqslant 0$,

$$\alpha_{j+1} m_{j+1} = m_j. \tag{6.2.13}$$

Iterating (6.2.13) we deduce that

$$m_k = m_0 \prod_{j=1}^{k} \frac{1}{\alpha_j}. \tag{6.2.14}$$

Let us return to the sequence (6.2.10). We need the following lemma.

Lemma 6.2.1. *There is a member m_ℓ of the sequence* (6.2.10) *such that $2U+1 \leqslant m_\ell \leqslant 4U^5$ and the corresponding V_ℓ^* or H_ℓ^*, depending on the parity of ℓ, exhibits all six types of corner cuts illustrated in Figure 6.2.3.*

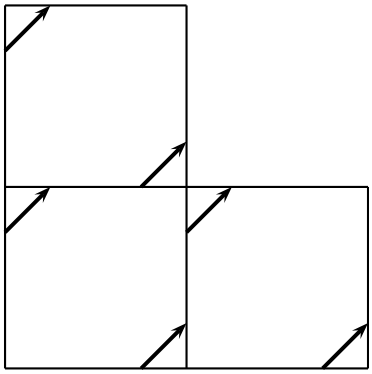

Figure 6.2.3: six types of corner cuts of the L-surface

Remark. The requirement $m_\ell \geqslant 2U+1$ is motivated by a later application of (6.2.14), while the other requirement $m_\ell \leqslant 3U^4$ will be clear from the proof of the lemma.

Before we can prove Lemma 6.2.1, we need to introduce the concept of *almost vertical units* of an almost vertical L-line and *almost horizontal units* of an almost horizontal L-line.

Suppose that V is an almost vertical L-line of slope $\gamma > 1$. An almost vertical unit of this L-line is a finite segment of V, of length $(1+\gamma^{-2})^{1/2}$, that goes from one horizontal edge of the L-shape to another horizontal edge. There are six different types of almost vertical units, illustrated in Figure 6.2.4.

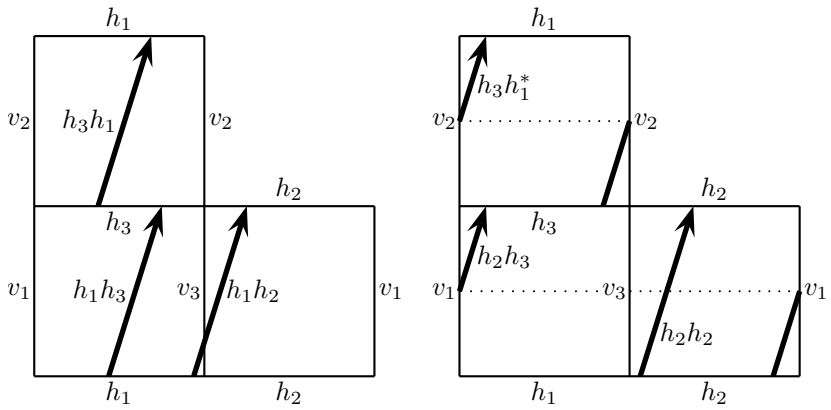

Figure 6.2.4: six types of almost vertical units

In Figure 6.2.4, the almost vertical unit h_1h_3 in the picture on the left starts from the edge h_1 and ends on the edge h_3, and is clearly of length $(1+\gamma^{-2})^{1/2}$ since its slope is γ. In the picture on the left, the almost vertical units h_1h_2 and h_3h_1 are also illustrated. Likewise, the almost vertical unit h_2h_2 is illustrated in the picture on the right. As shown in the picture on the right, the two almost vertical units h_2h_3 and $h_3h_1^*$ are each broken into two pieces. We can write $h_2h_3 = h_2v_1h_3$ to emphasize the fact that this almost vertical unit is broken at the edge v_1. Likewise, we can write $h_3h_1^* = h_3v_2h_1$ to emphasize the fact that this almost vertical unit is broken at the edge v_2. Note that h_3h_1 and $h_3h_1^*$ both start from the edge h_3 and end on the edge h_1. While the former is in one piece, the latter is broken at the edge v_2.

Suppose that H is an almost horizontal L-line of slope γ^{-1}, where $\gamma > 1$. An almost horizontal unit of this L-line is a finite segment of H, of length $(1+\gamma^{-2})^{1/2}$,

that goes from one vertical edge of the L-shape to another vertical edge. There are six different types of almost horizontal units, illustrated in Figure 6.2.5.

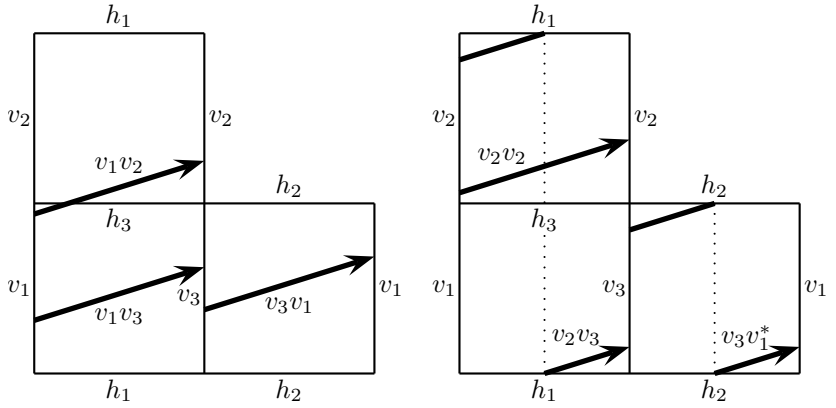

Figure 6.2.5: six types of almost horizontal units

Next we need to introduce the concept of *ancestor units*.

Consider first an almost horizontal L-line H_{2i+1}, with shortline V_{2i+2}. Then any almost vertical unit of V_{2i+2} is the shortcut of an almost horizontal detour crossing of a horizontal street, made up of some almost horizontal units of H_{2i+1}, together with some fractional units at the two ends. To illustrate this, the reader is referred to Figure 6.2.6.

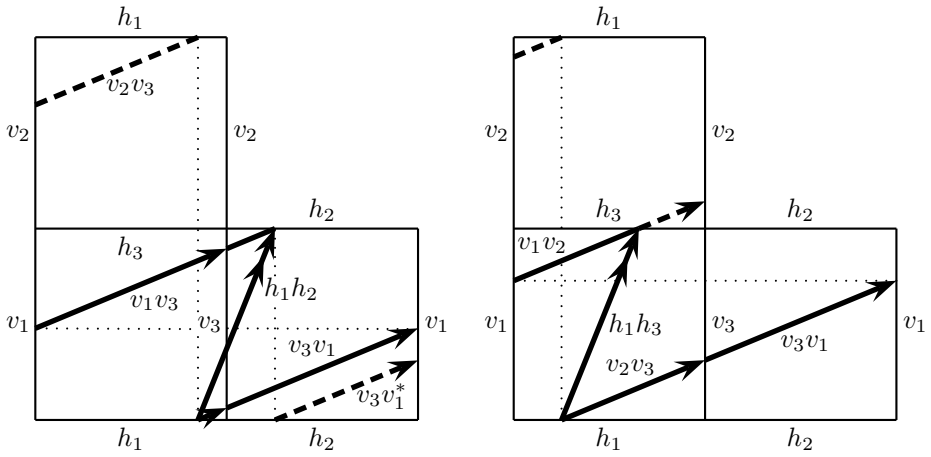

Figure 6.2.6: ancestor units of the almost vertical units h_1h_2 and h_1h_3

In the picture on the left, it is shown that the almost vertical unit h_1h_2 is the shortcut of an almost horizontal detour crossing of a horizontal street, made up of a fractional unit v_2v_3, followed by two complete units v_3v_1 and v_1v_3, and ending with a fractional unit $v_3v_1^*$.

In general, there may be extra copies of the whole units v_3v_1 and v_1v_3, if the slope of the almost horizontal detour crossing of the horizontal street is very small.

Extension Rule. Extend the fractional units at either end of the detour crossing to whole units.

Applying the Extension Rule, the ancestor units of h_1h_2 must contain types v_2v_3, v_3v_1, v_1v_3 and $v_3v_1^*$, and we denote this fact by writing

$$h_1h_2 \hookrightarrow v_2v_3, v_3v_1, v_1v_3, v_3v_1^*. \tag{6.2.15}$$

In the picture on the right, we start with the almost vertical unit h_1h_3. Using a similar analysis and applying the Extension Rule, the ancestor units of h_1h_3 must

contain types v_2v_3, v_3v_1 and v_1v_2, and we denote this fact by writing

$$h_1h_3 \hookrightarrow v_2v_3, v_3v_1, v_1v_2. \tag{6.2.16}$$

Analagous considerations give

$$h_2h_2 \hookrightarrow v_3v_1^*, v_1v_3, \tag{6.2.17}$$
$$h_2h_3 \hookrightarrow v_3v_1^*, v_1v_3, v_3v_1, v_1v_2, \tag{6.2.18}$$
$$h_3h_1 \hookrightarrow v_1v_2, v_2v_2, v_2v_3, \tag{6.2.19}$$
$$h_3h_1^* \hookrightarrow v_1v_2, v_2v_2, v_2v_3. \tag{6.2.20}$$

Consider next an almost vertical L-line V_{2i+2}, with shortline H_{2i+3}. Then any almost horizontal unit of H_{2i+3} is the shortcut of an almost vertical detour crossing of a vertical street, made up of some almost vertical units of V_{2i+2}, together with some fractional units at the two ends. Analogous to (6.2.15)–(6.2.20), we have

$$v_1v_2 \hookrightarrow h_2h_3, h_3h_1, h_1h_3, h_3h_1^*, \tag{6.2.21}$$
$$v_1v_3 \hookrightarrow h_2h_3, h_3h_1, h_1h_2, \tag{6.2.22}$$
$$v_2v_2 \hookrightarrow h_3h_1^*, h_1h_3, \tag{6.2.23}$$
$$v_2v_3 \hookrightarrow h_3h_1^*, h_1h_3, h_3h_1, h_1h_2, \tag{6.2.24}$$
$$v_3v_1 \hookrightarrow h_1h_2, h_2h_2, h_2h_3, \tag{6.2.25}$$
$$v_3v_1^* \hookrightarrow h_1h_2, h_2h_2, h_2h_3. \tag{6.2.26}$$

Consider now the chain

$$H_{2i+1} \to V_{2i+2} \to H_{2i+3} \to V_{2i+4}. \tag{6.2.27}$$

Starting with almost vertical units in V_{2i+4} and identifying their ancestors three times iteratively, using (6.2.15)–(6.2.26), we obtain

$$\begin{aligned} h_1h_2 &\hookrightarrow v_2v_3, v_3v_1, v_1v_3, v_3v_1^* \\ &\hookrightarrow h_3h_1^*, h_1h_3, h_3h_1, h_1h_2, h_2h_2, h_2h_3 \\ &\hookrightarrow v_1v_2, v_2v_2, v_2v_3, v_3v_1, v_1v_3, v_3v_1^*, \end{aligned} \tag{6.2.28}$$
$$\begin{aligned} h_1h_3 &\hookrightarrow v_2v_3, v_3v_1, v_1v_2 \\ &\hookrightarrow h_3h_1^*, h_1h_3, h_3h_1, h_1h_2, h_2h_2, h_2h_3 \\ &\hookrightarrow v_1v_2, v_2v_2, v_2v_3, v_3v_1, v_1v_3, v_3v_1^*, \end{aligned} \tag{6.2.29}$$
$$\begin{aligned} h_2h_2 &\hookrightarrow v_3v_1^*, v_1v_3 \\ &\hookrightarrow h_1h_2, h_2h_2, h_2h_3, h_3h_1 \\ &\hookrightarrow v_2v_3, v_3v_1, v_1v_3, v_3v_1^*, v_1v_2, v_2v_2, \end{aligned} \tag{6.2.30}$$
$$\begin{aligned} h_2h_3 &\hookrightarrow v_3v_1^*, v_1v_3, v_3v_1, v_1v_2 \\ &\hookrightarrow h_1h_2, h_2h_2, h_2h_3, h_3h_1, h_1h_3 \\ &\hookrightarrow v_2v_3, v_3v_1, v_1v_3, v_3v_1^*, v_1v_2, v_2v_2, \end{aligned} \tag{6.2.31}$$
$$\begin{aligned} h_3h_1 &\hookrightarrow v_1v_2, v_2v_2, v_2v_3 \\ &\hookrightarrow h_2h_3, h_3h_1, h_1h_3, h_3h_1^*, h_1h_2 \\ &\hookrightarrow v_3v_1^*, v_1v_3, v_3v_1, v_1v_2, v_2v_2, v_2v_3, \end{aligned} \tag{6.2.32}$$
$$\begin{aligned} h_3h_1^* &\hookrightarrow v_1v_2, v_2v_2, v_2v_3 \\ &\hookrightarrow h_2h_3, h_3h_1, h_1h_3, h_3h_1^*, h_1h_2 \\ &\hookrightarrow v_3v_1^*, v_1v_3, v_3v_1, v_1v_2, v_2v_2, v_2v_3. \end{aligned} \tag{6.2.33}$$

Proof of Lemma 6.2.1. Since V^* is long, we can clearly assume that $m_0 > 4U^5$. Let ℓ be the unique positive integer satisfying the inequalities

$$m_\ell \leqslant 4U^5 < m_{\ell-1}. \tag{6.2.34}$$

Then it follows from (6.2.11), (6.2.13) and (6.2.34) that

$$m_\ell \geqslant \frac{m_{\ell-1}}{U} \geqslant 4U^4 \geqslant 2U+1 \quad \text{and} \quad m_{\ell+3} \geqslant \frac{m_{\ell-1}}{U^4} \geqslant 4U. \tag{6.2.35}$$

Without loss of generality, suppose that ℓ is odd. To show that H_ℓ^* exhibits all six types of corner cuts illustrated in Figure 6.2.3, it suffices to show that it contains at least one copy of each of the three horizontal units v_1v_2, v_2v_3 and $v_3v_1^*$. We shall in fact show that H_ℓ^* contains at least one copy of each of the six types of horizontal units.

Note that it follows from the second set of inequalities in (6.2.35) that $m_{\ell+3} \geqslant 4$. This means that $V_{\ell+3}^*$ contains at least 3 whole almost vertical detour crossings of vertical streets. Take one such whole almost vertical detour crossing in the middle. This must contain one of the six almost vertical units. In finding its ancestors, the use of the Extension Rule is justified. The ancestors of this almost vertical unit contains various types of almost horizontal units, all of which must be in $H_{\ell+2}^*$. Their ancestors contain various types of almost vertical units, all of which must be in $V_{\ell+1}^*$. In turn, their ancestors contain various types of almost horizontal units, all of which must be in H_ℓ^*.

Taking the chain (6.2.27) to be the chain $H_\ell \to V_{\ell+1} \to H_{\ell+2} \to V_{\ell+3}$, and noting the ancestor relations (6.2.28)–(6.2.33), it is clear that H_ℓ^* contains at least one copy of each of the six types of horizontal units. This completes the proof of Lemma 6.2.1. □

Remark. Note that our proof of Lemma 6.2.1 here is a brute force exercise which does not give us any insight into what really is going on. Furthermore, this approach is only possible for the L-shape where we have very precise information on the almost horizontal and almost vertical units. If we consider surfaces other than this particular L-shape, the corresponding brute force exercise may well turn out to be an extremely umpleasant exercise. Indeed, in Section 6.4, we shall consider generalizations of the L-shape, leading to infinitely many analogs. Lemma 6.4.1 is the generalized version of Lemma 6.2.1, and we shall develop there a substantially simpler proof which also gives us more insight into the problem.

We next describe an iterative process for obtaining vertical and horizontal open intervals on the edges of the L-shape. The L-shape is the simplest interesting example of a polysquare. We adopt the following simple rule concerning where flow images in polysquares should lie.

Rule for Magnification in a Polysquare. Suppose, without loss of generality, that the edges of a polysquare $\mathcal{P}$ lie on lines of the form $x = x_0$ and $y = y_0$, where x_0 and y_0 are integers. Let I be an open interval lying entirely within an edge of $\mathcal{P}$, and let $\gamma > 1$.

(i) Suppose that I lies on a vertical edge of a square face of $\mathcal{P}$. Then there exist integers y_1 and y_2 satisfying $y_2 - y_1 = 1$ and such that the bottom edge of the square face lies on the line $y = y_1$ and the top edge of the square face lies on the line $y = y_2$. If we project I by the forward almost horizontal γ^{-1}-flow, then the image of I lies on edges of $\mathcal{P}$ that form part of the line $y = y_2$. If we project I by the reverse almost horizontal γ^{-1}-flow, then the image of I lies on edges of $\mathcal{P}$ that form part of the line $y = y_1$.

(ii) Suppose that I lies on a horizontal edge of a square face of $\mathcal{P}$. Then there exist integers x_1 and x_2 satisfying $x_2 - x_1 = 1$ and such that the left edge of the

square face lies on the line $x = x_1$ and the right edge of the square face lies on the line $x = x_2$. If we project I by the forward almost vertical γ-flow, then the image of I lies on edges of $\mathcal{P}$ that form part of the line $x = x_2$. If we project I by the reverse almost vertical γ-flow, then the image of I lies on edges of $\mathcal{P}$ that form part of the line $x = x_1$.

For the L-shape, the only possible choices for (x_1, x_2) and (y_1, y_2) are $(0, 1)$ and $(1, 2)$.

Suppose that I_0 is an open interval on a vertical edge of the L-shape. Figure 6.2.7 shows examples of this where I_0 lies on the vertical edge v_1 of the bottom left square face. This edge v_1 lies between the horizontal lines $y = 0$ and $y = 1$. We wish to project this interval to edges of the L-shape that lie on these two lines using the forward or reverse almost horizontal α_1^{-1}-flow.

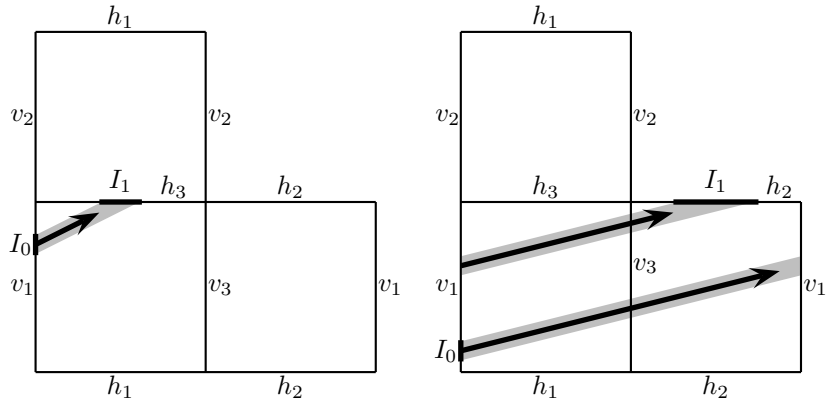

Figure 6.2.7: examples of good almost-horizontal flows for I_0

The forward almost horizontal α_1^{-1}-flow from left to right gives rise to an image of I_0 on horizontal edges that lie on the line $y = 1$. Clearly the image falls on either the edge h_3 of the bottom left square face or the top edge h_2 of the right square face, as shown in Figure 6.2.7, or it is split between these two edges.

Likewise, in view of the identification of the two vertical edges v_1 of the L-shape, the reverse almost horizontal α_1^{-1}-flow from right to left gives rise to an image of I_0 on horizontal edges that lie on the line $y = 0$. The image falls on either the bottom edge h_1 of the bottom left square face or the bottom edge h_2 of the right square face, or it is split between these two edges.

We say that this forward or reverse flow is *good* for the interval I_0 if the image does not hit a vertex of the L-shape and is an open interval on a single horizontal edge. The examples given in Figure 6.2.7 are good flows.

In this case, we define I_1 to be the corresponding open horizontal interval on the appropriate horizontal edge.

There are clearly instances when the forward almost horizontal α_1^{-1}-flow from left to right acting on an open vertical interval I_0 on some vertical edge of the L-shape fails to deliver an image that does not hit a vertex of the L-shape, resulting in one or more *splits*. This happens precisely when the flow encounters the top right vertex of one of the three constituent square faces of the L-shape, causing the flow to *split*. In this case, we say that this flow is *bad* for the interval I_0. The image I_1 will contain a split singularity and may be in multiple pieces. However, apart from these, its precise structure is not of any concern in our discussion. The more pertinent question is the effect of the split singularity. There are three separate cases.

Case 1. The flow hits the split singularity which is the top right vertex of the bottom left square face, as shown in the picture on the left in Figure 6.2.8.

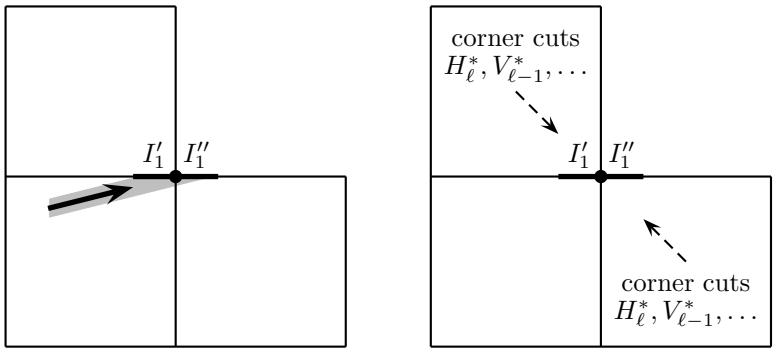

Figure 6.2.8: bad almost-horizontal α_1^{-1}-flow,
hitting the top right vertex of the bottom left square face

Case 2. The flow hits the split singularity which is the top right vertex of the top square face, as shown in the picture on the left in Figure 6.2.9, where we have placed the interval I_1' on the bottom edge, in view of edge identification.

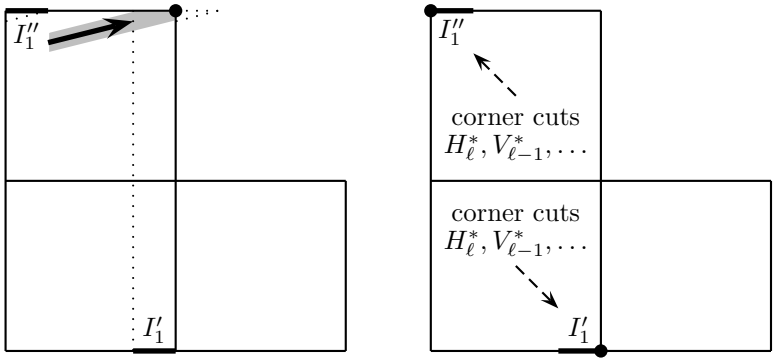

Figure 6.2.9: bad almost-horizontal α_1^{-1}-flow,
hitting the top right vertex of the top square face

Case 3. The flow hits the split singularity which is the top right vertex of the right square face, as shown in the picture on the left in Figure 6.2.10, where we have placed the interval I_1' on the bottom edge, in view of edge identification.

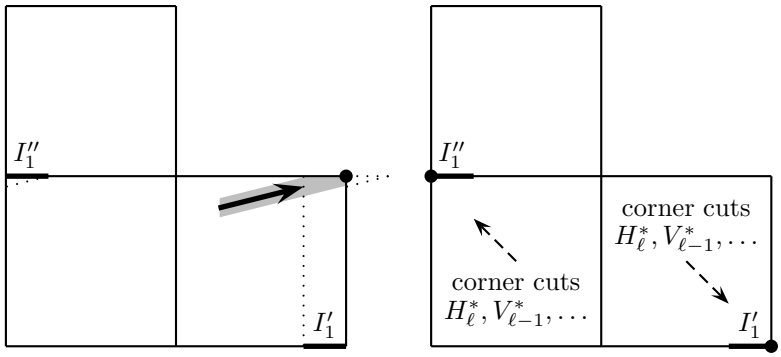

Figure 6.2.10: bad almost-horizontal α_1^{-1}-flow,
hitting the top right vertex of the right square face

We remark that in any of the three cases, the interval I_1'' can possibly take up a whole edge of the L-shape or even more.

There are also instances when the reverse almost horizontal α_1^{-1}-flow from right to left acting on an open vertical interval I_0 on some vertical edge of the L-shape fails to deliver an image that does not hit a vertex of the L-shape. This happens precisely when the flow encounters the bottom left vertex of one of the three constituent square faces of the L-shape, causing the flow to *split*.

Assume for the time being that the forward almost horizontal α_1^{-1}-flow from left to right or or the reverse almost horizontal α_1^{-1}-flow from right to left takes the open interval I_0 to a single open interval on an appropriate horizontal edge without capturing any vertex of the L-shape along the way, and that this leads to an open interval I_1, as shown in the picture on the left in Figure 6.2.11.

We may apply the forward almost vertical α_2-flow from left to right on the interval I_1. This may result in a single open interval I_2 on an appropriate vertical edge of the L-shape, as shown in the picture on the right in Figure 6.2.11, or the flow encounters the top right vertex of one of the three constituent square faces of the L-shape.

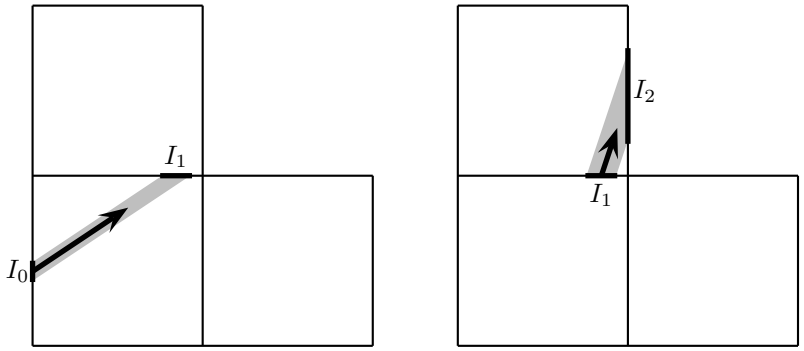

Figure 6.2.11: chain $I_0 \to I_1 \to I_2$ given by a good α_1^{-1} flow and a good α_2-flow

We may also apply the reverse almost vertical α_2-flow from right to left on the interval I_1. This may result in a single open interval I_2 on an appropriate vertical edge of the L-shape, or the flow encounters the bottom left vertex of one of the three constituent square faces of the L-shape.

And so on.

We thus have an iterative process, bearing in mind that the process may cease when a flow encounters a vertex of one of the three constituent square faces of the L-shape.

Suppose for the moment that we have some chain

$$I_0 \to I_1 \to I_2 \to I_3 \to I_4 \to \cdots \tag{6.2.36}$$

of alternate open vertical and horizontal intervals on appropriate edges of the L-shape. Owing to the slopes, these tilted projections magnify the intervals, as can clearly been seen in Figure 6.2.11. It is easy to give a quantitative description of the *magnification process* (6.2.36). It is clear from Figure 6.2.11 that

$$\frac{\text{length}(I_1)}{\text{length}(I_0)} = \alpha_1 \quad \text{and} \quad \frac{\text{length}(I_2)}{\text{length}(I_1)} = \alpha_2,$$

and so on.

Suppose that I_0 is a V^*-free open interval on some vertical edge of the L-shape, so that it does not contain any edge-cutting point of V^*. The forward or reverse almost horizontal α_1^{-1}-flow projects I_0 to an open interval I_1 on some appropriate horizontal edge of the L-shape. By the same edge cutting property, I_1 does not contain any edge-cutting points of H_1^*. The forward or reverse almost vertical α_2-flow projects I_1 to an open vertical interval I_2 on some appropriate vertical edge of the L-shape. By the same edge cutting property, I_2 does not contain any edge-cutting points of V_2^*. And so on.

Lemma 6.2.2. *Every V^*-free open interval I_0 on a vertical edge of the L-shape satisfies*

$$\text{length}(I_0) \leqslant \frac{2}{\alpha_1\alpha_2\alpha_3\cdots\alpha_{\ell-1}\alpha_\ell}, \tag{6.2.37}$$

where ℓ is the index of m_ℓ in Lemma 6.2.1. If there are several such indices, we choose the smallest one.

Proof. Suppose on the contrary that

$$\text{length}(I_0) > \frac{2}{\alpha_1\alpha_2\alpha_3\cdots\alpha_{\ell-1}\alpha_\ell}. \tag{6.2.38}$$

We shall prove that the forward or reverse α_1^{-1}-flow projects I_0 to an H_1^*-free interval I_1 on some horizontal edge of the L-shape, so that I_1 does not contain a split singularity.

Suppose on the contrary that this is not the case. For convenience, we assume that we are using the forward α_1^{-1}-flow, and the flow hits the top right vertex of the bottom left square face, as described in Case 1 earlier. The other two cases, as well as the case of reverse α_1^{-1}-flow, can be treated in almost the same way, with only very minor modifications. The similarities and differences of the three cases concerning the forward α_1^{-1}-flow are illustrated in Figures 6.2.8–6.2.10.

We define the *temporary* intervals I_1' and I_1'' as indicated in the picture on the left in Figure 6.2.8. Here the interval I_1'' cannot be the whole top edge of the right square face, for otherwise I_1'', and hence also I_1, would contain an edge-cutting point of H_1^*, a contradiction.

Without loss of generality, suppose that the index ℓ of m_ℓ in Lemma 6.2.1 is odd, so that the corresponding L-line segment is the almost horizontal H_ℓ^*. By Lemma 6.2.1, H_ℓ^* exhibits all six types of corner cuts. Figure 6.2.12 shows part of the top square face of the L-shape as well as a corner cut of H_ℓ^*.

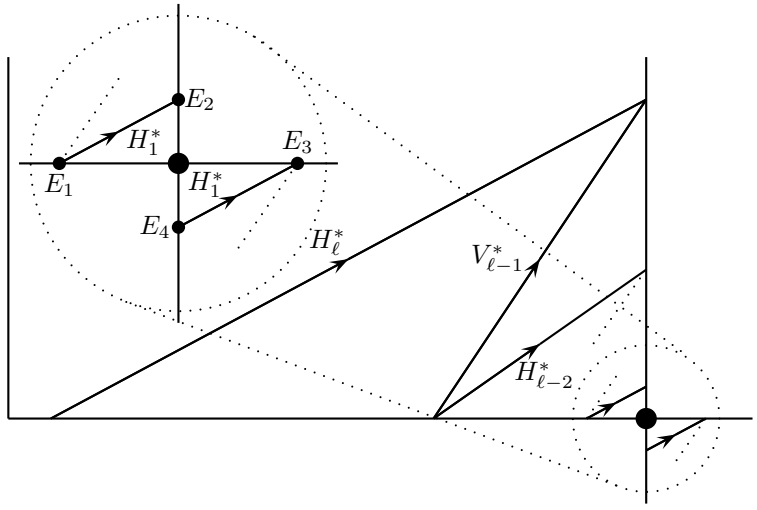

Figure 6.2.12: zigzagging towards the split singularity

By the same edge cutting property, each end of this corner cut of H_ℓ^* is the end of a corner cut of $V_{\ell-1}^*$, and as shown in Figure 6.2.12, we can pick one which is closer to the split singularity, indicated by the big dot. From the corner cut of $V_{\ell-1}^*$, we can find a corner cut of $H_{\ell-2}^*$ that is again closer to the split singularity, and so on. Eventually we arrive at a corner cut of H_1^*. This is very close to the split singularity; in Figure 6.2.12, the parts within the dotted circles are magnified. We denote by E_1 and E_2 the endpoints of the corner cut of H_1^* in the top square face.

An analogous argument can be carried out in the right square face, with corner cuts getting closer to the same split singularity. We denote by E_3 and E_4 the endpoints of a corresponding corner cut of H_1^* in this square face.

Our next step is to estimate the distances of these endpoints from the split singularity. We shall show that they are "exponentially close" to the split singularity.

It is clear from Figure 6.2.12 that the distance of the furthest point on the corner cut of H_ℓ^* from the split singularity is less than 1. Since H_ℓ^* has slope α_ℓ^{-1}, it follows that the distance of the furthest point on the corner cut of $V_{\ell-1}^*$ from the split singularity is less than α_ℓ^{-1}. Since $V_{\ell-1}^*$ has slope $\alpha_{\ell-1}$, it follows that the distance of the furthest point on the corner cut of $H_{\ell-2}^*$ from the split singularity is less than $\alpha_\ell^{-1}\alpha_{\ell-1}^{-1}$. Clearly E_1 is the point on the corner cut of H_1^* which is furthest from the split singularity. Iterating, we conclude that the distance of E_1 from the split singularity is less than

$$\frac{1}{\alpha_\ell\alpha_{\ell 1}\alpha_{\ell-2}\cdots\alpha_3\alpha_2}.$$

Similarly, the distance of E_3 from the split singularity is less than this same quantity. Hence the distance distance(E_1, E_3) between E_1 and E_3 satisfies the inequality

$$\text{distance}(E_1, E_3) < \frac{2}{\alpha_\ell\alpha_{\ell 1}\alpha_{\ell-2}\cdots\alpha_3\alpha_2}. \tag{6.2.39}$$

The forward α_1^{-1}-flow projects the V^*-free interval I_0 to an interval I_1 on some horizontal edges of the L-shape, temporarily represented by I_1' and I_1'' as shown in Figure 6.2.8, and containing the split singularity.

Under the assumption (6.2.38), it follows that

$$\text{length}(I_1') + \text{length}(I_1'') = \alpha_1\,\text{length}(I_0) > \frac{2}{\alpha_2\alpha_3\alpha_4\cdots\alpha_{\ell-1}\alpha_\ell}. \tag{6.2.40}$$

Combining (6.2.39) and (6.2.40), we conclude that

$$\text{distance}(E_1, E_3) < \text{length}(I_1') + \text{length}(I_1''). \tag{6.2.41}$$

Since the points E_1 and E_3 fall on different sides of the split singularity, the inequality (6.2.41) implies that $I_1' \cup I_1''$ must contain at least one of these two points, and so an edge-cutting point of H_1^*, clearly contradicting that I_1 is H_1^*-free. Thus I_1 does not contain a split singularity, so does not split and therefore is a single interval, with

$$\text{length}(I_1) = \alpha_1\,\text{length}(I_0) > \frac{2}{\alpha_2\alpha_3\alpha_4\cdots\alpha_{\ell-1}\alpha_\ell}.$$

The forward or reverse α_2-flow projects I_1 to I_2, which is a V_2^*-free interval on some vertical edge of the L-shape. With the roles of (6.2.38), I_0 and I_1 replaced respectively by (6.2.40), I_1 and I_2, an analogous argument shows that I_2 does not contain a split singularity, so does not split and is therefore a single interval, and

$$\text{length}(I_2) = \alpha_2\,\text{length}(I_1) > \frac{2}{\alpha_3\alpha_4\alpha_5\cdots\alpha_{\ell-1}\alpha_\ell}. \tag{6.2.42}$$

We now keep repeating this argument.

At the end we obtain an analog of (6.2.40) and (6.2.42), that $I_{\ell-1}$ is a $V_{\ell-1}^*$-free interval on some vertical edge of the L-shape, and

$$\text{length}(I_{\ell-1}) = \alpha_{\ell-1}\cdots\alpha_1\,\text{length}(I_0) > \frac{2}{\alpha_\ell}.$$

We now consider the effect of the forward or reverse α_ℓ^{-1}-flow on $I_{\ell-1}$.

Figure 6.2.13 illustrates the interval $I_{\ell-1}$ and its projection by the forward α_ℓ^{-1}-flow. Consider the horizontal line that contains the top edge of a square face of the L-shape that contains $I_{\ell-1}$ as part of its left edge. Suppose that a line of slope

α_ℓ^{-1} that passes through the top end point of $I_{\ell-1}$ intersects this horizontal line at a point A. Then a line of the same slope α_ℓ^{-1} that passes through the bottom end point of $I_{\ell-1}$ intersects the same horizontal line at a point B which is a distance of precisely $\alpha_\ell \,\mathrm{length}(I_{\ell-1}) > 2$ to the right of A. The interval AB must therefore contain a subinterval J of length 1 that can be identified with a horizontal edge of the L-shape. This means that I_ℓ must contain a whole edge of the L-shape, and therefore cannot be H_ℓ^*-free.

A similar conclusion can be drawn if we use the reverse α_ℓ^{-1}-flow on $I_{\ell-1}$.

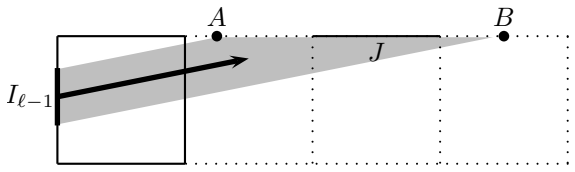

Figure 6.2.13: $I_{\ell-1}$ and its projection by the α_ℓ^{-1}-flow

We therefore arrive at a contradiction. This contradiction proves that (6.2.38) is false, and completes the proof of Lemma 6.2.2. □

We recall (6.2.9), that

$$\mathrm{length}(V^*) = m_0(1+\alpha^2)^{1/2},$$

as well as (6.2.14) with $k = \ell$, that

$$m_\ell = m_0 \prod_{j=1}^{\ell} \frac{1}{\alpha_j}.$$

It follows that

$$\mathrm{length}(V^*) = (1+\alpha^2)^{1/2} m_\ell \alpha_1\alpha_2\alpha_3\cdots\alpha_{\ell-1}\alpha_\ell,$$

which can be rewritten in the form

$$\frac{2}{\alpha_1\alpha_2\alpha_3\cdots\alpha_{\ell-1}\alpha_\ell} = \frac{2(1+\alpha^2)^{1/2} m_\ell}{\mathrm{length}(V^*)}. \tag{6.2.43}$$

Recall that the integer U, given by (6.2.11), is an upper bound of the continued fraction digits of the badly approximable number α. It then follows from (6.2.37), (6.2.43) and Lemma 6.2.1 that every V^*-free vertical interval I_0 on the boundary of the L-shape satisfies

$$\mathrm{length}(I_0) \leqslant \frac{12U^5}{\mathrm{length}(V^*)}. \tag{6.2.44}$$

In general, V^* can be taken to be an arbitrary segment of the L-line V, so the inequality (6.2.44) proves superdensity under the condition that V has a slope α which is a badly approximable number with even continued fraction digits. This completes the proof of Theorem 6.1.1. □

6.3. **Adapting the method of size-magnification for the L-solid.**

Proof of Theorem 6.1.2. First we introduce a convenient labelling for the faces of the L-solid; see Figure 6.1.4 and Figures 6.3.1–6.3.2 below.

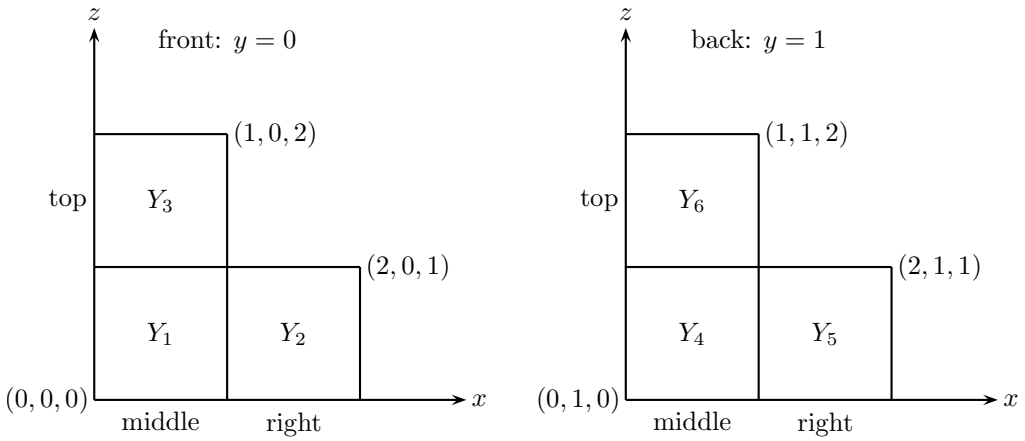

Figure 6.3.1: labelling the front and back faces of the L-solid

The picture on the left in Figure 6.3.1 shows the 3 front faces of the L-solid, with $y = 0$. The front top square face Y_3 has vertices $(0, 0, 1), (1, 0, 1), (0, 0, 2), (1, 0, 2)$. We denote this fact by

$$Y_3 = \mathrm{SQ}\{(0, 0, 1), (1, 0, 1), (0, 0, 2), (1, 0, 2)\}.$$

The front middle and front right square faces are denoted respectively by

$$Y_1 = \mathrm{SQ}\{(0, 0, 0), (1, 0, 0), (0, 0, 1), (1, 0, 1)\},$$
$$Y_2 = \mathrm{SQ}\{(1, 0, 0), (2, 0, 0), (1, 0, 1), (2, 0, 1)\}.$$

The picture on the right in Figure 6.3.1 shows the 3 back faces of the L-solid, with $y = 1$. The back top, back middle and back right square faces are denoted respectively by

$$Y_6 = \mathrm{SQ}\{(0, 1, 1), (1, 1, 1), (0, 1, 2), (1, 1, 2)\},$$
$$Y_4 = \mathrm{SQ}\{(0, 1, 0), (1, 1, 0), (0, 1, 1), (1, 1, 1)\},$$
$$Y_5 = \mathrm{SQ}\{(1, 1, 0), (2, 1, 0), (1, 1, 1), (2, 1, 1)\}.$$

These 6 square faces are all perpendicular to the y-axis, which explains the use of letter Y.

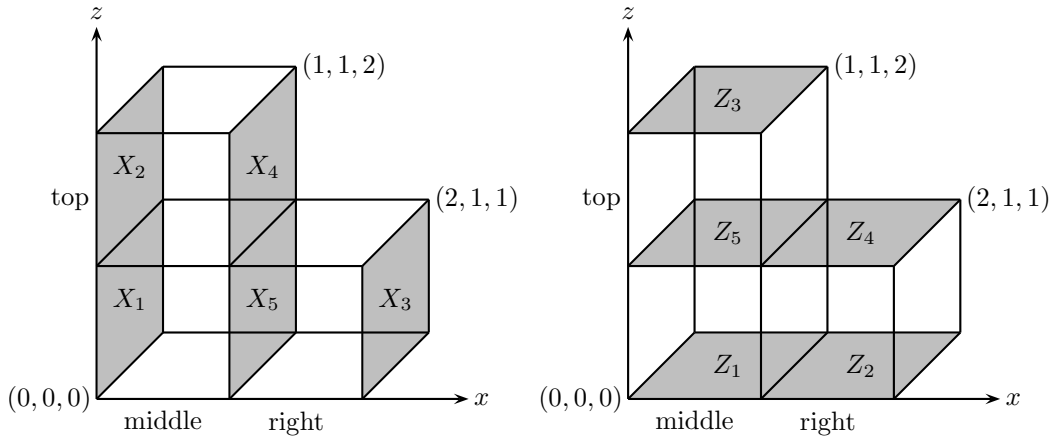

Figure 6.3.2: labelling the rest of the faces of the L-solid

Next, we see from Figure 6.3.2 that between the front and back faces, there are 4 faces on the boundary of the L-solid that are perpendicular to the x-axis, denoted

by

$$X_1 = \mathrm{SQ}\{(0,0,0),(0,1,0),(0,0,1),(0,1,1)\},$$
$$X_2 = \mathrm{SQ}\{(0,0,1),(0,1,1),(0,0,2),(0,1,2)\},$$
$$X_3 = \mathrm{SQ}\{(2,0,0),(2,1,0),(2,0,1),(2,1,1)\},$$
$$X_4 = \mathrm{SQ}\{(1,0,1),(1,1,1),(1,0,2),(1,1,2)\},$$

another 4 faces on the boundary of the L-solid that are perpendicular to the z-axis, denoted by

$$Z_1 = \mathrm{SQ}\{(0,0,0),(1,0,0),(0,1,0),(1,1,0)\},$$
$$Z_2 = \mathrm{SQ}\{(1,0,0),(2,0,0),(1,1,0),(2,1,0)\},$$
$$Z_3 = \mathrm{SQ}\{(0,0,2),(1,0,2),(0,1,2),(1,1,2)\},$$
$$Z_4 = \mathrm{SQ}\{(1,0,1),(2,0,1),(1,1,1),(2,1,1)\},$$

as well as two inside faces

$$X_5 = \mathrm{SQ}\{(1,0,0),(1,1,0),(1,0,1),(1,1,1)\},$$
$$Z_5 = \mathrm{SQ}\{(0,0,1),(1,0,1),(0,1,1),(1,1,1)\}.$$

Let $k \geqslant 1$ be an arbitrary but fixed integer. Assume that an s-L-line $\mathcal{L}_k$ starts from the origin $\mathbf{0} = (0,0,0)$ and ends at a point $C = (1,x,y)$ on the inside square face X_5, and in between hits the square face Z_3 on k separate occasions; see Figure 6.3.3, which shows the special case $k = 1$.

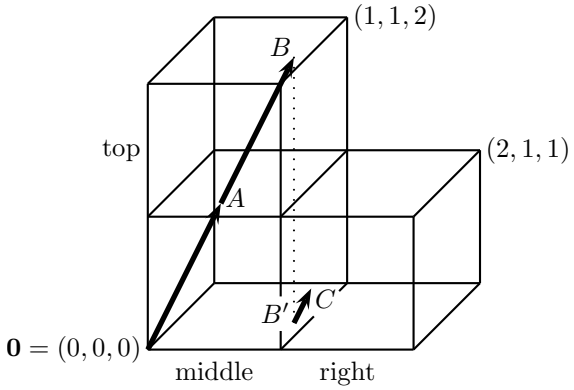

Figure 6.3.3: first detour crossing in the L-solid: the case $k = 1$

Let B denote the point on the square face Z_3 that $\mathcal{L}_k$ hits on the last occasion before it bounces down to the point B' and continues towards the point C.

Let A denote the point on the inside square face Z_5 that $\mathcal{L}_k$ hits on the first occasion, and assume that $A = (x,y,1)$, so that its coordinates form a permutation of the coordinates of $C = (1,x,y)$ with the same quantities x and y. Then $B = (2kx, 2ky, 2)$ and $B' = (2kx, 2ky, 0)$. The geometric fact that the two vectors $\mathbf{0}A$ and $B'C$ are parallel gives rise to the equations

$$\frac{1-2kx}{x} = \frac{x-2ky}{y} = \frac{y-0}{1}.$$

The first equality reduces to $y = x^2$. Substituting this into the right hand side and then equating with the left hand side, we conclude that

$$y = x^2 \quad \text{and} \quad x^3 + 2kx - 1 = 0.$$

Note that the cubic polynomial $x^3 + 2kx - 1$ is strictly increasing and has precisely one root α_k satisfying

$$\frac{1}{2k+1} < \alpha_k < \frac{1}{2k}. \tag{6.3.1}$$

We now take $x = \alpha_k$ and $y = \alpha_k^2$, and consider the particular segment of the s-L-line $\mathcal{L}_k$ with direction vector $\mathbf{v}_0 = (\alpha_k, \alpha_k^2, 1)$ illustrated in Figure 6.3.3. Starting from the origin $\mathbf{0} = (0, 0, 0)$, this s-L-line segment exhibits an up-and-down zigzagging, and finally ends its journey at the point $C = (1, \alpha_k, \alpha_k^2)$ on the middle square face X_5. It represents a *left to right detour crossing* inside a tower-like 3-dimensional "street", where the latter is the union of the middle cube and the top cube. Observe that with $0 < \alpha_k < 1$, the s-L-line $\mathcal{L}_k$ goes to the right faster than it goes to the back, and so crosses from one X-face to another faster than crossing from one Y-face to another.

The straight line segment joining the two endpoints $\mathbf{0}$ and $C = (1, \alpha_k, \alpha_k^2)$ of this detour crossing is called the *shortcut* of this detour crossing. This is an analog of the shortline concept in Section 6.2 for the L-shape.

The first extension of this particular zigzagging segment of the s-L-line $\mathcal{L}_k$ with direction vector $\mathbf{v}_0 = (\alpha_k, \alpha_k^2, 1)$ starts from the point $C = (1, \alpha_k, \alpha_k^2)$ on the square face X_5 and goes to the point $D = (2, 2\alpha_k, 2\alpha_k^2)$ on the right face X_3; see Figure 6.3.4. This zigzagging extension hits the square face Z_4 on $2k$ separate occasions, at the points $(1 + i\alpha_k - \alpha_k^3, \alpha_k + i\alpha_k^2 - \alpha_k^4, 1)$, $1 \leqslant i \leqslant 2k$, before ending at the point D on the square face X_3.

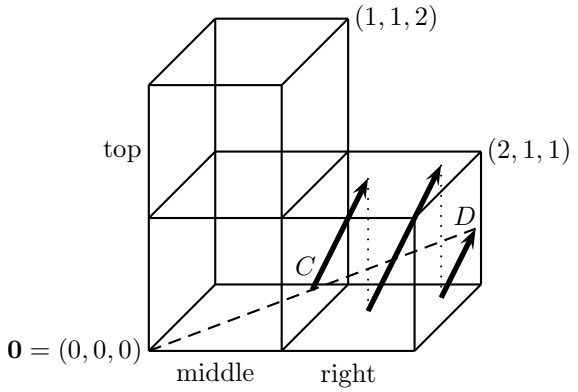

Figure 6.3.4: second detour crossing in the L-solid: the case $k = 1$

This zigzagging second segment of the s-L-line $\mathcal{L}_k$ from C to D with direction vector $\mathbf{v}_0$ represents a *left to right detour crossing* inside a 3-dimensional "street", which is simply the right cube. Again the straight line segment joining the two endpoints C and D of this detour crossing is called the *shortcut* of this detour crossing.

These two shortcuts, *i.e.*, the two straight line segments $\mathbf{0}C$ and CD, with endpoints $\mathbf{0} = (0, 0, 0)$, $C = (1, \alpha_k, \alpha_k^2)$ and $D = (2, 2\alpha_k, 2\alpha_k^2)$, are clearly collinear. In fact, C is the midpoint of the line segment $\mathbf{0}D$.

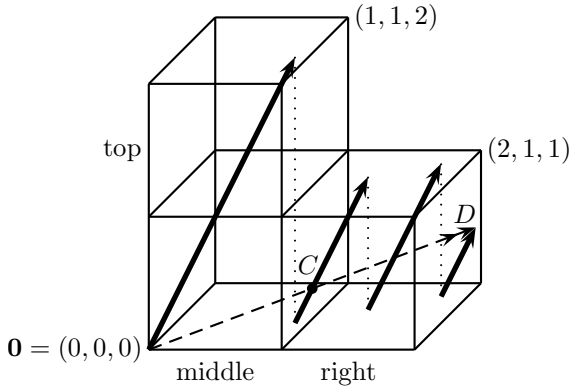

Figure 6.3.5: detour crossing and its shortline in the L-solid: the case $k = 1$

It is easy to see that this "collinearity" of the shortcuts is preserved as we continue and take the third, fourth and subsequent segments of the s-L-line $\mathcal{L}_k$ starting from the origin with direction vector $\mathbf{v}_0 = (\alpha_k, \alpha_k^2, 1)$. This collinearity means precisely that these consecutive shortcuts together form another s-L-line $\mathcal{L}_k^*$ starting from the origin, but it has a new direction vector $\mathbf{v}_1 = (1, \alpha_k, \alpha_k^2)$ obtained by a permutation of the coordinates of $\mathbf{v}_0$. We refer to this new s-L-line $\mathcal{L}_k^*$ as the *shortline* of the original s-L-line $\mathcal{L}_k$. Formally

$$\mathbf{S}(\mathcal{L}_k) = \mathcal{L}_k^*,$$

where $\mathbf{S}$ denotes the *shortline operation*. In the special case $k = 1$, Figure 6.3.5 is basically Figures 6.3.3–6.3.4 put together. It shows the two parts of the zigzagging $\mathcal{L}_k$ from $\mathbf{0}$ to D, with the point C separating the two parts. It also shows the corresponding shortline segment of $\mathcal{L}_k^*$, indicated by the dashed arrow, from $\mathbf{0}$ to D.

The crucial fact is that the s-L-line $\mathcal{L}_k$ and its shortline $\mathcal{L}_k^*$ hit every square face X_i, $1 \leqslant i \leqslant 5$, at precisely the same points, like C and D in Figures 6.3.4–6.3.5. We refer to this observation as the *X-face hitting property* of the infinite s-L-line $\mathcal{L}_k$ and its shortline $\mathcal{L}_k^*$.

The direction vector $\mathbf{v}_1 = (1, \alpha_k, \alpha_k^2)$ is clearly obtained from the direction vector $\mathbf{v}_0 = (\alpha_k, \alpha_k^2, 1)$ by a left shift in the cyclic permutation of the coordinates

$$1 \to \alpha_k \to \alpha_k^2 \to 1.$$

Applying a second left shift in this cyclic permutation, we obtain in turn a new direction vector $\mathbf{v}_2 = (\alpha_k^2, 1, \alpha_k)$. It is easy to see that the analogous shortline of the s-L-line $\mathcal{L}_k^*$ is a new s-L-line $\mathcal{L}_k^{**}$ that starts at the origin and has direction vector $\mathbf{v}_2$. Formally,

$$\mathbf{S}(\mathcal{L}_k^*) = \mathcal{L}_k^{**}.$$

Note that $\mathcal{L}_k^*$ consists of *front to back detour crossings*, and $\mathcal{L}_k^{**}$ is the union of the corresponding shortcuts. Observe that with $0 < \alpha_k < 1$, the s-L-line $\mathcal{L}_k^*$ goes to the back faster than it goes up, and so crosses from one Y-face to another faster than crossing from one Z-face to another.

Again the crucial fact is that the s-L-line $\mathcal{L}_k^*$ and its shortline $\mathcal{L}_k^{**}$ hit every square face Y_i, $1 \leqslant i \leqslant 6$, at precisely the same points. We refer to this observation as the *Y-face hitting property* of the infinite s-L-line $\mathcal{L}_k^*$ and its shortline $\mathcal{L}_k^{**}$.

Applying a third left shift in the cyclic permutation, we return to the original direction vector $\mathbf{v}_0 = (\alpha_k, \alpha_k^2, 1)$. It is easy to see that the analogous shortline of the s-L-line $\mathcal{L}_k^{**}$ is the original s-L-line $\mathcal{L}_k$ that starts at the origin and has direction vector $\mathbf{v}_0$. Formally,

$$\mathbf{S}(\mathcal{L}_k^{**}) = \mathcal{L}_k.$$

Note that $\mathcal{L}_k^{**}$ consists of *bottom to top detour crossings*, and $\mathcal{L}_k$ is the union of the corresponding shortcuts. Observe that with $0 < \alpha_k < 1$, the s-L-line $\mathcal{L}_k^{**}$ goes up faster than it goes to the right, and so crosses from one Z-face to another faster than crossing from one X-face to another.

Again the crucial fact is that the s-L-line $\mathcal{L}_k^{**}$ and its shortline $\mathcal{L}_k$ hit every square face Z_i, $1 \leqslant i \leqslant 5$, at precisely the same points. We refer to this observation as the *Z-face hitting property* of the infinite s-L-line $\mathcal{L}_k^{**}$ and its shortline $\mathcal{L}_k$.

The basic idea of the proof of Theorem 6.1.2 is the same as that of Theorem 6.1.1, namely, iterated magnification of empty sets, *i.e.*, sets that do not intersect the geodesic. In the case of Theorem 6.1.1 these empty sets are intervals with no edge-cutting points. Here these empty sets are convex sets on faces with no face-hitting points.

The L-solid is the simplest interesting example of a polycube. By a *cube atom*, we mean one of the unit cubes that make up the polycube. We adopt the following simple rule concerning where flow images in polycubes should lie.

Rule for Magnification in a Polycube. Suppose, without loss of generality, that the faces of a polycube $\mathcal{P}$ lie on planes of the form $x = x_0$, $y = y_0$ and $z = z_0$, where x_0, y_0 and z_0 are integers. Let S be a convex set lying entirely within a square face of $\mathcal{P}$, and let $\mathbf{v}$ be a 3-dimensional vector with positive coordinates.

(i) Suppose that S lies on an X-face of a cube atom of $\mathcal{P}$. Then there exist integers y_1 and y_2 satisfying $y_2 - y_1 = 1$ and such that the front Y-face of the cube atom lies on the plane $y = y_1$ and the back Y-face of the cube atom lies on the plane $y = y_2$. If we project S by the forward $\mathbf{v}$-flow, then the image of S lies on square faces of $\mathcal{P}$ that form part of the plane $y = y_2$. If we project S by the reverse $\mathbf{v}$-flow, then the image of S lies on square faces of $\mathcal{P}$ that form part of the plane $y = y_1$.

(ii) Suppose that S lies on a Y-face of a cube atom of $\mathcal{P}$. Then there exist integers z_1 and z_2 satisfying $z_2 - z_1 = 1$ and such that the bottom Z-face of the cube atom lies on the plane $z = z_1$ and the top Z-face of the cube atom lies on the plane $z = z_2$. If we project S by the forward $\mathbf{v}$-flow, then the image of S lies on square faces of $\mathcal{P}$ that form part of the plane $z = z_2$. If we project S by the reverse $\mathbf{v}$-flow, then the image of S lies on square faces of $\mathcal{P}$ that form part of the plane $z = z_1$.

(iii) Suppose that S lies on a Z-face of a cube atom of $\mathcal{P}$. Then there exist integers x_1 and x_2 satisfying $x_2 - x_1 = 1$ and such that the left X-face of the cube atom lies on the plane $x = x_1$ and the right X-face of the cube atom lies on the plane $x = x_2$. If we project S by the forward $\mathbf{v}$-flow, then the image of S lies on square faces of $\mathcal{P}$ that form part of the plane $x = x_2$. If we project S by the reverse $\mathbf{v}$-flow, then the image of S lies on square faces of $\mathcal{P}$ that form part of the plane $x = x_1$.

For the L-solid, the only possible choices for (x_1, x_2) and (z_1, z_2) are $(0, 1)$ and $(1, 2)$, and the only possible choice for (y_1, y_2) is $(0, 1)$.

We consider *iterated area magnification* of convex sets on faces by using the three X-Y-Z-face hitting properties and the 3-periodicity of the shortline process. We elaborate on this.

Figure 6.3.6 illustrates area magnification via tilted parallel projection. In order to visualize the parallel projection a little better, we have included an extra copy of three unit square faces, indicated by the dashed line squares, on the plane $y = 1$ in cartesian 3-space that can be identified with the square faces Y_4, Y_5, Y_6 of the L-solid. We start with a parallelogram $ABCD$ on the square face X_3. Using the $\mathbf{v}_1$-flow indicated by the short thick arrow, where $\mathbf{v}_1 = (1, \alpha_k, \alpha_k^2)$ is the direction vector of the shortline $\mathcal{L}_k^*$ of the s-L-line $\mathcal{L}_k$, we project the parallelogram on to the plane $y = 1$.

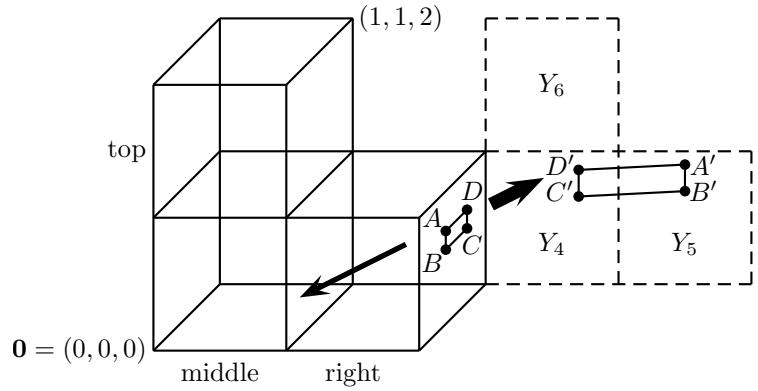

Figure 6.3.6: magnifying the area via tilted parallel projection

For simplicity, suppose that it is projected on to unit squares identified with $Y_4 \cup Y_5$, as shown. This tilted parallel projection maps the parallelogram $ABCD$ to a new parallelogram $A'B'C'D'$, and the area of $A'B'C'D'$ is $1/\alpha_k$ times the area of $ABCD$.

Indeed, let $(2, a+y, b+z)$ be an arbitrary point of the parallelogram $ABCD$. Keeping a and b as fixed constants and running the variables y and z in short intervals centered at zero, we obtain an "area element". Assume that the $\mathbf{v}_1$-flow maps the point $(2, a, b)$ in the parallelogram $ABCD$ to a point $(c, 1, d)$ in the new parallelogram $A'B'C'D'$ on the plane $y = 1$ in cartesian 3-space. Then the $\mathbf{v}_1$-flow also maps

$$(2, a+y, b+z) \quad \text{to} \quad \left(c - \frac{y}{\alpha_k}, 1, d + z - y\alpha_k\right)$$

in $A'B'C'D'$. The relevant undelying linear transformation in variables y and z is the 2-dimensional map

$$(y, z) \longrightarrow \left(-\frac{y}{\alpha_k}, z - y\alpha_k\right),$$

represented in matrix form by

$$\begin{pmatrix} -1/\alpha_k & 0 \\ -\alpha_k & 1 \end{pmatrix} \begin{pmatrix} y \\ z \end{pmatrix} = \begin{pmatrix} -y/\alpha_k \\ z - y\alpha_k \end{pmatrix}.$$

The area magnification factor, which is the absolute value of the determinant of the transition matrix, is therefore $1/\alpha_k$.

Next we explain how this area magnification can be used to study density. Let $L_k(0)$ be a "long" initial segment of the s-L-line $\mathcal{L}_k$, and let $S_0 = ABCD$ be an $L_k(0)$-free square on an X-face, *i.e.*, the square $S_0 = ABCD$ is "empty" in the sense that it does not contain any point of $L_k(0)$. Note that $L_k(0)$ consists of a number of *whole* left to right detour crossings, starting initially at the origin, and a *fractional* left to right detour crossing at the end. These detour crossings have the same length, and this common length is easily computed using Pythagoras's theorem to be

$$\text{length(detour crossing)} = \frac{1}{\alpha_k}(1 + \alpha_k^2 + \alpha_k^4)^{1/2}, \tag{6.3.2}$$

so there exists a positive real number m_0 such that

$$\text{length}(L_k(0)) = \frac{m_0}{\alpha_k}(1 + \alpha_k^2 + \alpha_k^4)^{1/2}. \tag{6.3.3}$$

Each whole detour crossing in $L_k(0)$ has a shortcut. The last fractional detour crossing in $L_k(0)$, if extended to a full detour crossing, also has a shortcut. For this last fractional detour crossing, we shorten its shortcut by the same fraction and at the appropriate end to obtain a fractional shortcut. We then take the union of these shortcuts and this fractional shortcut. This union is an initial segment of the s-L-line $\mathcal{L}_k^*$, the shortline of the s-L-line $\mathcal{L}_k$, that we denote by $L_k(1)$. Then $L_k(1)$ consists of a number of *whole* front to back detour crossings, starting initially at the origin, and a *fractional* front to back detour crossing at the end. These detour crossings have the same length, and this common length is also given by (6.3.2), so there exists a positive real number m_1 such that

$$\text{length}(L_k(1)) = \frac{m_1}{\alpha_k}(1 + \alpha_k^2 + \alpha_k^4)^{1/2}. \tag{6.3.4}$$

The shortline relation then implies the relation

$$m_1 = \alpha_k m_0, \tag{6.3.5}$$

the analog of (6.2.12).

Using the X-face hitting property, we deduce that the $\mathbf{v}_1$-flow maps the $L_k(0)$-free square $S_0 = ABCD$ on an X-face to an $L_k(1)$-free parallelogram $S_0' = A'B'C'D'$ on some Y-face(s). This $L_k(1)$-free set S_0' is not necessarily contained in a single Y-face. For example, in Figure 6.3.6, the short thick arrow pointing up indicates the $\mathbf{v}_1$-flow that maps S_0 to S_0', and S_0' intersects two Y-faces, namely Y_4 and Y_5. It is easy to see that if $S_0 = ABCD$ has diameter less than α_k^2, then the $\mathbf{v}_1$-flow image $S_0' = A'B'C'D'$ has at most 4 convex parts, where each one is located on some Y-face. Let S_1 denote the part having the largest area. Then the area of S_1 is at least $(4\alpha_k)^{-1}$ times the area of S_0.

It is easy to work with convex sets. They have the convenient properties that the intersection of convex sets is convex, and the parallel projection of a convex set is convex.

The possible loss of a factor 4 is a novel feature of this section. We do not have a similar loss in the proof of Theorem 6.1.1, since the trick of "exponentially fast zigzagging to a street corner" prevents such loss in Section 6.2; see Figure 6.2.2. Unfortunately we do not know how we can adapt this trick to higher dimensions. This loss explains why we cannot prove superdensity.

Remark. We do have some partial compensation here, as we can enhance the argument by replacing the threshold "diameter less than α_k^2" by the more generous threshold "diameter less than α_k", and replacing the restriction "at most 4 convex parts" by the stronger restriction "at most 2 convex parts". This is not a crucial part of our technique, but nevertheless gives a good insight into the geometrical complexity that we have to deal with. The new idea is to involve the *reverse flow*, which gives us *two options* to choose from. To explain this, we return to Figure 6.3.6, where we have used the $\mathbf{v}_1$-flow. Note that we can also use the reverse flow, *i.e.*, the $(-\mathbf{v}_1)$-flow indicated by the longer arrow pointing to the left. Using the X-face hitting property, we deduce that this $(-\mathbf{v}_1)$-flow maps the $L_k(0)$-free square S_0 to an $L_k(1)$-free parallelogram S_0'' on some Y-face(s), where S_0'' is different from S_0'.

It is very revealing to have these two options, namely to choose between the $\mathbf{v}_1$-flow and the *reverse* $(-\mathbf{v}_1)$-flow. For instance, consider the convex parts of S_0'' on (possibly) different Y-faces. Then the convex part having the largest area on some Y-face can be a better choice for S_1 than the analogous subset S_1 of S_0' obtained earlier using the forward flow. In other words, we now have the two options $S_1(S_0')$ and $S_1(S_0'')$, and can, if we wish, choose the one with the larger area located on some Y-face and call it S_1.

For illustration, let S_0 be the square with vertices

$$(0, \tfrac{1}{3}, 1), \quad (0, \tfrac{1}{3}, 1-\alpha_k), \quad (0, \tfrac{1}{3}+\alpha_k, 1-\alpha_k), \quad (0, \tfrac{1}{3}+\alpha_k, 1)$$

on the left most X-face X_1, and we use the $\mathbf{v}_1$-flow to project S_0 to some Y-face(s). The horizontal line segment with endpoints

$$(0, \tfrac{1}{3}, 1-\alpha_k^2) \quad \text{and} \quad (0, \tfrac{1}{3}+\alpha_k, 1-\alpha_k^2)$$

lies in S_0. The vector $\mathbf{v}_1 = (1, \alpha_k, \alpha_k^2)$ sends this line segment to a line segment with endpoints

$$(1, \tfrac{1}{3}+\alpha_k, 1) \quad \text{and} \quad (1, \tfrac{1}{3}+2\alpha_k, 1)$$

on the "dangerous" splitting edge $(1, y, 1)$, $0 \leqslant y \leqslant 1$, the common edge of the top and right cubes. Worse still, note that for every integer $1 \leqslant i \leqslant 2/3\alpha_k - 1$, the horizontal line segment with endpoints

$$(0, \tfrac{1}{3}, 1-i\alpha_k^2) \quad \text{and} \quad (0, \tfrac{1}{3}+\alpha_k, 1-i\alpha_k^2)$$

lies in S_0. The vector $i\mathbf{v}_1$ sends this line segment to a line segment in cartesian 3-space with endpoints

$$(i, \tfrac{1}{3} + i\alpha_k, 1) \quad \text{and} \quad (i, \tfrac{1}{3} + (i+1)\alpha_k, 1)$$

which forms part of the line segment $(i, y, 1)$, $0 \leqslant y \leqslant 1$. This in turn is identified in the L-solid with the "dangerous" splitting edge $(1, y, 1)$, $0 \leqslant y \leqslant 1$, if i is odd, and with the "dangerous" splitting edge $(2, y, 1)$, $0 \leqslant y \leqslant 1$, if i is even. Since $\alpha_k < 1/2k$, it follows that the $\mathbf{v}_1$-image S_0' of S_0 has about $4k/3$ convex parts on the Y-faces, caused by the splitting effect of the "dangerous" edges.

On the other hand, by the identification of faces of the L-solid, the same square S_0 has vertices

$$(2, \tfrac{1}{3}, 1), \quad (2, \tfrac{1}{3}, 1 - \alpha_k), \quad (2, \tfrac{1}{3} + \alpha_k, 1 - \alpha_k), \quad (2, \tfrac{1}{3} + \alpha_k, 1)$$

on the right most X-face X_3. In cartesian 3-space, this square is projected to the plane $y = 0$ by the vector $-\mathbf{v}_1$, where the image is a parallelogram with vertices

$$\left(2 - \frac{1}{3\alpha_k}, 0, 1 - \frac{\alpha_k}{3}\right), \quad \left(2 - \frac{1}{3\alpha_k}, 0, 1 - \frac{4\alpha_k}{3}\right),$$
$$\left(1 - \frac{1}{3\alpha_k}, 0, 1 - \frac{4\alpha_k}{3} - \alpha_k^2\right), \quad \left(1 - \frac{1}{3\alpha_k}, 0, 1 - \frac{\alpha_k}{3} - \alpha_k^2\right).$$

Clearly the projection never hits the planes $z = 0$ or $z = 1$ in between, and any point $(x, 0, z)$ in this parallelogram must satisfy

$$1 - \frac{1}{3\alpha_k} \leqslant x \leqslant 2 - \frac{1}{3\alpha_k} \quad \text{and} \quad 0 < 1 - \frac{4\alpha_k}{3} - \alpha_k^2 \leqslant z \leqslant 1 - \frac{\alpha_k}{3} < 1.$$

Identification of the faces of the L-solid leads us to conclude that this image parallelogram must fall within at most two Y-faces of the L-solid, leading to at most 2 convex parts. In particular, the number of parts is *independent* of k.

This last discussion can be extended to establish the general case as follows. Suppose that S_0 is a convex set with diameter less than α_k on an X-face X_1 or X_3. (The argument in the case when S_0 is on an X-face X_2 or X_4 requires only minimal modification.) Then clearly S_0 is contained in an aligned square of side length α_k on this X-face. Without loss of generality, we can take S_0 to be this aligned square.

Suppose first of all that S_0 is closer to the top edge than to the bottom edge of this X-face, or is equidistant from both. In view of face identification, we can assume that it is on X_3. Suppose that S_0 has vertices

$$(2, a, c), \quad (2, b, c), \quad (2, b, d), \quad (2, a, d),$$

where

$$0 \leqslant a < b \leqslant 1 \quad \text{and} \quad 0 \leqslant c < d \leqslant 1. \tag{6.3.6}$$

Then

$$b - a = \alpha_k \quad \text{and} \quad c \geqslant \frac{1}{2} - \frac{\alpha_k}{2}. \tag{6.3.7}$$

In cartesian 3-space, this square is projected to the plane $y = 0$ by the vector $-\mathbf{v}_1$, where the image is a parallelogram with vertices

$$\left(2 - \frac{a}{\alpha_k}, 0, c - a\alpha_k\right), \quad \left(2 - \frac{b}{\alpha_k}, 0, c - b\alpha_k\right),$$
$$\left(2 - \frac{b}{\alpha_k}, 0, d - b\alpha_k\right), \quad \left(2 - \frac{a}{\alpha_k}, 0, d - a\alpha_k\right).$$

Any point $(x, 0, z)$ in this parallelogram must satisfy

$$2 - \frac{b}{\alpha_k} \leqslant x \leqslant 2 - \frac{a}{\alpha_k} \quad \text{and} \quad c - b\alpha_k \leqslant z \leqslant d - a\alpha_k.$$

In view of (6.3.6) and (6.3.7), and noting that $\alpha_k < 1/2k$, we have

$$c - b\alpha_k \geqslant c - \alpha_k \geqslant \frac{1}{2} - \frac{3\alpha_k}{2} > \frac{1}{2} - \frac{3}{4k} > 0$$

as long as $k \geqslant 2$, and $d - a\alpha_k < 1$ trivially. Thus $0 < z < 1$. Clearly the projection never hits the planes $z = 0$ or $z = 1$ in between, and (6.3.7) also guarantees that the variable x falls into an interval of length at most 1. Identification of the faces of the L-solid now leads us to conclude that this image parallelogram must fall within at most two Y-faces of the L-solid, leading to at most 2 convex parts.

Suppose next that S_0 is closer to the bottom edge than to the top edge of this X-face. In view of face identification, we can assume that it is on X_1. We can then draw a similar conclusion by using the vector $\mathbf{v}_1$ and symmetry arguments, with the point in the middle of the face X_5 acting as the point of symmetry.

Starting with a convex set S_0 on an X-face of the L-solid, irrespective of whether its diameter is less than α_k or not, we can now adopt the following strategy to find a new convex set S_1 that is located on a single Y-face. We consider the $\mathbf{v}_1$-flow image S_0' and the $(-\mathbf{v}_1)$-flow image S_0'' of S_0. Each of S_0' and S_0'' has a number of convex parts, each of which is located on a single Y-face. Note that these parts are contained in Y-faces on the plane $y = 1$ if we use the forward $\mathbf{v}_1$-flow, and contained in Y-faces on the plane $y = 0$ if we use the reverse $\mathbf{v}_1$-flow. We now take S_1 to be the convex subset, located on a single Y-face, of one of these two sets S_0' and S_0'' that has the largest area. Then S_1 is $L_k(1)$-free.

Suppose further that the diameter of S_0 is less than α_k. Then at least one of the two flow images S_0' and S_0'' has at most two convex parts, each of which is located on a single Y-face. It follows that S_1 has area at least $(2\alpha_k)^{-1}$ times the area of S_0.

Remark. Irrespective of whether the diameter is less than α_k, it is clear that if the flow image of S_0 falls into at most N convex parts, each located on a single Y-face, where N is a positive integer, then the largest part S_1 has area at least $(N\alpha_k)^{-1}$ times the area of S_0.

Recall that $L_k(1)$ consists of a number of *whole* front to back detour crossings, starting initially at the origin, and a *fractional* front to back detour crossing at the end. Each whole detour crossing in $L_k(1)$ has a shortcut. The last fractional detour crossing in $L_k(1)$, if extended to a full detour crossing, also has a shortcut. For this last fractional detour crossing, we shorten its shortcut by the same fraction and at the appropriate end to obtain a fractional shortcut. We then take the union of these shortcuts and this fractional shortcut. This union is an initial segment of the s-L-line $\mathcal{L}_k^{**}$, the shortline of the s-L-line $\mathcal{L}_k^*$, that we denote by $L_k(2)$. Then $L_k(2)$ consists of a number of *whole* bottom to top detour crossings, starting initially at the origin, and a *fractional* bottom to top detour crossing at the end. These detour crossings have the same length, and this common length is also given by (6.3.2), so there exists a positive real number m_2 such that

$$\text{length}(L_k(2)) = \frac{m_2}{\alpha_k}(1 + \alpha_k^2 + \alpha_k^4)^{1/2}. \tag{6.3.8}$$

The shortline relation then implies the relation

$$m_2 = \alpha_k m_1, \tag{6.3.9}$$

the analog of (6.3.5).

We now repeat a similar area magnification argument above on this $L_k(1)$-free convex set S_1. However, we need to exercise some care in this second magnification step. Note that the set S_1 is contained in some Y-face. Clearly there exist integers z_1 and z_2 such that $z_2 - z_1 = 1$, the bottom edge of this Y-face intersects the plane

$z = z_1$ and the top edge of this Y-face intersects the plane $z = z_2$. We now use the forward $\mathbf{v}_2$-flow to project S_1 to Z-faces on the plane $z = z_2$, and use the reverse $\mathbf{v}_2$-flow to project S_1 to Z-faces on the plane $z = z_1$. Using the Y-face hitting property, we deduce, like before, that the forward $\mathbf{v}_2$-flow maps the set S_1 to an $L_k(2)$-free convex set S_1', and the reverse $(-\mathbf{v}_2)$-flow maps the set S_1 to an $L_k(2)$-free convex set S_1''. Each of S_1' and S_1'' has a number of convex parts, each of which is located on a single Z-face. We now take S_2 to be the convex subset, located on a single Z-face, of one of these two sets S_1' and S_1'' that has the largest area. Then S_2 is $L_k(2)$-free.

Suppose further that the diameter of S_1 is less than α_k. Then at least one of the two flow images S_1' and S_1'' has at most two convex parts, each of which is located on a single Z-face. It follows that S_2 has area at least $(2\alpha_k)^{-1}$ times the area of S_1.

Recall that $L_k(2)$ consists of a number of *whole* bottom to top detour crossings, starting initially at the origin, and a *fractional* bottom to top detour crossing at the end. Each whole detour crossing in $L_k(2)$ has a shortcut. The last fractional detour crossing in $L_k(2)$, if extended to a full detour crossing, also has a shortcut. For this last fractional detour crossing, we shorten its shortcut by the same fraction and at the appropriate end to obtain a fractional shortcut. We then take the union of these shortcuts and this fractional shortcut. This union is an initial segment of the s-L-line $\mathcal{L}_k$, the shortline of the s-L-line $\mathcal{L}_k^{**}$, that we denote by $L_k(3)$. Then $L_k(3)$ consists of a number of *whole* left to right detour crossings, starting initially at the origin, and a *fractional* left to right detour crossing at the end. These detour crossings have the same length, and this common length is also given by (6.3.2), so there exists a positive real number m_3 such that

$$\text{length}(L_k(3)) = \frac{m_3}{\alpha_k}(1 + \alpha_k^2 + \alpha_k^4)^{1/2}. \tag{6.3.10}$$

The shortline relation then implies the relation

$$m_3 = \alpha_k m_2, \tag{6.3.11}$$

the analog of (6.3.5).

We now repeat a similar area magnification argument above on this $L_k(2)$-free convex set S_2. Again, we need to exercise some care in this third magnification step. Note that the set S_2 is contained in some Z-face. Clearly there exist integers x_1 and x_2 such that $x_2 - x_1 = 1$, the left edge of this Z-face intersects the plane $x = x_1$ and the right edge of this Z-face intersects the plane $x = x_2$. We now use the forward $\mathbf{v}_0$-flow to project S_2 to X-faces on the plane $x = x_2$, and use the reverse $\mathbf{v}_0$-flow to project S_2 to X-faces on the plane $x = x_1$. Using the Z-face hitting property, we deduce that the forward $\mathbf{v}_3 = \mathbf{v}_0$-flow maps the set S_2 to an $L_k(3)$-free convex set S_2', and the reverse $(-\mathbf{v}_0)$-flow maps the set S_2 to an $L_k(3)$-free convex set S_2''. Each of S_2' and S_2'' has a number of convex parts, each of which is located on a single X-face. We now take S_3 to be the convex subset, located on a single X-face, of one of these two sets S_2' and S_2'' that has the largest area. Then S_3 is $L_k(3)$-free.

Suppose further that the diameter of S_2 is less than α_k. Then at least one of the two flow images S_2' and S_2'' has at most two convex parts, each of which is located on a single X-face. It follows that S_3 has area at least $(2\alpha_k)^{-1}$ times the area of S_2.

And so on, we keep iterating this process.

We are now almost ready to describe our magnification process. However, before we do so, we wish to illustrate the motivation behind a key step of the process. We consider a simple case where there is no splitting of the flow image. Our discussion here will be heuristic in nature. For ease of description, we shall take some liberty and make some unjustified simplifications along the way.

Suppose that we start with an aligned square S_0 on the square face X_1. Suppose also that the image of S_0 under the forward $\mathbf{v}_1$-flow is the convex set S_1 which lies

entirely on the square face Y_4, and that the image of S_1 under the reverse $-\mathbf{v}_2$-flow is the convex set S_2 which lies entirely on the square face Z_1, as shown in the picture on the left in Figure 6.3.7.

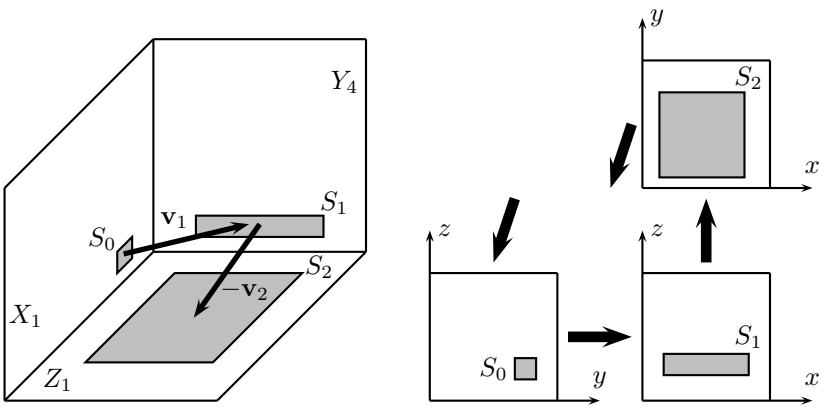

Figure 6.3.7: illustrating a key step of the magnification process

The forward $\mathbf{v}_1$-flow maps the square S_0 on the square face X_1 to a parallelogram S_1 on the square face Y_4. Recall that $\mathbf{v}_1 = (1, \alpha_k, \alpha_k^2)$. Note that α_k is small, so that α_k^2 is a lot smaller. The images under the forward $\mathbf{v}_1$-flow of the two edges of the square S_0 which are parallel to the z-axis are line segments parallel to the z-axis, and their lengths are hardly affected. Meanwhile, the images under the forward $\mathbf{v}_1$-flow of the two edges of the square S_0 which are parallel to the y-axis are line segments almost parallel to the x-axis, and their lengths are magnified by a factor roughly equal to α_k^{-1}. Let us now imagine that S_1 is simply a rectangle with sides parallel to the x-axis and the z-axis, where the sides parallel to the x-axis are longer than the sides parallel to the z-axis by a factor α_k^{-1}. Thus, as we go from S_0 to S_1, one direction of S is stretched a lot more than another.

The reverse $-\mathbf{v}_2$-flow maps the "rectangle" S_1 on the square face Y_4 to a parallelogram S_2 on the square face Z_1. Recall that $\mathbf{v}_2 = (\alpha_k^2, 1, \alpha_k)$. The images under the reverse $-\mathbf{v}_2$-flow of the two longer edges of the rectangle S_1 which are parallel to the x-axis are line segments parallel to the x-axis, and their lengths are hardly affected. Meanwhile, the images under the reverse $-\mathbf{v}_2$-flow of the two shorter edges of the rectangle S_1 which are parallel to the z-axis are line segments almost parallel to the y-axis, and their lengths are magnified by a factor roughly equal to α_k^{-1}, so are now roughly the same as the lengths of the two edges that are parallel to the x-axis. In other words, S_2 is almost like a square. Thus, as we go from S_1 to S_2, the shorter side is S_1 is now compensated by a similar stretching.

Not every step of the magnification process gives a similar magnification. Our first consideration is to guarantee that even if a magnification does not take part, we do not have any significant setback. In the worst case scenario, note that the image of a convex set on a single square face under a forward or reverse flow may split into at most $2\alpha_k^{-1}+2$ parts. As an illustration, take S_i to be the whole X-face with vertices $(1,0,0)$, $(1,0,1)$, $(1,1,0)$ and $(1,1,1)$. It gets mapped on to the plane $y=0$ by the reverse $(-\mathbf{v}_1)$-flow, where $\mathbf{v}_1 = (1, \alpha_k, \alpha_k^2)$. The image is a parallelogram, and the four vertices of the X-face are mapped respectively to

$$(1,0,0), \quad (1,0,1), \quad (1-\alpha_k^{-1}, 0, -\alpha_k), \quad (1-\alpha_k^{-1}, 0, 1-\alpha_k).$$

This parallelogram has x-span, *i.e.*, distance between extreme points in the x-direction, equal to α_k^{-1}, and z-span equal to $1+\alpha_k$, and falls into at most two rows of unit squares and at most $\alpha_k^{-1}+1$ columns of unit squares. If we now take S_{i+1} to be the largest convex subset that fits into a unit square, then S_{i+1} has area at least $(3\alpha_k^{-1}\alpha_k)^{-1} = 1/3$ times the area of S_i.

Standard Magnification Process. Throughout, the symbols $c_0, c_1, c_2, c_3, \ldots$ all represent positive absolute constants which may depend on the value of each other but not on the values of the numbers k or α_k.

Let c_0 be a large positive integer, to be determined later.

We start our process with an $L_k(0)$-free convex set S_0 on an X-face. At each stage $i \geqslant 0$, we have a convex set S_i on a square face. For ease of description, let us assume that S_i lies on an X-face. The description if S_i lies on a Y-face or Z-face has only minor differences of details.

There are two possibilities: (A_i) S_i contains at least one of the c_0^2 standard congruent subsquares of side length c_0^{-1} of the X-face containing it, *i.e.*, any subsquare obtained by the standard $c_0 \times c_0$ subdivision of the X-face containing S_i. (B_i) S_i does not contain any of the c_0^2 standard congruent subsquares of side length c_0^{-1} of the X-face containing it.

In case (A_i), we stop and do not proceed any further, and simply make the observation that

$$\mathrm{area}(S_i) \geqslant c_0^{-2}.$$

In case (B_i), we consider the image, on planes of the form $y = 0$ or $y = 1$ in cartesian 3-space, of S_i under the forward $\mathbf{v}_1$-flow and the reverse $(-\mathbf{v}_1)$-flow. There are two possibilities: (A_{i+1}) The image of S_i under the forward $\mathbf{v}_1$-flow or the reverse $(-\mathbf{v}_1)$-flow contains at least one of the c_0^2 standard congruent subsquares of side length c_0^{-1} of the Y-face containing it. (B_{i+1}) The image of S_i under neither the forward $\mathbf{v}_1$-flow nor the reverse $(-\mathbf{v}_1)$-flow contains any of the c_0^2 standard congruent subsquares of side length c_0^{-1} of the X-face containing it.

In case (A_{i+1}), we define S_{i+1} to be the largest convex subset of the image of S_i under the appropriate flow that contains such a standard congruent subsquare, stop and do not proceed any further, and make the observation that

$$\frac{\mathrm{area}(S_{i+1})}{\mathrm{area}(S_i)} \geqslant c_0^{-2} \quad \text{and} \quad \mathrm{area}(S_{i+1}) \geqslant c_0^{-2}, \tag{6.3.12}$$

where the first inequality comes from the trivial observation that $\mathrm{area}(S_i) \leqslant 1$.

In case (B_{i+1}), we have two possibilities.

$\circ$ Case 1. If the image of S_i under the forward $\mathbf{v}_1$-flow or the reverse $(-\mathbf{v}_1)$-flow splits into at most 4 convex parts, each contained in a single square that can be identified with a Y-face, then we take S_{i+1} to be the largest of these parts. Then

$$\frac{\mathrm{area}(S_{i+1})}{\mathrm{area}(S_i)} > (4\alpha_k)^{-1}, \tag{6.3.13}$$

and we move on to the next step $i + 1$.

$\circ$ Case 2. If the image of S_i under neither the forward $\mathbf{v}_1$-flow nor the reverse $(-\mathbf{v}_1)$-flow splits into at most 4 convex parts, each contained in a single square that can be identified with a Y-face, then the splitting results in at least 5 convex parts. Again, we take S_{i+1} to be the largest of these parts. Under the worst case scenario, S_{i+1} has area at least $1/3$ times the area of S_i. We then consider the image, on planes of the form $z = 0$, $z = 1$ or $z = 2$ in cartesian 3-space, of S_{i+1} under the forward $\mathbf{v}_2$-flow and the reverse $(-\mathbf{v}_2)$-flow. There are two possibilities: (A_{i+2}) The image of S_{i+1} under the forward $\mathbf{v}_2$-flow or the reverse $(-\mathbf{v}_2)$-flow contains at least one of the c_0^2 standard congruent subsquares of side length c_0^{-1} of the Z-face containing it. (B_{i+2}) The image of S_{i+1} under neither the forward $\mathbf{v}_2$-flow nor the reverse $(-\mathbf{v}_2)$-flow contains any of the c_0^2 standard congruent subsquares of side length c_0^{-1} of the Z-face containing it.

In case (A_{i+2}), we define S_{i+2} to be the largest convex subset of the image of S_{i+1} under the appropriate flow that contains such a standard congruent subsquare, stop

and do not proceed any further, and make the observation that

$$\frac{\text{area}(S_{i+1})}{\text{area}(S_i)} > \frac{1}{3}, \quad \frac{\text{area}(S_{i+2})}{\text{area}(S_{i+1})} \geqslant c_0^{-2} \quad \text{and} \quad \text{area}(S_{i+2}) \geqslant c_0^{-2}, \tag{6.3.14}$$

where the middle inequality comes from the trivial observation that $\text{area}(S_{i+1}) \leqslant 1$.

In case (B_{i+2}), we use the following simple geometric result.

Lemma 6.3.1. *Suppose that for a convex set S_i on an X-face of the L-solid, neither the forward $\mathbf{v}_1$-flow nor the reverse $(-\mathbf{v}_1)$-flow results in at most 4 convex parts, each contained in a Y-face. Then there exists a positive absolute constant c_1 such that the x-span of S_{i+1} is at least equal to c_1.*

Proof. Since S_i sits on an X-face, its image under the appropriate forward or reverse flow lies on the plane $y = 0$ or $y = 1$ in cartesian 3-space. Recall from our earlier discussion concerning the worst case scenario that the image of the whole square face fits into two rows of unit squares on this plane, each of which can be identified with a Y-face. It follows that if the image of S_i falls into a fifth unit square, then it means that it will intersect unit squares on at least three consecutive columns. If S_{i+1} comes from one of the unit squares in the middle columns, then clearly the x-span is bounded below by a positive absolute constant. On the other hand, if S_{i+1} comes from one of the unit squares in the columns at either end, then it has to intersect this unit square "substantially" in order to have any chance of being the biggest convex subset, and "substantially" means that its x-span has to be bounded below by a positive absolute constant. □

We now investigate the case (B_{i+2}) of Case 2 more closely. Note that it follows from Lemma 6.3.1 that S_{i+1} contains a line segment of length at least c_1 whose direction is bounded away from the direction of the z-axis. Let us look at S_{i+1} more closely in Figure 6.3.8 below. Suppose, for instance, that it is contained in the square face Y_4. Let L_x denote a line segment joining two extreme points of S_{i+1} in the x-direction. Then this line segment is bounded away from the direction of the z-axis. Let L_z denote a chord of S_{i+1} in the z-direction.

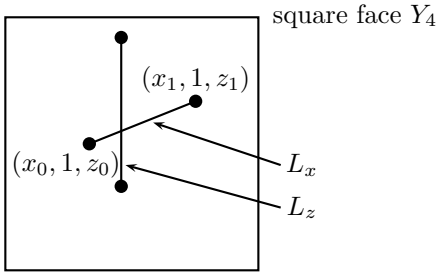

Figure 6.3.8: part of the image of the convex set S_{i+1} when L_x is not parallel to the x-axis

Suppose that the two endpoints of L_x are given by $(x_0, 1, z_0)$ and $(x_1, 1, z_1)$, where $x_0 < x_1$. Then it is clear that there exist positive absolute constants $c_2 \leqslant 1$ and c_3, depending at most on the constant c_1, such that

$$x_1 - x_0 \geqslant c_2 \quad \text{and} \quad \left| \frac{z_1 - z_0}{x_1 - x_0} \right| \leqslant c_3.$$

The reverse $(-\mathbf{v}_2)$-flow maps the entire square face Y_4 to the plane $z = 0$ in cartesian 3-space, and its image is bounded between the planes $x = -1$ and $x = 1$. In particular, the image of S_{i+1} under the same flow lies within two columns of unit squares on the plane $z = 0$, each of which can be identified with a Z-face. The two

endpoints of L_x are mapped respectively to the points

$$(x_0 - z_0\alpha_k, 1 - z_0\alpha_k^{-1}, 0) \quad \text{and} \quad (x_1 - z_1\alpha_k, 1 - z_1\alpha_k^{-1}, 0),$$

so the x-span of the image of L_x is equal to

$$x_1 - x_0 - (z_1 - z_0)\alpha_k = x_1 - x_0 + O(\alpha_k).$$

Clearly there exists a positive absolute constant c_4 such that

$$x_1 - x_0 - (z_1 - z_0)\alpha_k \geqslant c_4.$$

Meanwhile, the y-span of the image of L_x is equal to $|z_1 - z_0|\alpha_k^{-1}$. We illustrate these in Figure 6.3.9.

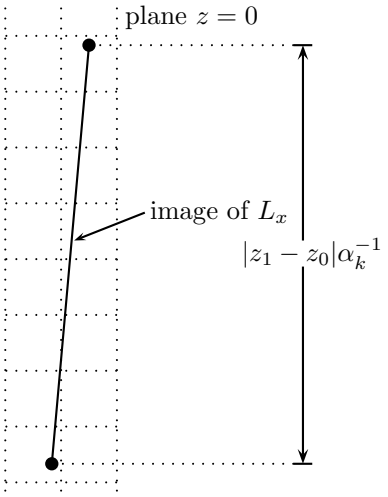

Figure 6.3.9: part of the image of the convex set S_{i+1}
when L_x is not parallel to the x-axis

How we proceed from this point is governed by the size of the z-span $|z_1 - z_0|$ of L_x. There are two possibilities, one when this is small, corresponding to the case L_x is close to being parallel to the x-axis, and the other when this is not so small, corresponding to the case when L_x is not so close to being parallel to the x-axis.

◦ Case 2.1. Suppose that $|z_1 - z_0| \leqslant \alpha_k^{1/2}$. Then the image of L_x has slope not exceeding $c_4^{-1}\alpha_k^{-1/2}$ and y-span not exceeding $\alpha_k^{-1/2}$.

Consider the image on the plane $z = 0$ of a typical chord L_z under the reverse $(-\mathbf{v}_2)$-flow. It is a line segment with slope α_k^{-2}.

Suppose that the length of the image of each of these chords L_z is at most $\alpha_k^{-1/2}$. Then the y-span of the image of S_{i+1} does not exceed $3\alpha_k^{-1/2}$, so the image of S_{i+1} is contained in at most $6\alpha_k^{-1/2} + 2 \leqslant 7\alpha_k^{-1/2}$ unit squares, and splits into at most this number of convex parts, each contained in a single square that can be identified with a Z-face. We now take S_{i+2} to be the largest of these parts. Then

$$\frac{\text{area}(S_{i+1})}{\text{area}(S_i)} > \frac{1}{3} \quad \text{and} \quad \frac{\text{area}(S_{i+2})}{\text{area}(S_{i+1})} \geqslant (49\alpha_k)^{-1/2}, \tag{6.3.15}$$

and we move on to the next step $i + 2$.

Suppose that the length of the image of one of these chords L_z exceeds $\alpha_k^{-1/2}$. Note that, in the orientation in Figure 6.3.9, the slope of the image of L_z is α_k^{-2}, while the span of the image of L_x is at least c_4 and its slope is at most $c_4^{-1}\alpha_k^{-1/2}$. The convex hull of the four endpoints of the images of L_x and L_z is contained in the image of S_{i+1} and has x-span at least c_4. It follows that the image of S_{i+1} must contain some squares of side length c_5, where c_5 is a positive absolute constant depending at most on c_4. Thus if the constant c_0 at the beginning of our discussion

is chosen sufficiently large in terms of c_5, then this case is already covered under case (A_{i+2}).

◦ Case 2.2. Suppose that $|z_1 - z_0| > \alpha_k^{1/2}$. Then the image of L_x has slope exceeding $c_4^{-1}\alpha_k^{-1/2}$ and y-span exceeding $\alpha_k^{-1/2}$. The image of S_{i+1} splits into many convex parts, each contained in a single square that can be identified with a Z-face. We take S_{i+2} to be the largest of these parts. Under the worst case scenario, S_{i+2} has area at least $1/3$ times the area of S_{i+1}. We then consider the image, on planes of the form $x = 0$, $x = 1$ or $x = 2$ in cartesian 3-space, of S_{i+2} under the forward $\mathbf{v}_0$-flow and the reverse $(-\mathbf{v}_0)$-flow. There are two possibilities: (A_{i+3}) The image of S_{i+2} under the forward $\mathbf{v}_0$-flow or the reverse $(-\mathbf{v}_0)$-flow contains at least one of the c_0^2 standard congruent subsquares of side length c_0^{-1} of the X-face containing it. (B_{i+3}) The image of S_{i+2} under neither the forward $\mathbf{v}_0$-flow nor the reverse $(-\mathbf{v}_0)$-flow contains any of the c_0^2 standard congruent subsquares of side length c_0^{-1} of the X-face containing it.

In case (A_{i+3}), we define S_{i+3} to be the largest convex subset of the image of S_{i+2} under the appropriate flow that contains such a standard congruent subsquare, stop and do not proceed any further, and make the observation that

$$\frac{\mathrm{area}(S_{i+1})}{\mathrm{area}(S_i)} > \frac{1}{3}, \quad \frac{\mathrm{area}(S_{i+2})}{\mathrm{area}(S_{i+1})} > \frac{1}{3}, \quad \frac{\mathrm{area}(S_{i+3})}{\mathrm{area}(S_{i+2})} \geqslant c_0^{-2} \quad \text{and} \quad \mathrm{area}(S_{i+3}) \geqslant c_0^{-2}, \tag{6.3.16}$$

where the third inequality comes from the trivial observation that $\mathrm{area}(S_{i+2}) \leqslant 1$.

In case (B_{i+3}), we can claim that, analogous to Lemma 6.3.1, there is a positive absolute constant c_6 such that S_{i+2} contains a section of the image of L_x with y-span at least c_6. Let us denote this section of the image of L_x by L_y, and look at S_{i+2} more closely in the picture on the left in Figure 6.3.10 below. Suppose, for instance, that S_{i+2} is contained in the square face X_1. Let L'_x denote a chord of S_{i+2} in the x-direction.

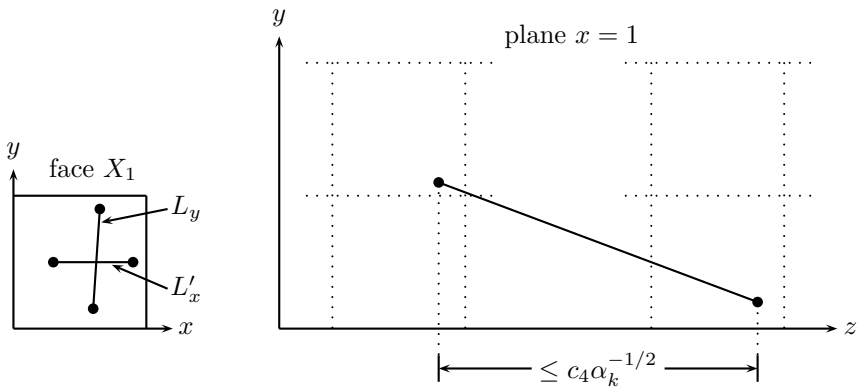

Figure 6.3.10: part of the convex set S_{i+2} and part of its image

Suppose that the two endpoints of L_y are given by $(x_0, y_0, 0)$ and $(x_1, y_1, 0)$, where $y_0 < y_1$. Then

$$y_1 - y_0 \geqslant c_6 \quad \text{and} \quad \left|\frac{x_1 - x_0}{y_1 - y_0}\right| < c_4\alpha_k^{1/2}. \tag{6.3.17}$$

The forward $\mathbf{v}_0$-flow maps the entire square face X_1 to the plane $x = 1$ in cartesian 3-space, and the image is bounded between the planes $y = 0$ and $y = 2$. In particular, the image of S_{i+2} under the same flow lies within two rows of unit squares on the plane $x = 1$, in the orientation of the picture on the right in Figure 6.3.10. The two endpoints of L_y are mapped respectively to the points

$$(1, y_0 + (1 - x_0)\alpha_k, (1 - x_0)\alpha_k^{-1}) \quad \text{and} \quad (1, y_1 + (1 - x_1)\alpha_k, (1 - x_1)\alpha_k^{-1}),$$

so the y-span of the image of L_y is equal to

$$y_1 - y_0 - (x_1 - x_0)\alpha_k = (y_1 - y_0) + O(\alpha_k).$$

Clearly there exists a positive absolute constant c_7 such that

$$y_1 - y_0 - (x_1 - x_0)\alpha_k \geqslant c_7.$$

Meanwhile, the z-span of the image of L_y is equal to $|x_1 - x_0|\alpha_k^{-1} < c_4\alpha_k^{-1/2}$, in view of (6.3.17).

Consider the image on the plane $x = 1$ of a typical chord L'_x that intersects L_y under the forward $\mathbf{v}_0$-flow. It is a line segment of slope α_k^2, in the orientation of the picture on the right in Figure 6.3.10.

Suppose that the length of the image of one of these chords L'_x that intersects L_y exceeds $\alpha_k^{-1/2}$. Note that, in the orientation of the picture on the right in Figure 6.3.10, the slope of the image of L'_x is α_k^2, while the span of the image of L_y is at least c_7 and its slope is at least $c_4^{-1}\alpha_k^{1/2}$. The convex hull of the four endpoints of the images of L_y and L'_x is contained in the image of S_{i+2} and has y-span at least c_7. It follows that the image of S_{i+2} must contain some squares of side length c_8, where c_8 is a positive absolute constant depending at most on c_4 and c_7. Thus if the constant c_0 at the beginning of our discussion is chosen sufficiently large in terms of c_8, then this case is already covered under case (A_{i+3}).

Suppose that the length of the image of each of these chords L'_x that intersects L_y is at most $\alpha_k^{-1/2}$. Then by convexity, the length of the image of *every* chord L'_x of S_{i+2} is at most $c_7^{-1}\alpha_k^{-1/2}$. A simple calculation then shows that there exists a positive absolute constant $c_9 \geqslant 1$, depending at most on c_4 and c_7, such that the z-span of the image of S_{i+2} does not exceed $c_9\alpha_k^{-1/2}$, so the image of S_{i+2} is contained in at most $2c_9\alpha_k^{-1/2} + 2 \leqslant 3c_9\alpha_k^{-1/2}$ unit squares, and splits into at most this number of convex parts, each contained in a single square that can be identified with an X-face. We now take S_{i+3} to be the largest of these parts. Then

$$\frac{\mathrm{area}(S_{i+1})}{\mathrm{area}(S_i)} > \frac{1}{3}, \quad \frac{\mathrm{area}(S_{i+2})}{\mathrm{area}(S_{i+1})} > \frac{1}{3} \quad \text{and} \quad \frac{\mathrm{area}(S_{i+3})}{\mathrm{area}(S_{i+2})} \geqslant (9c_9\alpha_k)^{-1/2}, \tag{6.3.18}$$

and we move on to the next step $i + 3$.

Suppose that the process stops at the step $i = i_0$, where S_{i_0} contains at least one of the c_0^2 standard congruent subsquares of side length c_0^{-1} of the square face containing it. We now analyze the total area growth originating from the steps

$$S_0 \to S_1 \to S_2 \to \ldots \to S_{i_0}.$$

Let c_0^* be a sufficiently small positive absolute constant, depending at most on c_9. In our magnification process, there are three different instances when we have a good area growth, do not stop but proceed on to the next step. The first instance arises from Case 1 within case (B_{i+1}). There the inequality (6.3.13) can be rewritten in the form

$$\frac{\mathrm{area}(S_{i+1})}{\mathrm{area}(S_i)} > (4\alpha_k)^{-1} > c_0^*\alpha_k^{-1/6}. \tag{6.3.19}$$

The second instance arises from Case 2.1 within case (B_{i+2}). There the inequality (6.3.15) can be rewritten in the form

$$\frac{\mathrm{area}(S_{i+2})}{\mathrm{area}(S_i)} > \frac{1}{3}(49\alpha_k)^{-1/2} > \left(c_0^*\alpha_k^{-1/6}\right)^2. \tag{6.3.20}$$

The last instance arises from Case 2.2 within case (B_{i+2}). For the case (B_{i+3}), the inequality (6.3.18) can be rewritten in the form

$$\frac{\text{area}(S_{i+3})}{\text{area}(S_i)} > \frac{1}{27}(c_9\alpha_k)^{-1/2} > \left(c_0^*\alpha_k^{-1/6}\right)^3. \tag{6.3.21}$$

On the other hand, there are three instances when our magnification process stops, corresponding to the cases (A_{i+1}), (A_{i+2}) and (A_{i+3}). Corresponding to these, we have inequalities (6.3.12), (6.3.14) and (6.3.16), which can be rewritten respectively in the form

$$\frac{\text{area}(S_{i+1})}{\text{area}(S_i)} \geqslant c_0^{-2} > (3c_0)^{-2}, \tag{6.3.22}$$

$$\frac{\text{area}(S_{i+2})}{\text{area}(S_i)} > \frac{1}{3}c_0^{-2} > (3c_0)^{-2}, \tag{6.3.23}$$

$$\frac{\text{area}(S_{i+3})}{\text{area}(S_i)} > \frac{1}{9}c_0^{-2} > (3c_0)^{-2}. \tag{6.3.24}$$

A stopping case (A_{i+1}) with $i+1 = i_0$ corresponds to the processes

$$S_0 \to S_1 \to S_2 \to \ldots \to S_{i_0-1} \quad \text{and} \quad S_{i_0-1} \to S_{i_0}.$$

Using (6.3.19)–(6.3.21) for the left hand chain and (6.3.22) for the right hand chain, we obtain respectively

$$\frac{\text{area}(S_{i_0-1})}{\text{area}(S_0)} > \left(c_0^*\alpha_k^{-1/6}\right)^{i_0-1} \quad \text{and} \quad \frac{\text{area}(S_{i_0})}{\text{area}(S_{i_0-1})} > (3c_0)^{-2},$$

and so

$$\frac{1}{\text{area}(S_0)} > (3c_0)^{-2}\left(c_0^*\alpha_k^{-1/6}\right)^{i_0-1}, \tag{6.3.25}$$

noting that $\text{area}(S_{i_0}) \leqslant 1$. A stopping case ($A_{i+2}$) with $i+2 = i_0$ corresponds to the processes

$$S_0 \to S_1 \to S_2 \to \ldots \to S_{i_0-2} \quad \text{and} \quad S_{i_0-2} \to S_{i_0-1} \to S_{i_0}.$$

Using (6.3.19)–(6.3.21) for the left hand chain and (6.3.23) for the right hand chain, we obtain respectively

$$\frac{\text{area}(S_{i_0-2})}{\text{area}(S_0)} > \left(c_0^*\alpha_k^{-1/6}\right)^{i_0-2} \quad \text{and} \quad \frac{\text{area}(S_{i_0})}{\text{area}(S_{i_0-2})} > (3c_0)^{-2},$$

and so

$$\frac{1}{\text{area}(S_0)} > (3c_0)^{-2}\left(c_0^*\alpha_k^{-1/6}\right)^{i_0-2}. \tag{6.3.26}$$

A stopping case (A_{i+3}) with $i+3 = i_0$ corresponds to the processes

$$S_0 \to S_1 \to S_2 \to \ldots \to S_{i_0-3} \quad \text{and} \quad S_{i_0-3} \to S_{i_0-2} \to S_{i_0-1} \to S_{i_0}.$$

Using (6.3.19)–(6.3.21) for the left hand chain and (6.3.24) for the right hand chain, we obtain respectively

$$\frac{\text{area}(S_{i_0-3})}{\text{area}(S_0)} > \left(c_0^*\alpha_k^{-1/6}\right)^{i_0-3} \quad \text{and} \quad \frac{\text{area}(S_{i_0})}{\text{area}(S_{i_0-3})} > (3c_0)^{-2},$$

and so

$$\frac{1}{\text{area}(S_0)} > (3c_0)^{-2}\left(c_0^*\alpha_k^{-1/6}\right)^{i_0-3}. \tag{6.3.27}$$

Next note that (6.3.3), (6.3.4), (6.3.8) and (6.3.10) can be generalized to

$$\text{length}(L_k(i)) = \frac{m_i}{\alpha_k}(1+\alpha_k^2+\alpha_k^4)^{1/2}, \quad 0 \leqslant i \leqslant i_0, \tag{6.3.28}$$

where m_i is some positive real number. The shortline relation then implies the relation

$$m_{i+1} = \alpha_k m_i, \quad 0 \leqslant i < i_0, \tag{6.3.29}$$

which is the general form of (6.3.5), (6.3.9) and (6.3.11).

Iterating (6.3.29), we deduce that

$$m_i = \alpha_k^i m_0. \tag{6.3.30}$$

Combining (6.3.28) and (6.3.30), we have

$$\text{length}(L_k(i)) = \alpha_k^i \,\text{length}(L_k(0)), \quad 0 \leqslant i \leqslant i_0.$$

Choosing $i = i_0$, this gives

$$\text{length}(L_k(i_0)) = \alpha_k^{i_0} \,\text{length}(L_k(0)). \tag{6.3.31}$$

Suppose that

$$\alpha_k^{i_0} \,\text{length}(L_k(0)) = C_k, \tag{6.3.32}$$

where C_k is a *sufficiently large* constant depending only on the given fixed integer $k \geqslant 1$. Then we have the following three facts:

(1) In view of (6.3.31) and (6.3.32), we have

$$\text{length}(L_k(i_0)) = C_k,$$

i.e., $L_k(i_0)$ is a "long" segment of $\mathcal{L}_k$ or $\mathcal{L}_k^*$ or $\mathcal{L}_k^{**}$.

(2) By definition the convex set S_{i_0} is disjoint from $L_k(i_0)$.

(3) The convex set S_{i_0} contains at least one of the c_0^2 standard congruent subsquares of side length c_0^{-1} of the square face containing it.

To show that these lead to a contradiction, we use the following lemma.

Lemma 6.3.2. *Let $k \geqslant 2c_0$ be an arbitrary integer. Then there is a threshold $C_k^\star$, depending at most on k, such that the initial segment $\mathcal{L}_k(t)$, $0 \leqslant t \leqslant C_k^\star$, of $\mathcal{L}_k$ intersects every one of the standard congruent subsquares of side length c_0^{-1} of the square faces Z_i, $1 \leqslant i \leqslant 5$, of the L-solid. Here, as usual, we use arc-length parametrization, so that the segment $\mathcal{L}_k(t)$, $0 \leqslant t \leqslant C_k^\star$, has length $C_k^\star$. Similarly, the initial segment $\mathcal{L}_k^*(t)$, $0 \leqslant t \leqslant C_k^\star$, of $\mathcal{L}_k^*$ intersects every one of the standard congruent subsquares of side length c_0^{-1} of the square faces X_i, $1 \leqslant i \leqslant 5$, of the L-solid, and the initial segment $\mathcal{L}_k^{**}(t)$, $0 \leqslant t \leqslant C_k^\star$, of $\mathcal{L}_k^{**}$ intersects every one of the standard congruent subsquares of side length c_0^{-1} of the square faces Y_i, $1 \leqslant i \leqslant 6$, of the L-solid.*

Proof. We shall only prove the assertion for $\mathcal{L}_k$, as the proof for the other two cases are similar. Every detour crossing of $\mathcal{L}_k$ has a shortcut which is part of $\mathcal{L}_k^*$. Consider the first two detour crossings of $\mathcal{L}_k$. The first starts at the origin $(0,0,0)$ and ends at the point $(1,\alpha_k,\alpha_k^2)$, and the second continues until the point $(2,2\alpha_k,2\alpha_k^2)$. The two short cuts are respectively the directed line segment joining $(0,0,0)$ and $(1,\alpha_k,\alpha_k^2)$ and the directed line segment joining $(1,\alpha_k,\alpha_k^2)$ and $(2,2\alpha_k,2\alpha_k^2)$. It is quite clear that the y-coordinate of every point on these two detour crossings as well as on both shortcuts satisfies $0 \leqslant y \leqslant 2\alpha_k$. On the other hand, if $k \geqslant 2c_0$, then noting that $\alpha_k < 1/2k$, we have $c_0^{-1} > 4\alpha_k$. In other words, both detour crossings and both shortcuts lie in the part of the L-solid where $0 < y < c_0^{-1}$. Figure 6.3.11 below represents the projection of part of the L-solid on to the plane $z = 0$. In the bottom strip, we show the projection of the first two detour crossings and their shortcuts,

as well as all the standard congruent subsquares of side length c_0^{-1} on the bottom row of the square faces Z_1 and Z_2.

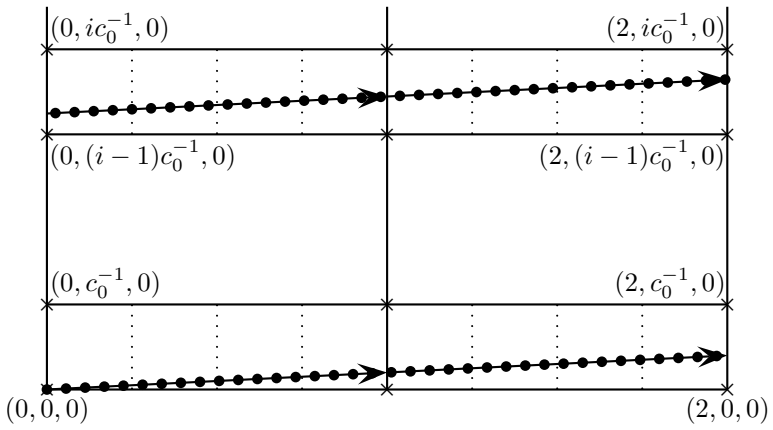

Figure 6.3.11: projection from above of $\mathcal{L}_k(t)$ and $\mathcal{L}_k^*(t)$

For $\mathcal{L}_k$, after it intersects one of the Z-faces, it intersects a Z-face again when the geodesic has progressed a distance α_k in the x-direction. In Figure 6.3.11, the dots represent the projection of these intersection points to the plane $z = 0$. The inequality $c_0^{-1} > 4\alpha_k$ ensures that there are at least three such consecutive points in each of the standard congruent subsquares of side length c_0^{-1} on the bottom row. For the first detour crossing, $\mathcal{L}_k$ intersects the square face Z_1, identified with the square face Z_3, and the square face Z_5 on alternate occasions, whereas for the second detour crossing, $\mathcal{L}_k$ intersects the square face Z_2, identified with the square face Z_4, on every occasion. It follows that the first two detour crossings of $\mathcal{L}_k$ together intersect every standard congruent subsquare of side length c_0^{-1} on the square faces Z_i, $1 \leqslant i \leqslant 5$, where $0 \leqslant y \leqslant c_0^{-1}$.

We now take the entirety of the first detour crossing of $\mathcal{L}_k^*$. It consists of shortcuts of detour crossings of $\mathcal{L}_k$, and we can extend the last "fractional" shortcut to a complete shortcut. We now let the initial segment $\mathcal{L}_k(t)$, $0 \leqslant t \leqslant C_k^\star$, of $\mathcal{L}_k$ to be the union of these detour crossings of $\mathcal{L}_k$. The length of this initial segment is approximately

$$\alpha_k^{-2}(1 + \alpha_k^2 + \alpha_k^4)^{1/2} < 2\alpha_k^{-2}.$$

For each integer $1 \leqslant i \leqslant c_0$, consider the part of the L-solid where $(i-1)c_0^{-1} < y < ic_0^{-1}$. The condition $c_0^{-1} > 4\alpha_k$ ensures that we can find two detour crossings of $\mathcal{L}_k$ in the initial segment defined above that lie in this part of the L-solid; see the top strip in Figure 6.3.11. An analogous argument shows that these two detour crossings of $\mathcal{L}_k$ together intersect every standard congruent subsquare of side length c_0^{-1} on the square faces Z_i, $1 \leqslant i \leqslant 5$, where $(i-1)c_0^{-1} \leqslant y <\leqslant ic_0^{-1}$.

This completes the proof of the lemma. □

Notice that if we apply Lemma 6.3.2 with the choice $C_k = C_k^\star$ in (6.3.32), then the three facts (1)–(3) contradict each other.

Indeed, if (6.3.32) holds with $C_k = C_k^\star$, *i.e.*, if

$$\text{length}(L_k(0)) = C_k^\star \left(\frac{1}{\alpha_k}\right)^{i_0}, \tag{6.3.33}$$

then the contradiction implies that the starting hypothesis is false. In other words, the first convex set S_0 of the sequence S_i cannot be $L_k(0)$-free, meaning that the square $S_0 = ABCD$ must intersect $L_k(0)$.

Write $c_0^{**} = (c_0^*)^6$. Then (6.3.25)–(6.3.27) combine to give

$$\left(\frac{3c_0}{\sqrt{\text{area}(S_0)}} \right)^{12} > \left(\frac{c_0^{**}}{\alpha_k} \right)^{i_0-3}. \tag{6.3.34}$$

Given any $\varepsilon > 0$, take k_0 to be an integer satisfying

$$k_0 \geqslant \frac{1}{2c_0^{**}} \left(\frac{1}{c_0^{**}} \right)^{12/\varepsilon}.$$

Then for any integer $k > k_0$, we have, in view of (6.3.1),

$$\left(\frac{c_0^{**}}{\alpha_k} \right)^{\varepsilon/12} > (2kc_0^{**})^{\varepsilon/12} \geqslant \frac{1}{c_0^{**}}. \tag{6.3.35}$$

Combining (6.3.34) and (6.3.35), we have

$$\left(\frac{3c_0}{\sqrt{\text{area}(S_0)}} \right)^{12+\varepsilon} > \left(\frac{c_0^{**}}{\alpha_k} \right)^{i_0-3} \left(\frac{1}{c_0^{**}} \right)^{i_0-3} = \left(\frac{1}{\alpha_k} \right)^{i_0-3}.$$

Together with (6.3.33), we now conclude that

$$\text{length}(L_k(0)) = C_k^\star \alpha_k^{-3} \left(\frac{1}{\alpha_k} \right)^{i_0-3} < C_k^\star \alpha_k^{-3} \left(\frac{3c_0}{\sqrt{\text{area}(S_0)}} \right)^{12+\varepsilon}.$$

This gives a conclusion that is substantially weaker than that stated in Theorem 6.1.2 in the special case of $\mathcal{L}_k$ when the half-infinite s-L-line of direction $(\alpha_k, \alpha_k^2, 1)$ *starts from the origin*. Note that $\sqrt{\text{area}(S_0)}$ is the side length of the square S_0.

The reader will recognize that we have lost a factor of 6 somewhere in the argument. It is clear that if the term $\alpha_k^{-1/6}$ in the estimates (6.3.19)–(6.3.21) could be replaced by α_k^{-1}, then the same could be done in the estimates (6.3.25)–(6.3.27), and our argument would give the desired result.

We can easily improve on the Basic Magnification Process for those initial steps when the diameter of the convex set S_i does not exceed α_k. We have already discussed that at the time of the introduction of the reverse flow which, together with the forward flow, ensures that we can always find a convex set S_{i+1} such that

$$\frac{\text{area}(S_{i+1})}{\text{area}(S_i)} > (2\alpha_k)^{-1}. \tag{6.3.36}$$

Suppose that the index $i = i_1$ is the first instance when the diameter of S_i exceeds α_k, so that an estimate of the form (6.3.36) can no longer be guaranteed. If we can show that there exists an absolute constant c_{10} such that the steps

$$S_{i_1} \to S_{i_1+1} \to S_{i_1+2} \to \ldots \to S_{i_0},$$

with $i_0 - i_1 \leqslant c_{10}$, leads to a convex set S_{i_0} that contains at least one of the c_0^2 standard congruent subsquares of side length c_0^{-1} of the square face containing it, then this should be enough to give the desired result for any fixed $\varepsilon > 0$. Unfortunately, not every such convex set S_{i_1} allows us to achieve this. We clearly need more input into the convex set S_0 at the beginning of the process in order to generate an appropriate convex set S_{i_1}.

To illustrate our new idea, recall our earlier discussion of starting with a parallelogram $ABCD$ on the plane $x = 2$ in cartesian 3-space and magnifying it by projecting it by the vector $\mathbf{v}_1 = (1, \alpha_k, \alpha_k^2)$ to a parallelogram $A'B'C'D'$ on the plane $y = 1$. We shall follow that by two further magnifications by projections by the vectors $\mathbf{v}_2 = (\alpha_k^2, 1, \alpha_k)$ and $\mathbf{v}_0 = (\alpha_k, \alpha_k^2, 1)$, thus completing a 3-step magnification process.

More precisely, let us consider a parallelogram S_0 on a plane $x = x_0^*$ in cartesian 3-space, where x_0^* is an integer.

As a first step, let us project S_0 by the vector $\mathbf{v}_1 = (1, \alpha_k, \alpha_k^2)$ to a parallelogram S_1 on a plane $y = y_1^*$, where y_1^* is an integer, with the point $(x_0^*, c_1, c_2) \in S_0$ at the center projected to the point $(c_3, y_1^*, c_4) \in S_1$. If $\mathbf{v}_1 = (1, \alpha_k, \alpha_k^2)$ projects a point $(x_0^*, c_1 + y_0, c_2 + z_0) \in S_0$ to the point $(c_3 + x_1, y_1^*, c_4 + z_1) \in S_1$, then simple calculation shows that

$$x_1 = -\frac{y_0}{\alpha_k} = \frac{z_1 - z_0}{\alpha_k^2}.$$

Hence $x_1 = -\alpha_k^{-1} y_0$ and $z_1 = z_0 - \alpha_k y_0$, and so

$$\begin{pmatrix} x_1 \\ z_1 \end{pmatrix} = \begin{pmatrix} -\alpha_k^{-1} & 0 \\ -\alpha_k & 1 \end{pmatrix} \begin{pmatrix} y_0 \\ z_0 \end{pmatrix}. \tag{6.3.37}$$

As a second step, let us project S_1 by the vector $\mathbf{v}_2 = (\alpha_k^2, 1, \alpha_k)$ to a parallelogram S_2 on a plane $z = z_2^*$, where z_2^* is an integer, with the point $(c_3, y_1^*, c_4) \in S_1$ at the center projected to the point $(c_5, c_6, z_2^*) \in S_2$. If $\mathbf{v}_2 = (\alpha_k^2, 1, \alpha_k)$ projects a point $(c_3 + x_1, y_1^*, c_4 + z_1) \in S_1$ to the point $(c_5 + x_2, c_6 + y_2, z_2^*) \in S_2$, then simple calculation shows that

$$\frac{x_2 - x_1}{\alpha_k^2} = y_2 = -\frac{z_1}{\alpha_k}.$$

Hence $x_2 = x_1 - \alpha_k z_1$ and $y_2 = -\alpha_k^{-1} z_1$, and so

$$\begin{pmatrix} x_2 \\ y_2 \end{pmatrix} = \begin{pmatrix} 1 & -\alpha_k \\ 0 & -\alpha_k^{-1} \end{pmatrix} \begin{pmatrix} x_1 \\ z_1 \end{pmatrix}. \tag{6.3.38}$$

As a final step, let us project S_2 by the vector $\mathbf{v}_0 = (\alpha_k, \alpha_k^2, 1)$ to a parallelogram S_3 on a plane $x = x_3^*$, where x_3^* is an integer, with the point $(c_5, c_6, z_2^*) \in S_2$ at the center projected to the point $(x_3^*, c_7, c_8) \in S_3$. If $\mathbf{v}_0 = (\alpha_k, \alpha_k^2, 1)$ projects a point $(c_5 + x_2, c_6 + y_2, z_2^*) \in S_2$ to the point $(x_3^*, c_7 + y_3, c_8 + z_3) \in S_3$, then simple calculation shows that

$$-\frac{x_2}{\alpha_k} = \frac{y_3 - y_2}{\alpha_k^2} = z_3.$$

Hence $y_3 = y_2 - \alpha_k x_2$ and $z_3 = -\alpha_k^{-1} x_2$, and so

$$\begin{pmatrix} y_3 \\ z_3 \end{pmatrix} = \begin{pmatrix} -\alpha_k & 1 \\ -\alpha_k^{-1} & 0 \end{pmatrix} \begin{pmatrix} x_2 \\ y_2 \end{pmatrix}. \tag{6.3.39}$$

Combining (6.3.37)–(6.3.39), we see that this 3-step magnification has resulted in the transition

$$\begin{pmatrix} y_3 \\ z_3 \end{pmatrix} = \begin{pmatrix} -\alpha_k & 1 \\ -\alpha_k^{-1} & 0 \end{pmatrix} \begin{pmatrix} 1 & -\alpha_k \\ 0 & -\alpha_k^{-1} \end{pmatrix} \begin{pmatrix} -\alpha_k^{-1} & 0 \\ -\alpha_k & 1 \end{pmatrix} \begin{pmatrix} y \\ z \end{pmatrix}.$$

The transition matrix in question is

$$\mathcal{A} = \begin{pmatrix} -\alpha_k & 1 \\ -\alpha_k^{-1} & 0 \end{pmatrix} \begin{pmatrix} 1 & -\alpha_k \\ 0 & -\alpha_k^{-1} \end{pmatrix} \begin{pmatrix} -\alpha_k^{-1} & 0 \\ -\alpha_k & 1 \end{pmatrix} = \begin{pmatrix} 2 - \alpha_k^3 & \alpha_k^2 - \alpha_k^{-1} \\ \alpha_k^{-2} - \alpha_k & 1 \end{pmatrix}.$$

Remark. We have boldly claimed at the beginning of this paper that our technique is eigenvalue-free. So we ask our readers to grant us our indulgence just this once, given that we have already established time-quantitative density, albeit a somewhat weaker version, for this problem, without using eigenvalues and eigenvectors.

The eigenvalues of this matrix are the roots of the quadratic equation

$$\det \begin{pmatrix} 2 - \alpha_k^3 - \Lambda & \alpha_k^2 - \alpha_k^{-1} \\ \alpha_k^{-2} - \alpha_k & 1 - \Lambda \end{pmatrix} = 0,$$

or $\Lambda^2 - (3 - \alpha_k^3)\Lambda + \alpha_k^{-3} = 0$, with solutions

$$\Lambda_i = \frac{(3 - \alpha_k^3) \pm \mathrm{i}\sqrt{4\alpha_k^{-3} - (3 - \alpha_k^3)^2}}{2}, \quad i = 1, 2, \tag{6.3.40}$$

and corresponding eigenvectors

$$\mathbf{W}_i = \left(\frac{\Lambda_i - 1}{\alpha_k^{-2} - \alpha_k}, 1 \right), \quad i = 1, 2. \tag{6.3.41}$$

Note that the two eigenvalues are complex conjugates of each other, as are the first coordinates of the two eigenvectors. It follows that the two vectors

$$\mathbf{u}_1 = \mathbf{W}_1 + \mathbf{W}_2 \quad \text{and} \quad \mathbf{u}_2 = \frac{1}{\mathrm{i}}(\mathbf{W}_1 - \mathbf{W}_2) \tag{6.3.42}$$

have real coordinates. Indeed, $\mathbf{u}_1 = (u_{1,1}, u_{1,2})$, where

$$u_{1,1} = \frac{2 - \alpha_k^3}{\alpha_k^{-2} - \alpha_k} \quad \text{and} \quad u_{1,2} = 2,$$

and $\mathbf{u}_2 = (u_{2,1}, u_{2,2})$, where

$$u_{2,1} = \frac{\sqrt{4\alpha_k^{-3} - (3 - \alpha_k^3)^2}}{\alpha_k^{-2} - \alpha_k} \quad \text{and} \quad u_{2,2} = 0,$$

if we ensure that $u_{2,1}$ is positive. This is the motivation for modifying our present discussion in the following way.

As before, we start with a parallelogram S_0 on a plane $x = x_0^*$ in cartesian 3-space, but with some very special property attached to it. Omitting reference to the x-coordinate, we ensure that the non-parallel sides of S_0 are parallel to $\mathbf{u}_1$ and $\mathbf{u}_2$, with lengths respectively

$$\lambda|\mathbf{u}_1| = \lambda(u_{1,1}^2 + u_{1,2}^2)^{1/2} \quad \text{and} \quad \lambda|\mathbf{u}_2| = \lambda u_{2,1},$$

where $\lambda > 0$ is a small fixed real number.

The 3-step magnification process transforms S_0 into a parallelogram S_3 with non-parallel sides that are parallel to the vector

$$\mathbf{u}_1^{(1)} = \mathcal{A}\mathbf{u}_1 = \mathcal{A}(\mathbf{W}_1 + \mathbf{W}_2) = \mathcal{A}\mathbf{W}_1 + \mathcal{A}\mathbf{W}_2 = \Lambda_1\mathbf{W}_1 + \Lambda_2\mathbf{W}_2,$$

with real coordinates and of length

$$\lambda|\Lambda_1\mathbf{W}_1 + \Lambda_2\mathbf{W}_2|,$$

and to the vector

$$\mathbf{u}_2^{(1)} = \mathcal{A}\mathbf{u}_2 = \frac{1}{\mathrm{i}}\mathcal{A}(\mathbf{W}_1 - \mathbf{W}_2) = \frac{1}{\mathrm{i}}(\mathcal{A}\mathbf{W}_1 - \mathcal{A}\mathbf{W}_2) = \frac{1}{\mathrm{i}}(\Lambda_1\mathbf{W}_1 - \Lambda_2\mathbf{W}_2),$$

with real coordinates and of length

$$\lambda|\Lambda_1\mathbf{W}_1 - \Lambda_2\mathbf{W}_2|.$$

Indeed, this 3-step magnification process repeated $\ell \geqslant 1$ times transforms S_0 into a parallelogram $S_{3\ell}$ with non-parallel sides that are parallel to the vector

$$\mathbf{u}_1^{(\ell)} = \Lambda_1^\ell\mathbf{W}_1 + \Lambda_2^\ell\mathbf{W}_2,$$

with real coordinates and of length

$$\lambda|\Lambda_1^\ell\mathbf{W}_1 + \Lambda_2^\ell\mathbf{W}_2|, \tag{6.3.43}$$

and to the vector

$$\mathbf{u}_2^{(\ell)} = \frac{1}{\mathrm{i}}(\Lambda_1^\ell\mathbf{W}_1 - \Lambda_2^\ell\mathbf{W}_2),$$

with real coordinates and of length

$$\lambda|\Lambda_1^\ell \mathbf{W}_1 - \Lambda_2^\ell \mathbf{W}_2|. \tag{6.3.44}$$

We wish to understand how far the parallelogram $S_{3\ell}$ differs from the original parallelogram S_0. In particular, we wish to show that it does not look like a long "needle", with one side substantially longer than the other.

Assume that k is a fixed large integer.

First we estimate the area of $S_{3\ell}$. It is clear, since $u_{2,2} = 0$, that

$$\text{area}(S_0) = \lambda^2|u_{1,2}||u_{2,1}| = (4 + o_k(1))\lambda^2\alpha_k^{1/2}.$$

It then follows from the magnification process that

$$\text{area}(S_{3\ell}) = \alpha_k^{-3\ell}\,\text{area}(S_0) = (4 + o_k(1))\lambda^2\alpha_k^{-3\ell}\alpha_k^{1/2}. \tag{6.3.45}$$

Next, we estimate the maximum side length of $S_{3\ell}$. Note first of all that it clearly follows from (6.3.40)that

$$|\Lambda_i| = \alpha_k^{-3/2}, \quad i = 1, 2.$$

Combining this with (6.3.41), we see that

$$|\mathbf{W}_i| \leqslant 2, \quad i = 1, 2.$$

It follows, on noting that the side lengths of $S_{3\ell}$ are given by (6.3.43) and (6.3.44), that the maximum side length of $S_{3\ell}$ satisfies

$$\text{max-sidelength}(S_{3\ell}) \leqslant \lambda(|\Lambda_1|^\ell|\mathbf{W}_1| + |\Lambda_2|^\ell|\mathbf{W}_2|) \leqslant 4\lambda\alpha_k^{-3\ell/2}. \tag{6.3.46}$$

Combining (6.3.45) and (6.3.46), we deduce that

$$\frac{(\text{max-sidelength}(S_{3\ell}))^2}{\text{area}(S_{3\ell})} \leqslant \frac{4 + o_k(1)}{\alpha_k^{1/2}},$$

and so

$$\frac{(\text{diam}(S_{3\ell}))^2}{\text{area}(S_{3\ell})} \leqslant \frac{8 + o_k(1)}{\alpha_k^{1/2}}. \tag{6.3.47}$$

Let us now rework this 3-step magnification process $S_0 \to S_1 \to S_2 \to S_3$, discussed earlier, but no longer in cartesian 3-space.

Suppose that the special parallelogram S_0 is contained in a single X-face of the L-solid, on the plane $x = x_0^*$. We now project it by the vector $\mathbf{v}_1$ to Y-faces contained in an appropriate plane $y = y_1^*$, in accordance with our stringent convention for such projections. Let $\phi : S_0 \to S_1$ describe this map.

Suppose that $\text{diam}(S_0) \leqslant \alpha_k^3$. In view of the magnification process, we have $\text{diam}(S_1) \leqslant \alpha_k^2 < 1$, and so S_1 lies entirely within at most 4 standard unit squares on the plane $y = y_1^*$, separated by two perpendicular straight lines L_1' and L_1''. Let us project these two straight lines back to the plane $x = x_0^*$ by the inverse map ϕ^{-1}, and write

$$\mathscr{L}_1' = \phi^{-1}(L_1') \quad \text{and} \quad \mathscr{L}_1'' = \phi^{-1}(L_1''). \tag{6.3.48}$$

Consider a subset $S_0' \subset S_0$ and its image under the map ϕ. It is clear that if S_0' does not intersect either of the 2 straight lines (6.3.48), then its image is contained within a single unit square on the plane $y = y_1^*$, and therefore no *splitting* occurs during this magnification.

Remark. Our argument breaks down here if we have not set up properly the Rule for Magnification in a Polycube which dictates which faces the flow images must lie in. For general finite polycubes, without this restriction, parts of S_1 may lie in unit square faces on different planes $y = y_1$ and $y = y_2$, and there may then be more lines that a subset $S_0' \subset S_0$ must not intersect in order that its image is contained in a single Y-face of the L-solid. This complication does not arise in this step for

the L-solid, as the L-solid has only front and back Y-faces. But then the L-solid has X-faces that lie on 3 different planes, as well as Z-faces that lie on 3 different planes, so this complication may possibly arise in the next two steps.

Lemma 6.3.3 ("geometric lemma"). *If the unit square* $[0,1]^2$ *is divided into* 81 *congruent subsquares of side length* $1/9$ *in the standard way, then given any* 2 *straight lines on the plane containing the unit square* $[0,1]^2$*, there is at least one such subsquare that does not intersect either of these* 2 *straight lines.*

Proof. For a given line $\mathscr{L}$ on the plane, for any real number $r > 0$, let $\mathscr{L}(r)$ denote the set of points on the plane that have distance at most r from $\mathscr{L}$. It is easy to see that

$$\text{area}(\mathscr{L}(r) \cap [0,1]^2) \leqslant 2r\sqrt{2}. \tag{6.3.49}$$

On the other hand, if $\mathscr{L}$ intersects one of the standard subsquares $\mathscr{S}$ of side length $1/9$ in $[0,1]^2$, then since the diameter of $\mathscr{S}$ is $\sqrt{2}/9$, it is clear that $\mathscr{S} \subset \mathscr{L}(\sqrt{2}/9)$. Putting $r = \sqrt{2}/9$ in (6.3.49), we see that

$$\sum_{\mathscr{S} \cap \mathscr{L} \neq \emptyset} \text{area}(\mathscr{S}) \leqslant \text{area}\left(\mathscr{L}\left(\frac{\sqrt{2}}{9}\right) \cap [0,1]^2 \right) \leqslant \frac{4}{9}.$$

It follows that the total area of those congruent subsquares that intersect either of 2 given lines is at most $8/9$, so there exist some congruent subsquares that do not intersect any of these 2 straight lines. □

In other words, one of the 81 congruent sub-parallelograms $S_0' \subset S_0$ obtained by 9-fold division of each side of S_0 has image under ϕ which is contained in a single Y-face of the L-solid. We can also modify the next two magnification steps in the same spirit, noting that $\text{diam}(S_2) \leqslant \alpha_k < 1$ and $\text{diam}(S_3) \leqslant 1$, so that S_2 and S_3, and hence also their subsets, is each contained within at most 4 standard unit squares.

We are now ready to improve on our original magnification process.

Enhanced Magnification Process. Throughout, the symbols $c_0, c_1, c_2, c_3, \ldots$ all represent positive absolute constants which may depend on the value of each other but not on the values of the numbers k or α_k.

In particular, the constants $c_0, c_1, \ldots, c_9$ are the same as given in the Standard Magnification Process described earlier.

We start our process with an $L_k(0)$-free parallelogram S_0 on an X-face. Omitting reference to the x-coordinate, this parallelogram has its non-parallel sides parallel to the vectors $\mathbf{u}_1$ and $\mathbf{u}_2$ given in terms of (6.3.40)–(6.3.42).

Suppose that $\text{diam}(S_0) \leqslant \alpha_k^3$. There is at least one of the 531141 congruent sub-parallelograms obtained by 729-fold division of each side of S_0 that goes through the 3-step magnification without splitting at any stage, and leads to a parallelogram S_3 on some X-face. Clearly

$$\frac{\text{area}(S_3)}{\text{area}(S_0)} = \frac{\alpha_k^{-3}}{531141} = (81\alpha_k)^{-3}.$$

For any positive integer $i \geqslant 3$ which is a multiple of 3, suppose that the parallelogram S_i that lies on some X-face satisfies $\text{diam}(S_i) \leqslant \alpha_k^3$. Then there is at least one of the 531141 congruent sub-parallelograms obtained by 729-fold division of each side of S_i that goes through the 3-step magnification without splitting at any stage, and leads to a parallelogram S_{i+3} on some X-face. Clearly

$$\frac{\text{area}(S_{i+3})}{\text{area}(S_i)} = (81\alpha_k)^{-3}.$$

We repeat this process iteratively, and stop when we reach an index $i = i_1$ which is a multiple of 3 and such that $\mathrm{diam}(S_{i_1}) > \alpha_k^3$. Clearly we have

$$\frac{\mathrm{area}(S_{i_1})}{\mathrm{area}(S_0)} = (81\alpha_k)^{-i_1}. \tag{6.3.50}$$

We now proceed following the Standard Magnification Process, starting at $i = i_1$ and ending the process at $i = i_0$.

The estimates (6.3.25)–(6.3.27) and (6.3.34) are now enhanced by (6.3.50) and replaced by

$$\left(\frac{3c_0}{\sqrt{\mathrm{area}(S_0)}}\right)^2 > \left(\frac{1}{81\alpha_k}\right)^{i_1} \left(\frac{c_0^*}{\alpha_k^{1/6}}\right)^{i_0-i_1-3}. \tag{6.3.51}$$

Finally, note that in view of (6.3.47), we have

$$\mathrm{area}(S_{i_1}) \geqslant \frac{\alpha_k^{1/2}(\mathrm{diam}(S_{i_1}))^2}{8+o_k(1)} > \frac{1}{8+o_k(1)}\alpha_k^{13/2}.$$

This implies, in view of the area growth estimates (6.3.19)–(6.3.21) of the magnification process between $i = i_1$ and $i = i_0$, that there is a positive absolute constant c_{10} such that

$$i_0 - i_1 \leqslant c_{10}, \tag{6.3.52}$$

an absolutely vital part of our argument.

Again, if (6.3.33) holds, then Lemma 6.3.2 demonstrates that the three facts (1)–(3) immediately before it lead to a contradiction, implying that the starting hypothesis is false. In other words, the first parallelogram S_0 of the sequence S_i cannot be $L_k(0)$-free, meaning that it must intersect $L_k(0)$.

Let $c_{11} = 5(c_{10} - 3)/6$. In view of (6.3.52), we have

$$\left(\frac{c_0^*}{\alpha_k^{1/6}}\right)^{i_0-i_1-3} = \left(\frac{c_0^*}{\alpha_k}\right)^{i_0-i_1-3} \alpha_k^{5(i_0-i_1-3)/6} \geqslant \left(\frac{c_0^*}{\alpha_k}\right)^{i_0-i_1-3} \alpha_k^{c_{11}}. \tag{6.3.53}$$

On the other hand, let $c_0^{***} = \min\{1/81, c_0^*\}$. Then it follows from (6.3.51) and (6.3.53) that

$$\left(\frac{3c_0}{\sqrt{\mathrm{area}(S_0)}}\right)^2 > \left(\frac{c_0^{***}}{\alpha_k}\right)^{i_0-3} \alpha_k^{c_{11}}. \tag{6.3.54}$$

Given any $\varepsilon > 0$, take k_0 to be an integer satisfying

$$k_0 \geqslant \frac{1}{2c_0^{***}} \left(\frac{1}{c_0^{***}}\right)^{2/\varepsilon}.$$

Then for any integer $k > k_0$, we have, in view of (6.3.1),

$$\left(\frac{c_0^{***}}{\alpha_k}\right)^{\varepsilon/2} > (2kc_0^{***})^{\varepsilon/2} \geqslant \frac{1}{c_0^{***}}. \tag{6.3.55}$$

Combining (6.3.54) and (6.3.55), we have

$$\left(\frac{3c_0}{\sqrt{\mathrm{area}(S_0)}}\right)^{2+\varepsilon} > \left(\frac{c_0^{***}}{\alpha_k}\right)^{i_0-3} \alpha_k^{c_{11}} \left(\frac{1}{c_0^{***}}\right)^{i_0-3} \alpha_k^{c_{11}\varepsilon/2}.$$

We may clearly assume that $\varepsilon \leqslant 2$. Then

$$\left(\frac{3c_0}{\sqrt{\mathrm{area}(S_0)}}\right)^{2+\varepsilon} > \left(\frac{1}{\alpha_k}\right)^{i_0-3} \alpha_k^{2c_{11}}.$$

Together with (6.3.33), we now conclude that

$$\text{length}(L_k(0)) = C_k^\star \alpha_k^{-3} \left(\frac{1}{\alpha_k}\right)^{i_0-3} < C_k^\star \alpha_k^{-3-2c_{11}} \left(\frac{3c_0}{\sqrt{\text{area}(S_0)}}\right)^{2+\varepsilon}.$$

This gives the conclusion of Theorem 6.1.2 in the special case of $\mathcal{L}_k$ when the half-infinite s-L-line of direction $(\alpha_k, \alpha_k^2, 1)$ *starts from the origin*.

The general case when the half-infinite s-L-line $\mathcal{L}_k$ with direction vector $\mathbf{v}_0 = (\alpha_k, \alpha_k^2, 1)$ can start at any arbitrary but fixed point in the L-solid goes along a similar way.

Let $L_k(0)$ be a "long" initial segment of $\mathcal{L}_k$. We define $L_k(1), L_k(2), L_k(3), \ldots$ successively in a similar way. The Standard Magnification Process and Enhanced Magnification Process remain valid.

Finally, note that in the proof of Lemma 6.3.2, one never uses the assumption that $\mathcal{L}_k$ starts from the origin. In the general case, one simply takes $\mathcal{L}_k^*$ long enough to include a whole detour crossing. □

6.4. **Generalizations of Theorems 6.1.1 and 6.1.2.** We now switch from the L-surface to a large class of polysquare surfaces, and show how we can find superdense geodesics.

A finite *polysquare surface*, tiled with unit size squares, is a 2-dimensional manifold that consists of a finite number of unit size squares glued together in such a way that any two squares either are disjoint, or have a common vertex, or have a common edge. Note that some authors refer to such a surface as an *origami*. It is equipped with flat metric, so it is a Riemann surface, with possible conical singularity or singularities, where every square face has zero curvature. The total curvature $2\pi\chi(S)$ in the well known Gauss–Bonnet formula, where $\chi(S)$ is the Euler characteristic of the polysquare surface S, is concentrated in the finitely many conical singularities.

We require connectivity in the precise sense that any two squares are "joined" by a chain of squares such that any two consecutive members of the chain share a common edge.

One example is the L-surface, first introduced in Section 6.1. A more familiar example is the cube surface shown in Figure 6.4.1.

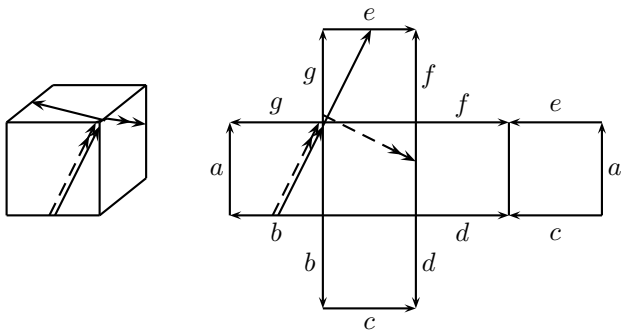

Figure 6.4.1: orbit singularity of geodesic flow on the cube surface leading to perpendicular directions on the net

It is well known that every polygonal surface has a plane model called the *net*, which is not uniquely determined. Similarly, every finite polysquare surface has a net. Such a net consists of two parts. The first part is a *polysquare region*, which is a finite, but not necessarily connected, subset of the lattice of squares on the plane. The second part of the net is a *complete boundary edge pairing with orientations* that defines which pair of edges on the boundary of the polysquare region are identified, according to the given orientation, to form a closed surface.

We restrict ourselves to *orientable* surfaces. If the polysquare region is a polygon, *orientability* of the surface is equivalent to the following simple "opposite orientation" requirement. As we go around the boundary, in every pair of the boundary pairing, the two edges in question must have opposite orientations.

The simplest boundary pairing with orientations comes from perpendicular translation as in the case of the L-surface. The boundary pairing in a net of the cube surface is more complicated; see Figure 6.4.1.

We study superdensity in geodesic flow on the cube surface. Similarly to the L-surface, geodesic flow on the cube surface has orbit-singularity at the vertices, so it is non-integrable. A novelty is that it is a 4-direction flow; see the picture on the right hand side in Figure 6.4.1.

There is a general trick to reduce a 4-direction geodesic flow on a polysquare surface to a 1-direction flow on a 4-times larger surface. We illustrate it on the cube surface. We take four 90-degree rotated copies of the net in Figure 6.4.1, and glue them together by making some specific edge-identifications between the different copies; see Figure 6.4.2.

Figure 6.4.2 shows a *translation surface*. It is obtained by gluing together the boundary edges with identical labels, which are parallel, so one is mapped to the other via translation. For example, the edge b_2 in the lower-left copy is identified with the edge b_2 in the lower-right copy of the net of the cube surface, and they are parallel vectors. And so on. This surface is a 4-fold covering of the cube surface, and its geodesics form a 1-direction flow.

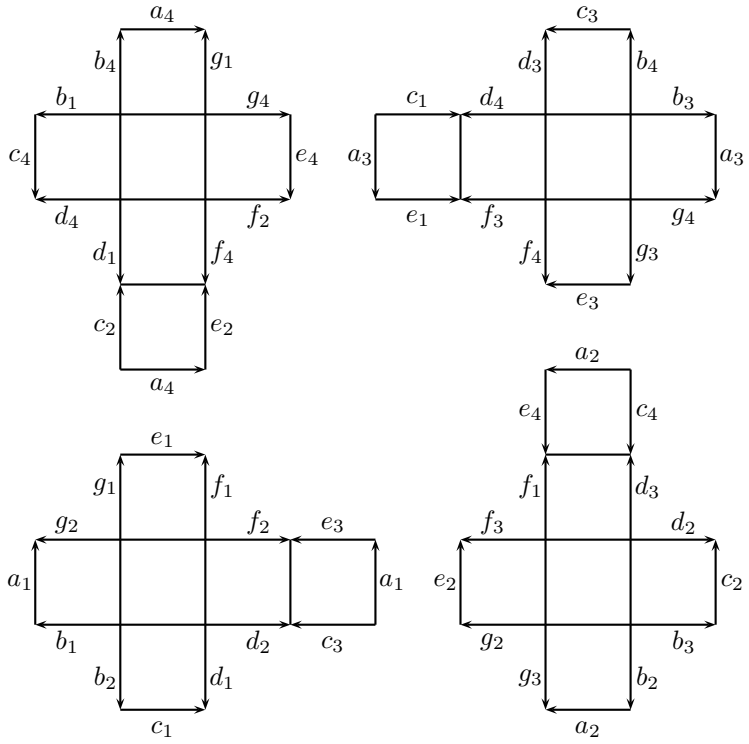

Figure 6.4.2: translation surface which is a 4-fold covering of the cube surface

This 4-copy construction works for any polysquare surface with 4-direction geodesic flow, thus explaining why it suffices to study 1-direction flow.

Similar 4-copy construction works for any billiard in a polysquare polygon. We refer to the polysquare polygon in Figure 6.4.3 as the "snake". Figure 6.4.3 shows how the "snake billiard" on the left is converted into a 1-direction flow on the right, where the 4-times larger polysquare surface obtained by gluing together 4 copies of the "snake" via iterated reflection across sides, called "unfolding", and using the

given boundary pairing which does not contain perpendicular pairs, and the result is a translation surface. We refer to this polysquare surface as the *snake-cross surface*.

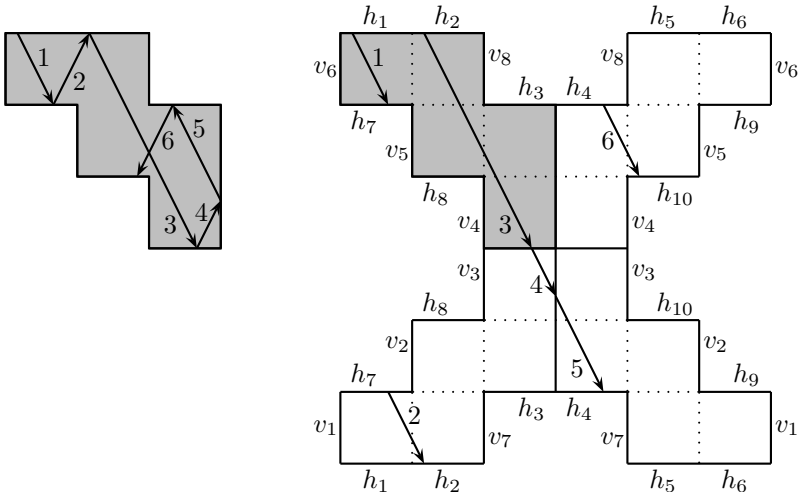

Figure 6.4.3: snake billiard and unfolding to obtain the snake-cross surface

It is a basic fact that a 1-direction geodesic flow on a polysquare surface *modulo one* is equivalent to the torus line flow in the unit square. Here *modulo one* means taking the fractional parts of the coordinates.

The next examples exhibit 1-direction geodesic flow, but there are novelties.

The polysquare surface on the left in Figure 6.4.4 has a missing square face, illustrated by the shaded region.

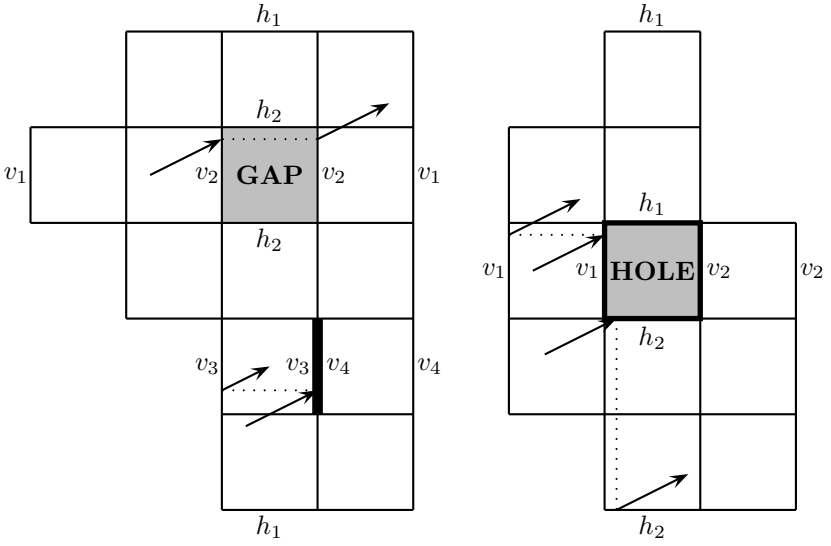

Figure 6.4.4: surfaces with gap, wall or hole

Note that the edge pairings make this missing part behave like a "gap". For instance, when a geodesic hits the edge v_2 on the left of this gap, it jumps to the corresponding point on the identified edge v_2 on the right of this gap, then continues on its way at the same slope. It also has a double edge, illustrated by the thick line segment, that behaves line a "wall". For instances, when a geodesic hits the edge v_3 on the left side of this wall, it jumps back to the corresponding point on the identified edge v_3 further back, then continues on its way at the same slope. Note that this surface has one vertical street of length 1, one vertical street of length 3, one vertical street of length 4, and one vertical street of length 5. It also has two horizontal streets of length 1, one horizontal street of length 2, and three horizontal

streets of length 3. So the street-LCM, the least common multiple of all the street lengths, is $3 \times 4 \times 5 = 60$.

The polysquare surface on the right in Figure 6.4.4 also has a missing square face, illustrated by the shaded region. But it behaves like a thick wall in both the horizontal and vertical direction. We shall call it a "hole".

Note that some of the boundary pairings are omitted from the pictures, since they come from the simplest form of perpendicular translation.

Remark. We use the words "gap", "wall" and "hole" purely for convenience. The precise details are given by the edge identification process.

We use the word "gap" when opposite edges of the missing square(s) are identified with each other. Thus when a geodesic reaches such an edge, it "jumps" over to the corresponding point on the identified edge, which is "ahead", and then continues on its way. It remains on the *same* street.

We use the word "hole" when opposite edges of the missing square(s) are not identified with each other, but instead with edges elsewhere. Thus, in the examples we have discussed so far, when a geodesic reaches such an edge, it finds that this edge is identified with another edge which is "behind". Any square on the other side of the missing square(s) is part of a *different* street.

Indeed, there can be missing squares that can be hybrid-gap-holes, in the sense that it may act like a gap in the horizontal direction and like a hole in the vertical direction. Furthermore, there may be edge identifications that make missing squares or walls far more complex than we have described so far. The important point always to bear in mind is that the edge pairings are the *be-all-and-end-alls*.

As Figure 6.4.2 shows, the analog street-LCM for the cube surface is 4, since every street has length 4.

Similarly, the analog street-LCM in Figure 6.4.3 is also 4, since every street has length 2 or 4.

We have the following generalization of Theorem 6.1.1.

Theorem 6.4.1. *Let $\mathcal{P}$ be an arbitrary finite polysquare surface. Let α be a badly approximable number with continued fraction expansion*

$$\alpha = [a_0; a_1, a_2, a_3, \ldots] = a_0 + \cfrac{1}{a_1 + \cfrac{1}{a_2 + \cfrac{1}{a_3 + \cdots}}} \tag{6.4.1}$$

such that for every $i \geqslant 0$, the digit a_i is divisible by the street-LCM of $\mathcal{P}$. Then any half-infinite 1-directional geodesic with slope α exhibits superdensity on $\mathcal{P}$.

Using unfolding such that as illustrated in Figure 6.4.3, we can show that a 4-directional billiard trajectory in a polysquare can be reduced to a 1-directional geodesic on the 4-copy version of the polysquare. Thus the conclusion of Theorem 6.4.1 applies also to billiards in a finite polysquare.

Let $\alpha > 0$ be any badly approximable number satisfying (6.4.1), with the extra restriction that every digit $a_i \geqslant 4$, $i \geqslant 1$, is divisible by 4. Theorem 6.4.1 implies that any geodesic on the cube surface with slope equal to this α exhibits superdensity. Similarly, any billiard trajectory in the snake region given in Figure 6.4.3 with initial slope equal to this α exhibits superdensity.

Let $\alpha > 0$ be any badly approximable number satisfying (6.4.1), with the extra restriction that every digit $a_i \geqslant 60$, $i \geqslant 1$, is divisible by 60. Theorem 6.4.1 implies that any geodesic on the surface in the picture on the left in Figure 6.4.4 with slope equal to this α exhibits superdensity.

As Theorem 6.4.1 is a generalization of Theorem 6.1.1, we can similarly formulate an analogous generalization of Theorem 6.1.2. It simply means that we increase the

dimension by one. The concept of *polycubes*, *i.e.*, cube-tiled solids, is a straightforward generalization of the concept of polysquare surfaces. For example, a 1-direction geodesic flow in a polycube *modulo one*, *i.e.*, taking the fractional parts of the coordinates, is equivalent to the torus line flow in the unit cube. The horizontal and vertical streets are of course replaced by the X-streets, Y-streets, and Z-streets. Such a "street" means a box $[0,\ell] \times [0,1] \times [0,1]$, where the long side is parallel to the x-axis, or a box $[0,1] \times [0,\ell] \times [0,1]$, where the long side is parallel to the y-axis, or a box $[0,1] \times [0,1] \times [0,\ell]$, where the long side is parallel to the z-axis. We call the integer parameter $\ell \geqslant 1$ the length of the street.

We have the following generalization of Theorem 6.1.2.

Theorem 6.4.2. *Let $\mathcal{P}$ be an arbitrary finite polycube, and let $h = h(\mathcal{P})$ denote the street-LCM of $\mathcal{P}$, i.e., the lowest common multiple of all the street lengths in $\mathcal{P}$. For any fixed constant $\varepsilon > 0$, there exist infinitely many explicit 3-dimensional vectors $\mathbf{v}_0$ such that every half-infinite 1-directional geodesic $\mathcal{L}(\mathbf{v}_0; t)$, $t \geqslant 0$, with direction vector $\mathbf{v}_0$ and arc-length parametrization, exhibits time-quantitative density in $\mathcal{P}$ in the following precise sense. There is an effectively computable threshold constant $C_0 = C_0(\varepsilon; h; \mathbf{v}_0)$ such that for every integer $n \geqslant C_0$ and every point Q in $\mathcal{P}$, the initial segment $\mathcal{L}(\mathbf{v}_0; t)$, $0 < t < n^{2+\varepsilon}$, gets $1/n$-close to Q.*

In particular, for any fixed constant $\varepsilon > 0$, there is a threshold $k_0 = k_0(\varepsilon)$ such that for every integer $k \geqslant k_0$, the root $\alpha = \alpha(k)$ of the cubic equation $x^3 + hkx - 1 = 0$ in the interval

$$\frac{1}{hk+1} < \alpha < \frac{1}{hk} \tag{6.4.2}$$

gives rise to a vector $\mathbf{v}_0 = (\alpha, \alpha^2, 1)$ that satisfies the requirements.

Using 3-dimensional unfolding, we can show that an 8-directional billiard trajectory in a polycube can be reduced to a 1-directional geodesic on the 8-copy version of the polycube. Thus the conclusion of Theorem 6.4.2 applies also to billiards in a finite polycube.

Theorem 6.4.2 also raises the following interesting question.

Open Problem 2. *Let $\mathcal{P}$ be an arbitrary finite polycube. Does there exist a half-infinite 1-directional geodesic that exhibits superdensity on $\mathcal{P}$?*

First we prove the 2-dimensional result.

Proof of Theorem 6.4.1. The proof is a fairly straightforward adaptation of the proof of Theorem 6.1.1. The key concept of *street* in the general case means a *maximal* size strip of ℓ consecutive unit squares, possibly punctuated by gaps but not separated by walls, arranged horizontally or vertically. We call ℓ the length of the street. The concept of *street corner*, such as those in Figures 6.2.2 and 6.2.3 for the L-shape, in the general case means the intersection of a horizontal side of a horizontal street and a vertical side of a vertical street.

The missing ingredient is a suitable analog of Lemma 6.2.1 in the general case. However, the discussion immediately after the statement of Lemma 6.2.1 and before its proof sets the tone of this discussion.

The reader may recall that our earlier discussion in connection with the proof of Lemma 6.2.1 involves working out ancestors of almost vertical units and almost horizontal units by brute force, where we diligently list ancestors at every stage and make use of the Extension Rule. Whereas for any *given* finite polysquare $\mathcal{P}$, we can repeat this brute force approach with a possibly extremely tedious exercise, in the general case, we have no precise information on the structure of the polysquare $\mathcal{P}$ to even contemplate such a crude approach. As it turns out, the solution is relatively simple.

Instead of listing all possible almost vertical units, we classify them into two types. Consider a given square of the polysquare surface, and consider almost vertical units that start from the bottom edge of this square. We say that the almost vertical unit is of type $\uparrow$ in the square if it starts from the bottom edge of the square and arrives at the top edge of the same square without intersecting a vertical side along the way, as shown in the picture on the left in Figure 6.4.5. We say that the almost vertical unit is of type $\nmid$ in the square if it starts from the bottom edge of the square but then hits the right edge of the same square, as shown in the picture on the right in Figure 6.4.5. Where the unit proceeds to after intersecting the right edge of the square depends on whether there is another square to the right.

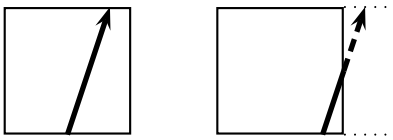

Figure 6.4.5: almost vertical units $\uparrow$ and $\nmid$ in the square

Likewise, instead of listing all possible almost horizontal units, we classify them into two types. Consider a given square of the polysquare surface, and consider almost horizontal units that start from the left edge of this square. We say that the almost horizontal unit is of type $\rightarrow$ in the square if it starts from the left edge of the square and arrives at the right edge of the same square without intersecting a horizontal side along the way, as shown in the picture on the left in Figure 6.4.6. We say that the almost vertical unit is of type $\mapsto$ in the square if it starts from the left edge of the square but then hits the top edge of the same square, as shown in the picture on the right in Figure 6.4.6. Where the unit proceeds to after intersecting the top edge of the square depends on whether there is another square above.

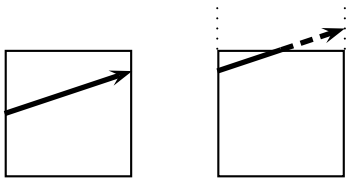

Figure 6.4.6: almost horizontal units $\rightarrow$ and $\mapsto$ in the square

Recall that Lemma 6.2.1 concerns exhibiting corner cuts. It is clear that a corner cut is a unit of type $\nmid$ or $\mapsto$, but not one of type $\uparrow$ or $\rightarrow$. We shall also start our ancestor process by assuming that the first unit is part of a much longer geodesic, so that we may use the Extension Rule.

First we define the $\mathcal{P}$-distance between any two distinct square faces S_1 and S_2 in the polysquare surface $\mathcal{P}$. We say that their $\mathcal{P}$-distance is 1 if they belong to the same horizontal street or vertical street. Otherwise, we consider a shortest sequence of alternate horizontal and vertical streets such that the first contains S_1, the last contains S_2, and any two consecutive streets intersect. Then the length of this sequence is the $\mathcal{P}$-distance between S_1 and S_2. In the picture on the left in Figure 6.4.7, the two square faces S_1 and S_2 have $\mathcal{P}$-distance 2, since the horizontal street containing S_1 intersects the vertical street containing S_2, although the vertical street containing S_1 may not necessarily intersect the horizontal street containing S_2. In the picture on the right, the two square faces S_1 and S_2 also have $\mathcal{P}$-distance 2, since the vertical street containing S_1 intersects the horizontal street containing S_2.

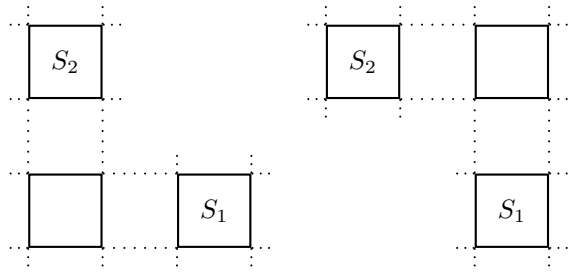

Figure 6.4.7: square faces S_1 and S_2 with $\mathcal{P}$-distance 2

The shortline process discussed earlier replaces a detour crossing with a shortcut. Here we study the reverse process. Given a finite almost vertical (resp. horizontal) geodesic, we can break it up into a number of *whole* units, and possibly two *fractional* units at the end. Each whole unit is the shortcut of an almost horizontal (resp. vertical) detour crossing. Each of the fractional units, if extended to a full unit, is also the shortcut of an almost horizontal (resp. vertical) detour crossing. For these, we shorten the almost horizontal (resp. vertical) detour crossing by the same fraction and at the appropriate end. We then take the union of these almost horizontal (resp. vertical) detour crossings and fractional almost horizontal (resp. vertical) detour crossings. The union is a finite almost horizontal (resp. vertical) geodesic. We call this the *ancestor geodesic* of the original almost vertical (resp. horizontal) geodesic.

Lemma 6.4.1. *Suppose that $\mathcal{P}$ is an arbitrary polysquare surface with finite street-LCM and with 1-direction almost vertical geodesic flow V of slope α which is an irrational number given by* (6.4.1)*, where every continued fraction digit is a positive integer multiple of the street-LCM of $\mathcal{P}$. Let K denote the $\mathcal{P}$-diameter, i.e. the maximum $\mathcal{P}$-distance between any two square faces of $\mathcal{P}$. Let $\mathcal{V}$ (resp. $\mathcal{H}$) denote a finite almost vertical (resp. horizontal) geodesic made up of 4 successive detour crossings of the i-generation shortline of V for some even (resp. odd) integer $i \geqslant 2K$. Then in every square face of $\mathcal{P}$, the $2K$-generation ancestor geodesic of $\mathcal{V}$ (resp. $\mathcal{H}$) gives rise to an almost vertical unit of type $\nmid$ (resp. horizontal unit of type $\nmid\!\!\mapsto$) in the square.*

We shall only prove Lemma 6.4.1 for $\mathcal{V}$, as the argument for $\mathcal{H}$ is similar. We need the following.

Replacement Rule. Replace a unit by another unit in the same detour crossing.

We first prove the following intermediate result.

Lemma 6.4.2. *Under the hypotheses of Lemma 6.4.1, suppose that S' and S'' are two square faces of $\mathcal{P}$ that lie on the same horizontal or vertical street. Suppose that A is an almost vertical unit of type $\uparrow$ or $\nmid$ in S'. Suppose further that the Extension Rule and the Replacement Rule apply. Then S'' contains an almost vertical unit of type $\uparrow$ or $\nmid$ in S'' that is a 2-generation ancestor of A or some almost vertical unit of type $\uparrow$ or $\nmid$ replacing A.*

Proof. (i) Suppose that S' and S'' lie on the same horizontal street. Consider the almost horizontal detour crossing for which A is the shortcut. This detour crossing must contain a fractional part of an almost horizontal unit of type $\nmid\!\!\mapsto$ that intersects the starting point of A. This fractional unit intersects the square face S'. Since the Extension Rule applies, we may assume that this fractional unit is extended to a full unit, as shown in Figure 6.4.8 if A is of type $\uparrow$ in S' and in Figure 6.4.9 if A is of type $\nmid$ in S'.

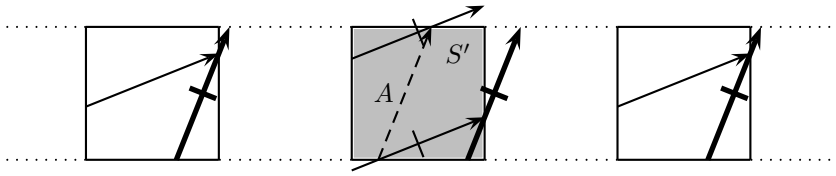

Figure 6.4.8: working along a horizontal street starting with a unit of type ↑

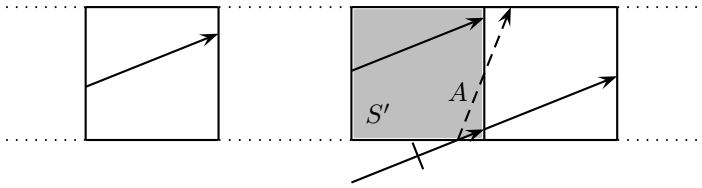

Figure 6.4.9: working along a horizontal street starting with a unit of type ↟

On the other hand, this almost horizontal detour crossing also gives rise to a unit of type → in every other square face that is in the same horizontal street that contains S'. Note that each of these almost horizontal units ↠ and → is a 1-generation ancestor of A, with the end point intersecting the right edge of the square. This almost horizontal unit is the shortcut of an almost vertical detour crossing that contains a fractional part of an almost vertical unit of type ↟ that intersects the end point of the almost horizontal unit under consideration. Since the Extension Rule applies, we may assume that this fractional unit is extended to a full unit, as shown in Figure 6.4.8 by the bold arrows (note that we have not inserted these in Figure 6.4.9), and this unit is a 2-generation ancestor of A.

In particular, each of the two square faces S' and S'' contains such a 2-generation ancestor of A.

(ii) Suppose that S' and S'' lie on the same vertical street. Note that the almost vertical unit A in the square face S' is part of an almost vertical detour crossing of the vertical street containing S'. This detour crossing has an almost vertical unit in every square face in this vertical street. Thus the square face S'' contains an almost vertical unit B that is in the same almost vertical detour crossing as A. Starting with B in S'' and considering the horizontal street containing S'', it follows from (i) that S'' contains a 2-generation ancestor of B. □

Proof of Lemma 6.4.1. Let A be an almost vertical unit in the two middle detour crossings in $\mathcal{V}$ that intersects the bottom edge of some square face S_1 in $\mathcal{P}$. Since any other square face S in $\mathcal{P}$ has $\mathcal{P}$-distance at most K from S_1, there exists a sequence of square faces $S_2, \ldots, S_L$, where $L \leqslant K$, such that any consecutive pair of square faces lie on the same horizontal or vertical street, and such that S_1 and S_2 lie on the same horizontal or vertical street, and S_L and S lie on the same horizontal or vertical street. Applying Lemma 6.4.2 iteratively at most K times gives us the desired result.

It remains to justify the use of the Extension Rule and Replacement Rule.

The Extension Rule means that ancestor units that are only *fractional* in the detour crossing for which A is the shortcut are counted in full. Such an ancestor unit is also part of the ancestry of an almost vertical unit in $\mathcal{V}$ adjoining A. To make sure that the unit ↟ at the end of the proof is a *genuine* 4-generation ancestor of some unit in $\mathcal{V}$, and not there merely as a consequence of the Extension Rule, we start with a geodesic $\mathcal{V}$ with four detour crossings and pick a unit A in the two middle detour crossings. The two detour crossings at either end of $\mathcal{V}$ then give us ample cover. These extra detour crossings also justify the use of the Replacement Rule. □

Lemma 6.4.1 is precisely the generalization of Lemma 6.2.1 that we need to complete the proof of Theorem 6.4.1. We can now prove Theorem 6.4.1 with a fairly straightforward adaptation of the *magnification process of empty intervals*, the basic idea of the proof of Theorem 6.1.1 for the L-surface, as long as the Rule for Magnification in a Polysquare is followed. □

The restriction that the continued fraction digits of α are divisible by the street-LCM in Theorem 6.4.1 implies that the superdense slopes α satisfying this digit condition form a nowhere dense set in the unit interval. There is, however, a simple geometric trick to extend this set of superdense slopes to a dense set in the unit interval for every polysquare surface.

The simple idea is that every polysquare surface generates infinitely many new polysquare surfaces as follows. Consider, for instance, the L-surface of 3 square faces. By drawing the two diagonals on each one of the 3 square faces, *i.e.*, putting a $\times$ in every square face, we obtain a new polysquare surface with 6 smaller square faces, each with half the area; see Figure 6.4.10. The genus remains the same. By using the boundary pairing in the picture on the right in Figure 6.4.10, we obtain the so-called *diagonal subdivision* surface of the L-surface, or DS-L-surface. Here the DS-L-surface is not in the usual horizontal-vertical position, but rotating the picture by 45 degrees does not alter the nature of the question at hand.

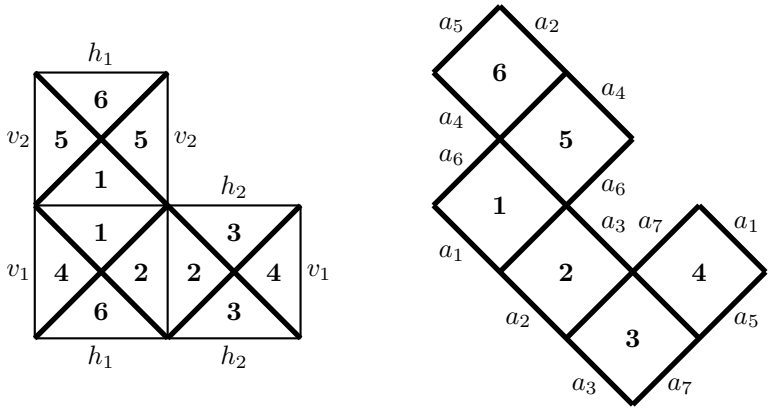

Figure 6.4.10: L-surface and DS-L-surface

The concept of diagonal decomposition into smaller squares has a far-reaching generalization. For example, Figure 6.4.11 below shows the $(k, 1)$-decomposition of a square face in the special cases $k = 2$ and $k = 3$.

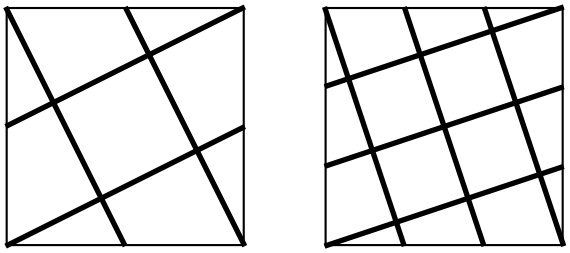

Figure 6.4.11: $(2, 1)$-decomposition and $(3, 1)$-decomposition

The full generalization comes from choosing an arbitrary integer ℓ satisfying $1 \leqslant \ell < k$ such that k and ℓ are relatively prime. Applying the corresponding (k, ℓ)-decomposition on every square face of of an arbitrary polysquare surface $\mathcal{P}$ with 1-direction geodesic flow, we obtain the polysquare surface (k, ℓ)-S-$\mathcal{P}$, where S stands for "subdivision". We emphasize the fact that the slope ℓ/k can be *any* rational number between 0 and 1, and of course the rationals form a dense set. The last step

is to apply Theorem 6.4.1 for an arbitrary polysquare surface (k, ℓ)-S-$\mathcal{P}$. Thus we obtain the following result.

Corollary of Theorem 6.4.1. *Let $\mathcal{P}$ be any finite polysquare surface with 1-direction geodesic flow. Then the set of slopes for which every infinite geodesic flow of this slope exhibits superdensity on $\mathcal{P}$ is dense in the unit interval.*

Next we switch to the 3-dimensional problem.

Proof of Theorem 6.4.2. Let $\mathcal{P}$ be a finite polycube with 1-direction geodesic flow. We refer to its unit size cubes as *cube atoms*. Assume that the set of street sizes is *bounded*, and let $h = h(\mathcal{P}) < \infty$ denote the street-LCM of $\mathcal{P}$, taking into account all of the X-streets, Y-streets and Z-streets. Consider the 1-direction geodesic flow with direction $\mathbf{v}_0 = (\alpha, \alpha^2, 1)$, where α is the root of the cubic equation $x^3 + hkx - 1 = 0$ in the interval (6.4.2).

We assume that the reader is familiar with the details of the proof of Theorem 6.1.2, and here we use analogous notation. Since $\mathbf{v}_0$ is almost parallel to the z-axis, we refer to a unit in direction $\mathbf{v}_0$ as a Z-unit. The ancestor units of a Z-unit are the Y-units in direction $\mathbf{v}_2 = (\alpha^2, 1, \alpha)$. The ancestor units of a Y-unit are the X-units in direction $\mathbf{v}_1 = (1, \alpha, \alpha^2)$. The ancestor units of an X-unit are the Z-units in direction $\mathbf{v}_0$.

Next we define the 3-dimensional $\mathcal{P}$-distance between any two distinct cube atoms H_1 and H_2 in a polycube $\mathcal{P}$ with finite street-LCM. If some X-street or Y-street or Z-street in $\mathcal{P}$ contains both H_1 and H_2, then the $\mathcal{P}$-distance between H_1 and H_2 is 1. Otherwise, we consider the shortest sequence of streets such that the first contains H_1, the last contains H_2, and any two consecutive streets in the sequence intersect. Then the length of this sequence is the $\mathcal{P}$-distance between H_1 and H_2.

We have the following analog of Lemma 6.4.1.

Lemma 6.4.3. *Suppose that $\mathcal{P}$ is a finite polycube with finite street-LCM equal to h and with 1-direction geodesic flow $\mathcal{L}$ with direction vector $\mathbf{v}_0$ as given in the statement of Theorem 6.4.2. Let K denote the $\mathcal{P}$-diameter, i.e. the maximum $\mathcal{P}$-distance between any two cube atoms of $\mathcal{P}$. Let $\mathcal{V}$ denote a finite geodesic made up of 4 successive detour crossings of the i-generation shortline of $\mathcal{L}$ for some integer $i \geqslant 3K$ which is a multiple of 3. Then in every cube atom H of $\mathcal{P}$, the $3K$-generation ancestor geodesic of $\mathcal{V}$ gives rise to a Z-unit in the cube atom that intersects the right X-face of H.*

We first prove the following intermediate result.

Lemma 6.4.4. *Under the hypotheses of Lemma 6.4.3, suppose that H' and H'' are two cube atoms of $\mathcal{P}$ that lie on the same X-street, Y-street or Z-street. Suppose that a Z-unit A intersects the right X-face of H', at a point closer to the back Y-face of H' than to the front Y-face of H'. Suppose further that $hk \geqslant 4$, and that the Extension Rule and the Replacement Rule apply. Then H'' contains a Z-unit that is a 3-generation ancestor of A or some Z-unit replacing A, and this Z-unit intersects the right X-face of H'', at a point closer to the back Y-face than to the front Y-face of H''.*

Proof. We first make a simple observation, illustrated in Figure 6.4.12 below which is the view from above the cube atom H'. Here the gray arrow represents the projection of the left-to-right detour crossing that contains the starting part of A, and the projection of the point at which A intersects the right X-face of H' is the point at the end of this arrow. Note that the y-span of a left-to-right detour crossing is equal to α, so it follows from $hk \geqslant 4$ and the assumption on the position of the

point of intersection of A with the right X-face that this detour crossing does not intersect any Y-face of $\mathcal{P}$.

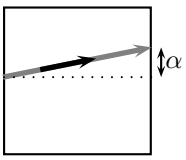

Figure 6.4.12: the view from above the cube atom H'
and the vertical projection of the left-to-right detour crossing
that contains the starting part of A

The condition $hk \geqslant 4$ also ensures that this detour crossing traverses the Z-street containing H' at least 4 times. In Figure 6.4.12, the black arrow represents one such occasion consisting entirely of Z-units. Note that such a traversal does not intersect any X-face or Y-face. We have therefore established the following.

$(*)$ Every cube atom on the same Z-street as H' contains a Z-unit with starting point on the bottom Z-face of the cube atom and end point on the top Z-face of the same cube atom.

In particular, we can now replace A with a Z-unit in H' which forms part of this traversal. Note that this unit has starting point on the bottom Z-face of H' and end point on the top Z-face of H'. Suppose that this Z-unit is A'.

The Z-unit A' is shown in Figure 6.4.13 below. Clearly it is the shortcut of a bottom to top detour crossing of the Y-street containing H'. By its construction, we have ensured that this detour crossing does not intersect any X-face of $\mathcal{P}$.

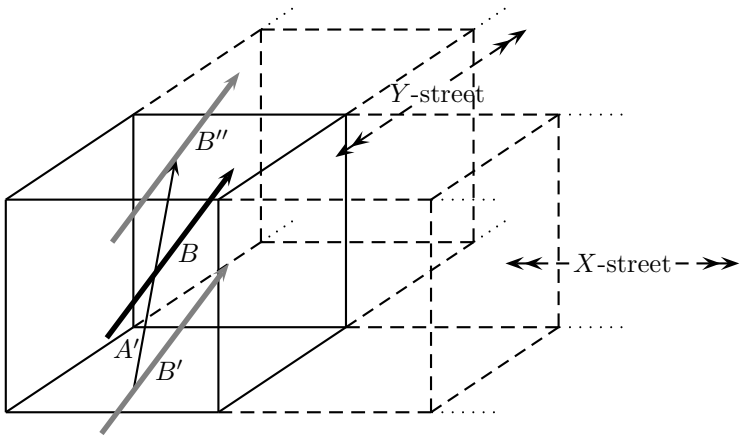

Figure 6.4.13: the cube atom H' and some units

The bottom to top detour crossing starts from the intersection of the Y-unit B' with A', and ends with the intersection of the Y-unit B'' with A'. The condition $hk \geqslant 4$ also ensures that this detour crossing traverses the Y-street containing H' at least 4 times, so it contains a Y-unit in every cube atom of the Y-street containing H', each with starting point on the front Y-face of the cube atom and end point on the back Y-face of the same cube atom. Clearly every such Y-unit is a 1-generation ancestor of A'. For the cube atom H', this Y-unit is given as B in Figure 6.4.13 with the dark thick arrow. We can summarize our argument thus far by as follows.

$(**)$ Every cube atom on the Y-street containing H' contains a Y-unit which is a 1-generation ancestor of A', with starting point on the front Y-face of the cube atom and end point on the back Y-face of the same cube atom.

Suppose first that H' and H'' are on the same X-street. Note that the Y-unit B is the shortcut of a front to back detour crossing of this X-street. By its construction, we have ensured that this detour crossing does not intersect any Z-face of $\mathcal{P}$. The condition $hk \geqslant 4$ also ensures that this detour crossing traverses the X-street containing H' at least 4 times, as shown in Figure 6.4.14 below.

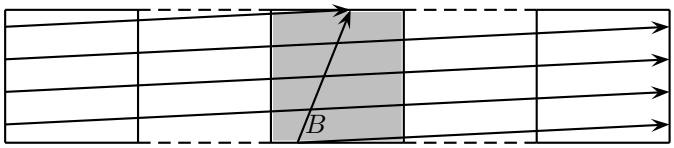

Figure 6.4.14: vertical view of detour crossing with shortcut B

This detour crossing gives rise to at least 4 X-units in H'', with end point on the right X-face of H''. The end point of at least one of these is clearly closer to the back Y-face than the front Y-face of H''. The X-unit with this endpoint is the shortcut of a left to right detour crossing, ending with a Z-unit that intersects this endpoint. Clearly this is a 3-generation ancestor of A' and intersects the right X-face of H'', at a point closer to the back Y-face than the front Y-face of H''.

Suppose next that H' and H'' are on the same Y-street. Then it follows from $(**)$ that H'' contains a Y-unit which is a 1-generation ancestor of A', with starting point on the front Y-face of the cube atom and end point on the back Y-face of the same cube atom. We now simply repeat the earlier argument on the X-street that contains H''.

Suppose finally that H' and H'' are on the same Z-street. Then it follows from $(*)$ that H'' contains a Z-unit in the same detour crossing that intersects A, with starting point on the bottom Z-face of the cube atom and end point on the top Z-face of the same cube atom. We now simply repeat the earlier argument on the X-street that contains H''. □

Proof of Lemma 6.4.3. Let A be a Z-unit in the two middle detour crossings of $\mathcal{V}$ that intersects the right X-face of some cube atom H_1 in $\mathcal{P}$.

If the intersection point is closer to the back Y-face than to the front Y-face of H_1, then since any other cube atom H in $\mathcal{P}$ has $\mathcal{P}$-distance at most K from H_1, applying Lemma 6.4.3 iteratively at most K times gives us the desired result.

On the other hand, if the intersection point is closer to the front Y-face than to the back Y-face of H_1, then we simply proceed to the next left to right detour crossing that crosses a Z-street that contains a cube atom H_0 that is in the same X-street as H_1. This new detour crossing contains the end part of A.

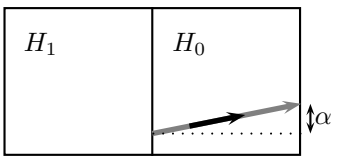

Figure 6.4.15: view from above: using the next detour crossing

We now choose a Z-unit A' in H_0 judiciously, and argue as before.

We can justify the use of the Extension Rule and Replacement Rule in the same way as for Lemma 6.4.1.

Finally, note that the condition $hk \geqslant 4$ in Lemma 6.4.3 is easily taken care of in Theorem 6.4.2 by choosing the threshold $k_0(\varepsilon)$ appropriately. □

As in the proof of Theorem 6.1.2 for the L-solid, we shall use the Enhanced Magnification Process. Then Lemma 6.4.3 is clearly not enough, as we want to show that some ancestor geodesic intersects every one of the c_0^2 standard congruent

subsquares of side length c_0^{-1} on a square face. To achieve this, we shall do some rescaling.

Corresponding to the finite polycube $\mathcal{P}$, we construct a polycube $c_0\mathcal{P}$ as follows. For every cube atom H in $\mathcal{P}$, we magnify H about the origin $\mathbf{0}$ by a factor c_0 to obtain a cube c_0H of side length c_0, and then split this big cube into c_0^3 cube atoms of unit side length in the natural way. It is not difficult to see that $c_0\mathcal{P}$ is a finite polycube. Furthermore, suppose that $R_1 \subset c_0H_1$ and $R_2 \subset c_0H_2$ are cube atoms of $c_0\mathcal{P}$, where H_1 and H_2 are cube atoms of $\mathcal{P}$, then it is not difficult to show that

$$c_0\mathcal{P}\text{-distance}(R_1, R_2) \leqslant \mathcal{P}\text{-distance}(H_1, H_2) + 3. \tag{6.4.3}$$

For any 1-direction geodesic flow $\mathcal{L}$ in $\mathcal{P}$ with arc length parametrization, where the length after time t is given by t, we consider the 1-direction geodesic flow

$$\mathcal{L}_{c_0} = \{c_0\mathbf{v} : \mathbf{v} \in \mathcal{L}\}$$

in $c_0\mathcal{P}$, with parametrization such that the length after time t is given by c_0t. Likewise, for any finite geodesic $\mathcal{V}$ in $\mathcal{P}$, we consider the finite geodesic

$$\mathcal{V}_{c_0} = \{c_0\mathbf{v} : \mathbf{v} \in \mathcal{V}\}$$

in $c_0\mathcal{P}$.

Lemma 6.4.5. *Suppose that $\mathcal{P}$ is a finite polycube with finite street-LCM and with 1-direction geodesic flow $\mathcal{L}$ with direction vector $\mathbf{v}_0$ as given in the statement of Theorem 6.4.2. Let K denote the $\mathcal{P}$-diameter. Let $\mathcal{V}$ denote a finite geodesic made up of 4 detour crossings of the i-generation shortline of $\mathcal{L}$ for some integer $i \geqslant 9(K+1)$ which is a multiple of 3. Then for every cube atom H of $\mathcal{P}$, the $9(K+1)$-generation ancestor geodesic of $\mathcal{V}$ intersects every one of the c_0^2 standard congruent subsquares of side length c_0^{-1} on the right X-face of H.*

Sketch of proof. We consider the geodesic $\mathcal{L}_{c_0}$ with direction vector $\mathbf{v}_0$ in the polycube $c_0\mathcal{P}$. Noting the inequality (6.4.3), we now apply Lemma 6.4.3 to $c_0\mathcal{P}$. Finally we rescale $c_0\mathcal{P}$ back to $\mathcal{P}$. □

We can now complete the proof of Theorem 6.4.2 in a similar fashion as for Theorem 6.1.2 in Section 6.3, as long as the Rule for Magnification in a Polycube is followed. □

6.5. **Time-quantitative density in a square-maze.** Here we describe a large class of *infinite* polysquare surfaces for which geodesic flow exhibits density. As usual, we are interested in the time-quantitative aspects of density.

We call an infinite polysquare surface a *square-maze* if the lengths of the horizontal and vertical streets are uniformly bounded. Let $\ell \geqslant 2$ be any integer. We call a square-maze an *ℓ-square-maze* if every street, whether horizontal or vertical, has length at most ℓ, and there is a street that has length equal to ℓ. We choose an arbitrary square face of $\mathcal{P}$, choose any of its 4 corner points, and refer to this particular corner point as the origin $\mathbf{0}$.

If geodesic flow on the square-maze is a 4-direction flow, like in the case of billiards, then of course we can apply the standard trick of a 4-copy construction as in Figure 6.4.2 or the trick of unfolding like in Figure 6.4.3. Such a geometric trick converts the original problem to an equivalent problem of geodesic flow on a different ("4-copy") square-maze with 1-direction flow.

The class of square-mazes forms a very rich family of infinite surfaces. Note that for a fixed positive integer ℓ there are completely different ℓ-square-mazes with completely different "growth-rate of the neighborhood", *i.e.*, the rate of growth of the number of square faces that are at a $\mathcal{P}$-distance at most N from a given

square face as a function of N. Nevertheless, somewhat surprisingly, this "growth-rate of the neighborhood" does not show up in our time-quantitative density result Theorem 6.5.1 below.

Along the way, we shall give examples of mazes that exhibit linear, or quadratic, or cubic, or exponential "growth-rate of the neighborhood".

We call our first example an "infinite shark"; see Figure 6.5.1 below. The alternating vertical "walls", from above and below, resemble shark-teeth, explaining the name. To get an infinite flat surface in Figure 6.5.1, we use the simplest perpendicular boundary pair identification: horizontal translation for vertical edges and vertical translation for horizontal edges. In the resulting surface every street has length 2, so it is a 2-square-maze.

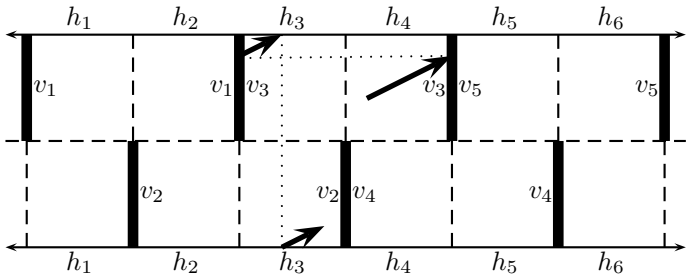

Figure 6.5.1: infinite shark surface as a 2-square-maze and 1-direction geodesic flow

For $\ell \geqslant 3$ we have the freedom to change the gaps between the teeth of the shark. This gives an uncountable set of *aperiodic* ℓ-square-mazes with linear growth-rate of the neighborhood similar to Figure 6.5.1.

By the way, already the set of all 2-square-mazes is uncountable. To justify this claim we can introduce the infinite staircase in Figure 6.5.2 below. Moving from left to right the staircase goes down, so we refer to it as a *down-staircase*. Reflecting it across a vertical line we obtain an infinite *up-staircase*.

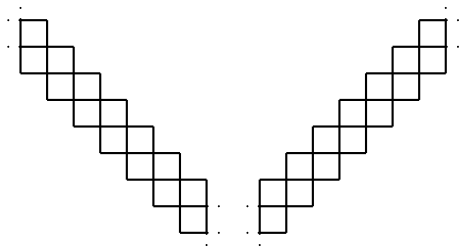

Figure 6.5.2: infinite down-staircase and infinite up-staircase

Figure 6.5.2 shows the infinite staircase region, which is a 45-degree "tilted tower" of infinitely many 2×1 rectangles. The infinite staircase *surface* is obtained from the infinite region by the simplest boundary identification: pairs of vertical boundary edges are identified by horizontal translation, and pairs of horizontal boundary edges are identified by vertical translation.

A 2-square-maze is intuitively an "infinite snake", where we have an infinite degree of freedom of going up-or-down and left-or-right and by using "walls" if necessary. For example, start with any finite down- or up-staircase surface, glue to it any finite shark surface, next glue to it any finite down- or up-staircase surface, next glue to it any finite shark surface, and so on. This simple construction already provides an uncountable set of 2-square-mazes. Of course every 2-square-maze has a linear growth-rate of the neighborhood.

Figure 6.5.3 shows a double-periodic 3-square-maze, which clearly exhibits quadratic growth-rate of the neighborhood. Here the building blocks are 3×3 squares

with "holes" in the middle, and these blocks are glued together by 1×1 squares in such a way that they form a 2-dimensional lattice (somewhat like $\mathbb{Z}^2$), creating further "holes". We use gray color for the "holes", which we also indicate by the letter **H**, and the boundary pair identification, some of which are indicated, ensures that these holes are *no-go zones* as opposed to the "gap" in Figure 6.4.4. Here every right vertical edge of a hole is identified with the left vertical edge (on the same horizontal street) of the next hole to the right, and every top horizontal edge of a hole is identified with the bottom horizontal edge (on the same vertical street) of the next hole above. Thus we obtain a surface where every street has length 3.

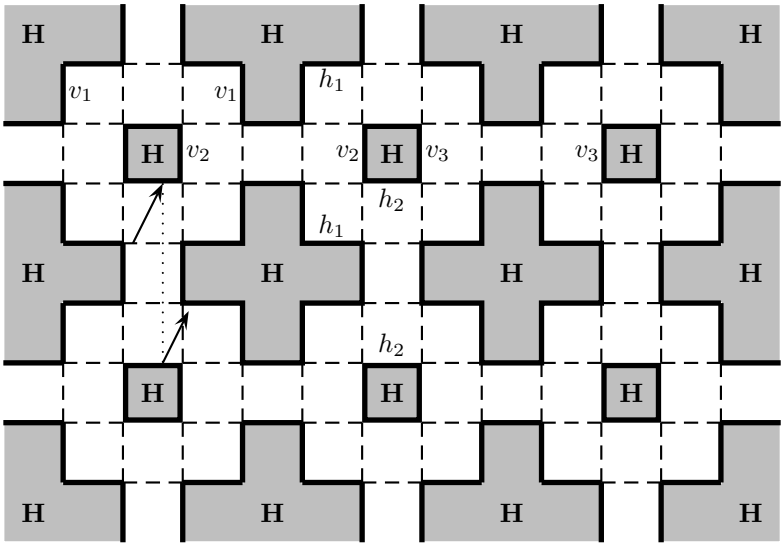

Figure 6.5.3: 3-square-maze with holes

Remark. All missing squares in this section are "holes".

If ℓ is substantially larger than 3, then we have all the freedom to change the size of the building blocks. For example, we can replace the 3×3 square with an 8×8 square, replace the hole size to 4×4, and locate the hole inside the $8\times$ square arbitrarily. This way we can construct an uncountable set of *aperiodic* ℓ-square-mazes with quadratic growth-rate of the neighborhood similar to that in Figure 6.5.3.

Another way to construct an uncountable set of *aperiodic* square-mazes is based on Figure 6.5.4. Type + on the left shows 4 unit size gray squares (holes) inside a 4×4 big square such that every row and column has one gray square and the distance between any two gray squares is at least one. Type − on the right shows another configuration of 4 gray squares with the same property. Divide the plane into 4×4 squares, and in each one place a type + or a type − configuration arbitrarily. The cardinality of the number of different infinite configurations is $2^{\mathbb{Z}^2}$. Thus we obtain an uncountable family of aperiodic j-square-mazes where $j \leqslant 6$. They all exhibit quadratic growth-rate of the neighborhood.

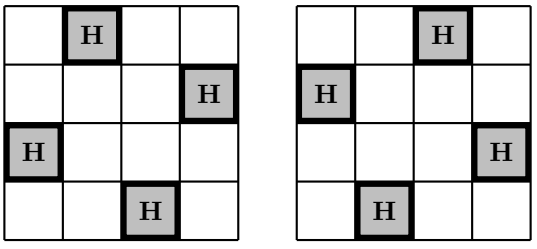

Figure 6.5.4: type + on the left and type − on the right

This idea can be generalized to larger square blocks. Let $p > 2$ be a prime, and consider a $p \times p$ block of unit size squares. For ease of description, suppose that the bottom left vertex is $(0, 0)$ and the top right vertex is (p, p), and that for every $0 \leqslant i, j < p$, $S(i, j)$ denotes the unit size square with bottom left vertex (i, j). Let q be a prime distinct from p. For every $0 \leqslant i < p$, let $0 \leqslant y_i < p$ be the unique solution of the congruence $y_i \equiv qi \bmod p$. Now consider a building block where each square $S(i, y_i)$, $0 \leqslant i < p$, is a unit size gray square (hole). Then every row and column of the $p \times p$ block has precisely one gray unit size square. We can call this the type (p, q) configuration. On the other hand, we can repeat the same argument with another prime q' different from both p and q, and obtain a type (p, q') configuration. Divide the plane into $p \times p$ squares, and in each one place a type (p, q) or a type (p, q') configuration arbitrarily. Thus we obtain an uncountable family of aperiodic j-square-mazes where $j \leqslant 2p - 2$.

Of course there are many, many more ways to construct an uncountable set of aperiodic square-mazes.

We shall prove the following result; see Theorem 6.5.1 below. For any integer $\ell \geqslant 2$, there is an infinite set of explicit badly approximable slopes, depending only on ℓ, such that any half-infinite geodesic having such a slope and starting from a face corner exhibits a precise form of *time-quantitative density* uniformly for all ℓ-square-mazes. We emphasize the surprising fact that the same slope works for *all* uncountably many ℓ-square-mazes.

Let $\mathcal{P}$ be an infinite polysquare surface with 1-direction geodesic flow. Assume that every street has length at most ℓ, *i.e.*, $\mathcal{P}$ is a j-square-maze for some $2 \leqslant j \leqslant \ell$.

Since every square face in $\mathcal{P}$ is the intersection of a horizontal and a vertical street, and $\mathcal{P}$ is square-face-connected by definition, we can define the concept of *$\mathcal{P}$-distance* between distinct square faces in $\mathcal{P}$ as in Section 6.4. We say that the $\mathcal{P}$-distance between two distinct square faces S_1 and S_2 is 1 if they belong to the same horizontal street or vertical street. Otherwise, we consider a shortest sequence of alternate horizontal and vertical streets such that the first contains S_1, the last contains S_2, and any two consecutive streets intersect. Then the length of this sequence is the $\mathcal{P}$-distance between S_1 and S_2. Note that the $\mathcal{P}$-distance is a metric on the collection of all square faces in $\mathcal{P}$ if we further define the $\mathcal{P}$-distance of any square face and itself to be 0.

We shall adopt the "magnification process" in the proof of Theorem 6.1.1, but do not use the trick of *exponentially fast zigzagging to a street corner*; see Figure 6.2.2. Thus the proof of Theorem 6.5.1 below is somewhat simpler than that of the proof of Theorem 6.1.1. For simplicity we restrict our attention to slopes of the form

$$\alpha = \alpha(a) = [a; a, a, a, \ldots] = a + \frac{1}{a + \frac{1}{a + \frac{1}{a + \cdots}}}, \tag{6.5.1}$$

where the common digit $a \geqslant \ell!$ is divisible by $\ell!$. This condition implies that every street length is a divisor of the common digit a in (6.5.1).

Theorem 6.5.1 ("time-quantitative density in a square-maze"). *For any fixed integer $\ell \geqslant 2$, let $\mathcal{P}$ be a j-square-maze for some $2 \leqslant j \leqslant \ell$. For any fixed constant $\varepsilon > 0$, there exist infinitely many numbers α of the form* (6.5.1)*, where $a \geqslant \ell!$ is divisible by $\ell!$, such that the half-infinite 1-directional geodesic $V(\alpha; t)$, $t \geqslant 0$, starting at the origin $\mathbf{0}$, with slope α and with arc-length parametrization, exhibits time-quantitative density in $\mathcal{P}$ in the following precise sense. For any square face S_0 of $\mathcal{P}$, there is an effectively computable threshold constant $c_0 = c_0(S_0; \varepsilon; \alpha)$ such that for every integer $n \geqslant c_0$ and every point $Q \in S_0$, the initial segment $V(\alpha; t)$, $0 < t < n^{3+\varepsilon}$, gets $1/n$-close to Q.*

Remarks. Theorem 6.5.1 covers a large class of infinite billiards. Let $\mathcal{P}$ be an infinite polysquare polygon such that every street is finite and has length at most ℓ. The holes become square obstacles. Hitting such an obstacle the point billiard bounces back the usual way. The 4-copy construction of the snake billiard in Figure 6.4.3 works for the infinite billiard on the table $\mathcal{P}$ equally well. The analogous construction converts this $\mathcal{P}$-billiard to a 1-direction flow in the union of four reflected copies of $\mathcal{P}$, glued together by boundary identification analogous to Figure 6.4.3. The only change is that the street length doubles, like the street length in the snake in the picture on the left in Figure 6.4.3 is 1 or 2, and the street length in the snake-cross surface in the picture on the right in Figure 6.4.3 is 2 or 4. So this union of four reflected copies of $\mathcal{P}$ glued together to form an infinite surface is a $2j$-square-maze for some $j \leqslant \ell$.

In terms of optics, the billiard form of Theorem 6.5.1 (resp. Theorem 6.6.1) is equivalent to the result that a single ray of light can *essentially illuminate* a whole infinite square-maze (resp. cube-maze), with reflecting boundaries ("mirrors"). The term "illumination" usually means that light reaches every point. Since the trajectory of a single reflecting ray in a square-maze (resp. cube-maze) has zero area (resp. volume), hitting every point is clearly impossible. The next best thing is to get arbitrarily close to every point, a density problem, and this is precisely what we mean by "essential illumination".

The infinite aperiodic billiards with square obstacles belong to the class that physicists call the *Ehrenfest wind-tree models*. In 1912 Ehrenfest and Ehrenfest wrote a long important encyclopaedia article on the foundations of statistical mechanics; see [7]. The Appendix of Section 5 in the first chapter of the article introduces a "much simplified model", as the Ehrenfests called it, to illustrate the works of Maxwell–Boltzmann. In this model a point particle (the "wind") moves freely on the plane and collides with the well known reflection law of geometric optics with an infinite number of irregularly placed congruent square scatterers (the "trees"). In the rest we refer to the particle ("wind") as a billiard, and call it the Ehrenfest wind-tree (billiard) model.

The Ehrenfests raised the problem of studying the individual billiard orbits in the wind-tree model. They wanted to understand the dynamics of this billiard model.

Unfortunately relatively little is known about the original aperiodic version of the problem. However, there are many recent results on the dynamics of the *periodic* version of the wind-tree model, introduced by Hardy and Weber [11] around 1980. It concerns the double-periodic arrangement of identical squares, or identical rectangles, where one obstacle is centered at each integer lattice point on the plane. We will return to the periodic wind-tree models in Sections 6.7 and 6.9. For a short summary of the known results, see the end of Section 6.9.

The best known result about the original aperiodic version of the problem is due to Sabogal and Troubetzkoy [24]. They can show that in a well-defined class of aperiodic wind-tree models, for a generic, in the sense of Baire, configuration of the obstacles, the wind-tree dynamics is ergodic in almost every direction. This is very interesting, but unfortunately their method does not give explicit results. They do not give any explicit configuration of the obstacles that is ergodic in almost every direction. They cannot even provide an explicit configuration that is ergodic in a single explicit direction.

In stark contrast, our method using Theorem 6.5.1 gives explicit results. Consider for example the concrete family of aperiodic j-mazes where $j \leqslant 6$ mentioned above, obtained by dividing the plane into 4×4 squares, and in each one placing the type $+$ or the type $-$ configuration in Figure 6.5.4 arbitrarily. It represents an uncountable family of explicit aperiodic configurations of the obstacles ("gray squares") for which

there are explicit billiard orbits exhibiting *density*. We cannot prove ergodicity, but we can prove a time-quantitative form of density of individual orbits. Note that ergodicity and time-quantitative density are not compatible, and neither one implies the other. Each says something relevant about the dynamics from two different viewpoints.

Open Problem 3. *Is the assumption that "the starting point $V(0)$ of V is a square corner" in Theorem 6.5.1 necessary? Can we have an arbitrary starting point?*

Proof of Theorem 6.5.1. As usual, we assume that every square face of $\mathcal{P}$ has side length one. We pick an arbitrary square face of $\mathcal{P}$, pick one of its 4 corner points, and call it $\mathbf{0}$.

Let $V(t) = V(\mathbf{0}; \alpha; t)$, $t \geqslant 0$, denote the almost vertical geodesic in $\mathcal{P}$ that starts from $\mathbf{0}$ and has slope α. Let $H(t) = H(\mathbf{0}; \alpha; t)$, $t \geqslant 0$, denote the almost horizontal geodesic in $\mathcal{P}$ that starts from $\mathbf{0}$ and has slope α^{-1}.

By hypothesis every street length in $\mathcal{P}$ is a divisor of the common digit a in (6.5.1), which implies that the almost horizontal $H(t)$, $t \geqslant 0$, and the almost vertical $V(t)$, $t \geqslant 0$, are *shortlines* of each other. That is, they are "mutual shortlines", where the concept of *shortline* is introduced at the beginning of Section 6.2.

We follow closely the argument in Section 6.2. First we recall the so-called *vertical same edge cutting property* of the shortline process, which says that the almost vertical $V(t)$, $t \geqslant 0$, and its shortline $H(t)$, $t \geqslant 0$, have precisely the same edge-cutting points on the vertical sides of vertical streets. We also have the analogous *horizontal same edge cutting property*, which says that the almost horizontal $H(t)$, $t \geqslant 0$, and its shortline $V(t)$, $t \geqslant 0$, have precisely the same edge-cutting points on the horizontal sides of horizontal streets.

Let V^* be a finite initial segment of $V(t)$, $t \geqslant 0$, and assume that V^* is "long". It is clear that V^* consists of a number of *whole* detour crossings and possibly a *fractional* detour crossing at the end. Clearly the length of V^* is some multiple of $(1 + \alpha^2)^{1/2}$, the common length of detour crossings of vertical streets. In other words,

$$\text{length}(V^*) = m_0(1 + \alpha^2)^{1/2} \quad \text{for some large positive real number } m_0. \tag{6.5.2}$$

Each whole detour crossing in V^* has a shortcut, which is part of the almost horizontal shortline H of V. The last fractional detour crossing in V^*, if extended to a full detour crossing, also has a shortcut, which is also part of the almost horizontal shortline H of V. For this last fractional detour crossing, we shorten its shortcut by the same fraction and at the appropriate end to obtain a fractional shortcut. We the take the union of these shortcuts and this fractional shortcut. This union is a segment of H that we denote by H_1^*. Clearly the length of H_1^* is some multiple of $(1 + \alpha^2)^{1/2}$, the common length of detour crossings of horizontal streets. In other words,

$$\text{length}(H_1^*) = m_1(1 + \alpha^2)^{1/2} \quad \text{for some real number } m_1.$$

We keep iterating this. Let

$$\text{length}(V_2^*) = m_2(1 + \alpha^2)^{1/2} \quad \text{for some real number } m_2,$$
$$\text{length}(H_3^*) = m_3(1 + \alpha^2)^{1/2} \quad \text{for some real number } m_3,$$

and so on. Consider the decreasing sequence

$$m_0 \geqslant m_1 \geqslant m_2 \geqslant m_3 \geqslant \cdots .$$

Repeating the argument of (6.2.12)–(6.2.14), we obtain the analogous result

$$m_k = m_0\alpha^{-k}. \tag{6.5.3}$$

Let I_0 be a V^*-free interval on a vertical edge of a square face on a vertical street of $\mathcal{P}$, so that I_0 and V^* are disjoint. It follows from the *vertical same edge cutting property* of the shortline process that the almost horizontal α^{-1}-flow projects ("tilted parallel projection") the interval I_0 to an H_1^*-free interval on a horizontal edge of a horizontal street of $\mathcal{P}$. The reader may want to go back to Figures 6.2.7 and 6.2.11 for illustration. Let I_1 denote this H_1^*-free interval. Then I_1 is a subinterval of a horizontal edge of a square face on a horizontal street *if* the α^{-1}-flow does not split the image. We now iterate this. It follows from the *horizontal same edge cutting property* of the shortline process that the almost vertical α-flow projects the interval I_1 to a V_2^*-free interval on a vertical edge of a vertical street of $\mathcal{P}$. Let I_2 denote this V_2^*-free interval. Then I_2 is a subinterval of a vertical edge of a square face on a vertical street *if* the α-flow does not split the image. And then the almost horizontal α^{-1}-flow projects the interval I_2 to an H_3^*-free interval on a horizontal edge of a horizontal street of $\mathcal{P}$. Let I_3 denote this H_3^*-free interval. Then I_3 is a subinterval of a horizontal edge of a square face on a horizontal street *if* the α^{-1}-flow does not split the image. And so on, always observing the Rule for Magnification in a Polysquare.

Remark. Unlike in Section 6.2, here we cannot use the trick of *exponentially fast zigzagging to a street corner*; see Figure 6.2.2. By using that trick in Section 6.2 we can prevent the appearance of "bad flow", when a singularity splits some image into *two* intervals. Here, similarly to the proof of Theorem 6.1.2 in Section 6.3, we have no choice but to accept the possibility of such splitting, and deal with it as a possible worst case scenario. It means that if splitting occurs, then of course we take the longer part.

It is well possible that already I_1, the α^{-1}-flow image of the starting V^*-free interval I_0, splits. Let $J_1 \subset I_1$ denote the longer part, so that J_1 is an H_1^*-free interval and a subinterval of a horizontal edge of a square face on a horizontal street of $\mathcal{P}$. Clearly $|J_1| \geqslant \min\{1, |I_0|\alpha/2\}$, where $|J|$ denotes the length of an interval J. In the next step the almost vertical α-flow projects the interval J_1 to a V_2^*-free interval, which may split. We take the longer part and denote it by J_2. Now J_2 is a V_2^*-free interval and a subinterval of a vertical edge of a square face on a vertical street of $\mathcal{P}$. Clearly $|J_2| \geqslant \min\{1, |J_1|\alpha/2\}$. And so on.

Thus this magnification process produces a chain of intervals

$$I_0 = J_0 \to J_1 \to J_2 \to J_3 \to \cdots \to J_k \to \cdots \tag{6.5.4}$$

such that, writing $V_0^* = V^*$, for every integer $i \geqslant 0$,

(1) J_{2i} is a V_{2i}^*-free interval and a subinterval of a vertical edge of a square face on a vertical street of $\mathcal{P}$;

(2) J_{2i+1} is an H_{2i+1}^*-free interval and a subinterval of a horizontal edge of a square face on a horizontal street of $\mathcal{P}$; and

(3) $|J_{i+1}| \geqslant \min\{1, |J_i|\alpha/2\}$.

It is not an accident that in (6.5.3) and (6.5.4) we use the same unspecified index k. We complete the proof of Theorem 6.5.1 by making an appropriate choice of this common index.

Let $k = k_0$ be the smallest even integer such that

$$|I_0|(\alpha/2)^k > 2. \tag{6.5.5}$$

Then it follows from (3) that $|J_{k_0}| = 1$. Combining this with (1), we conclude that J_{k_0} is a *whole* vertical edge of a square face on a vertical street of $\mathcal{P}$, and this vertical edge is $V_{k_0}^*$-free.

We recall that the square face corner $\mathbf{0}$ is the common starting point $V(0) = H(0) = \mathbf{0}$ of the two particular geodesics V and H that are shortlines of each other.

Let S_0 denote a square face of $\mathcal{P}$ that contains the common starting point $\mathbf{0}$. Let S_1 denote a square face of $\mathcal{P}$ that contains the V^*-free interval I_0, the first interval in the chain (6.5.4), on its left boundary, and let S_2 denote a square face of $\mathcal{P}$ that contains the $V^*_{k_0}$-free edge J_{k_0} on its right boundary.

For $0 \leqslant i, j \leqslant 2$, let $d(i,j)$ denote the $\mathcal{P}$-distance between the square faces S_i and S_j.

The upper bound $d(1,2) \leqslant k_0$ is a straightforward corollary of the k_0-step construction of the magnification process (6.5.4) with $k = k_0$. Indeed, in each step, the $\mathcal{P}$-distance increases by at most 1, as a consequence of the triangle inequality. Combining this with the triangle inequality we deduce that the $\mathcal{P}$-distance $d(0,2)$ between the square faces S_0 and S_2 has the upper bound

$$d(0,2) \leqslant d(0,1) + d(1,2) \leqslant d(0,1) + k_0. \tag{6.5.6}$$

We recall some key facts. First of all, J_{k_0} is a $V^*_{k_0}$-free edge on the boundary of the square face S_2 in $\mathcal{P}$. Next, by (6.5.2) and (6.5.3) we have a very good estimation for the length of $V^*_{k_0}$, given by

$$\text{length}(V^*_{k_0}) = m_{k_0}(1+\alpha^2)^{1/2} \quad \text{and} \quad \text{length}(V^*) = m_0(1+\alpha^2)^{1/2}, \tag{6.5.7}$$

where

$$m_{k_0} = m_0 \alpha^{-k_0}. \tag{6.5.8}$$

Next we apply a variant of Lemma 6.4.1 to our j-square-maze $\mathcal{P}$, where $2 \leqslant j \leqslant \ell$, noting that in the proof of Lemma 6.4.1, we have not used at all the fact that the polysquare surface is finite. We need to make some simple modification to Lemma 6.4.1 as we start the geodesic here at the origin $\mathbf{0}$, so that we can talk about the *first* detour crossing which is a *whole* detour crossing.

Lemma 6.5.1. *Suppose that $\mathcal{P}$ is an arbitrary polysquare surface with 1-direction geodesic flow V of slope α which is an irrational number given by (6.5.1), where the continued fraction digit a is a positive integer multiple of the street-LCM of $\mathcal{P}$. Let S' be a given square face of $\mathcal{P}$, and let $\mathcal{V}$ denote the finite almost vertical geodesic made up of the first 3 detour crossings of the i-generation shortline of V for some even integer $i \geqslant 4$. Suppose that a unit contained in the first two detour crossings in $\mathcal{V}$ intersects the bottom edge of S'. Then in every square face S'' of $\mathcal{P}$ for which the $\mathcal{P}$-distance between S' and S'' is at most 2, the 4-generation ancestor geodesic of $\mathcal{V}$ gives rise to an almost vertical unit of type $\nmid$ in the square.*

Remark. Note that the first detour crossing of V and of V^* are the same.

Let $h \geqslant 4$ be any integer that is divisible by 4. By using an $h/4$-times iteration of Lemma 6.5.1, we conclude that starting from an arbitrary almost vertical shortcut A in the square face S_1, every square face with $\mathcal{P}$-distance at most $h/2$ from S_1 has an almost vertical unit of type $\nmid$ that is an h-generation ancestor of some unit which is contained in full or in part in the first detour crossing of V^*.

We recall that V^* is a "long" initial segment of the special almost vertical $V(t)$, $t \geqslant 0$.

We start with 2 whole detour crossings of V^*, of total length $2(1+\alpha^2)^{1/2}$. The h-step shortcut-ancestor process, where at each stage we include fractional units proportionally, now gives rise to an initial segment of V^* with length

$$2\alpha^h(1+\alpha^2)^{1/2}. \tag{6.5.9}$$

We know that for every square face with $\mathcal{P}$-distance at most $h/2$ from the square face S_1, this initial segment of V^* of length (6.5.9) gives rise to an almost vertical unit of type $\nmid$ in the square.

We now specify parameter h to satisfy the the requirement that this segment is contained in $V^*_{k_0}$, so that

$$\text{length}(V^*_{k_0}) \geqslant 2\alpha^h(1+\alpha^2)^{1/2}. \tag{6.5.10}$$

Comparing (6.5.8) and (6.5.9), we see that a condition like

$$m_0\alpha^{-k_0} \geqslant 2\alpha^h \tag{6.5.11}$$

implies (6.5.10).

We next claim that

$$\frac{h}{2} < d(0,1) + k_0, \tag{6.5.12}$$

where $d(0,1)$ denotes the $\mathcal{P}$-distance between the square faces S_0 and S_1. The proof is by contradiction. Suppose on the contrary that (6.5.12) does not hold. Then it follows from (6.5.6) that $h/2 \geqslant d(0,2)$, and so for every square face with $\mathcal{P}$-distance at most $d(0,2)$ from the square face S_1, the particular initial segment of V^* of length (6.5.9) gives rise to an almost vertical unit of type $\dagger$ in the square. It then follows from (6.5.10) that for every square face with $\mathcal{P}$-distance at most $d(0,2)$ from the square face S_1, $V^*_{k_0}$ gives rise to an almost vertical unit of type $\dagger$ in the square. It follows that the right edge of the square face S_2 is not a $V^*_{k_0}$-free vertical edge. But this is a contradiction, since we know that J_{k_0} *is* a $V^*_{k_0}$-free vertical edge on the boundary of the square face S_2, and it is the whole edge. This contradiction proves (6.5.12).

Recall that $k = k_0$ is the smallest even integer such that (6.5.5) holds. This implies

$$2(\alpha/2)^{-k_0} < |I_0| \leqslant 2(\alpha/2)^{-k_0+2}.$$

Combining (6.5.7) and (6.5.11), we have

$$\text{length}(V^*) \geqslant 2(1+\alpha^2)^{1/2}\alpha^{h+k_0}. \tag{6.5.13}$$

In view of (6.5.12), it follows that the choice

$$\text{length}(V^*) \geqslant 2(1+\alpha^2)^{1/2}\alpha^{2d(0,1)+3k_0}$$

clearly implies the inequality (6.5.13).

We conclude, therefore, that if we specify the length of the initial segment V^* of the special geodesic $V(t)$, $t \geqslant 0$, starting from $\mathbf{0}$ with slope α, as

$$\text{length}(V^*) = C'(\alpha)\alpha^{2d+3k}, \tag{6.5.14}$$

then the longest V^*-free interval on any edge of a square face with $\mathcal{P}$-distance at most d from the square face S_0 is "short". More precisely, such a V^*-free interval has length roughly at most $2(\alpha/2)^{-k+2}$.

Let $\varepsilon > 0$ be arbitrarily small but fixed. We choose the integer variable n to satisfy

$$n \leqslant 2(\alpha/2)^{k-2} < n+1. \tag{6.5.15}$$

Then by (6.5.14) and (6.5.15),

$$\text{length}(V^*) = C'(\alpha)\alpha^{2d+3k} \leqslant C''(\alpha;d)n^{3+\varepsilon},$$

if the common continued fraction digit a of α in (6.5.1) is sufficiently large depending on $\varepsilon > 0$. This completes the proof of Theorem 6.5.1. □

Remark. An important consequence of the shortline method is that the dense geodesic exhibits *super-slow escape rate to infinity.*

We can describe this phenomenon in terms of the concept of the $\mathcal{P}$-diameter restricted to a finite geodesic. Suppose that L is a finite geodesic on a polysquare $\mathcal{P}$. To calculate the $\mathcal{P}$-diameter restricted to the geodesic L, we simply consider the

$\mathcal{P}$-distance between any two square faces of $\mathcal{P}$ visited by L, and find the maximum value among these.

Using the notation of the proof of Theorem 6.5.1, we consider the decreasing chain

$$V^* = V_0^* \to H_1^* \to V_2^* \to H_3^* \to \ldots \to V_{2i}^* \to H_{2i+1}^* \to \ldots$$

of geodesic segments. This is *decreasing exponentially fast*, in the sense that the ratio of the lengths of consecutive segments is equal to α. On the other hand, the shortline method implies that the $\mathcal{P}$-diameter restricted to any of these geodesic segments does not exceed the $\mathcal{P}$-diameter restricted to the next geodesic segment in the chain by more than 1. Thus the dense geodesic exhibits *logarithmic escape rate to infinity* in terms of the restricted $\mathcal{P}$-distances.

The growth-rate of the neighborhood of the polysquare surface in Figure 6.5.1 is linear, and the growth-rate of the neighborhood of the polysquare surface in Figure 6.5.3 is quadratic. To give an example of a polysquare surface for which the growth-rate of the neighborhood is cubic, we consider first an infinite polycube, *i.e.*, cube tiled solid, where the building blocks are illustrated in the picture on the left in Figure 6.5.5 below.

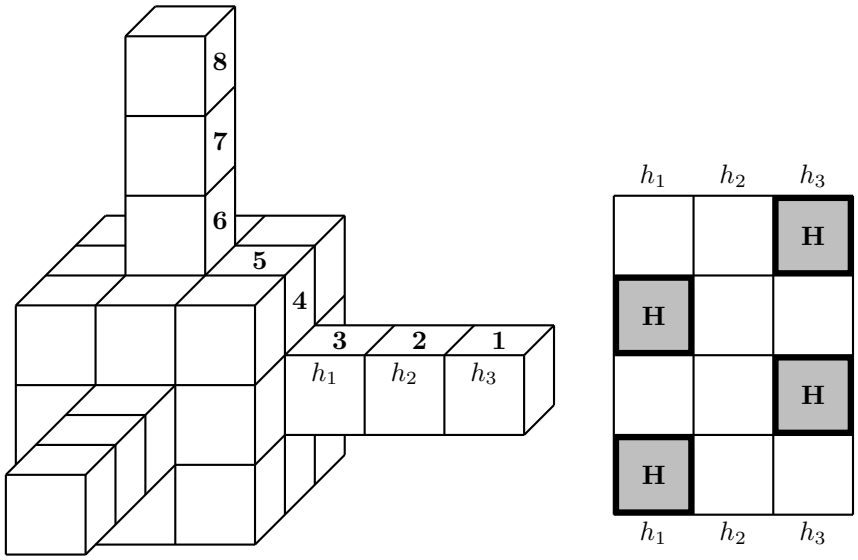

Figure 6.5.5: polycube and holes on the corridor

More precisely, consider all integer lattice points $\mathbf{n} = (n_1, n_2, n_3) \in \mathbb{Z}^3$ such that every coordinate n_i is divisible by 6, and place an aligned $3 \times 3 \times 3$ cube centered at each such lattice point $\mathbf{n}$. We then join these $3 \times 3 \times 3$ cubes by corridors. These are $1 \times 1 \times 3$ boxes, with the two ends attached to the middle squares on the relevant faces of the neighboring $3 \times 3 \times 3$ cubes.

The polysquare surface of this infinite polycube typically exhibits cubic growth-rate of the neighborhood. However, this is an infinite polysquare surface with infinitely long streets. To turn this into an ℓ-square-maze, we shall limit the street sizes by replacing some square faces by holes. In fact, we shall replace some square faces on the corridors by holes.

The 12 square faces of a typical corridor forms a polysquare surface which is a 4×3 rectangle with edge pairings given in the picture on the right in Figure 6.5.5. We now replace four of these square faces by holes as shown. The resulting surface is triple-periodic, so the growth-rate of the neighborhood is cubic.

Without the holes, a typical street of this polysquare surface that involves square faces of the corridors is illustrated by the sequence of square faces annotated by **1** – **8**. With the presence of holes, it is clear that the length of any such street is at

most 6. On the other hand, a street that is made up of square faces arising from a $3 \times 3 \times 3$ cube is at most 12; consider, for instance, a street arising from the top 12 vertical square faces. We conclude, therefore, that with the presence of these holes, we have a 12-square-maze.

For an integer ℓ substantially larger than 12, we have the freedom to change the lengths of the corridors and the arrangement of the holes. This way we can easily construct an uncountable family of ℓ-square-mazes for which the growth-rate of the neighborhood is cubic.

We can go even further. Given any integer $d \geqslant 4$, it is not difficult to construct an uncountable family of square-mazes for which the growth-rate of the neighborhood is a d-th power.

What is more, it is easy to achieve *exponential* growth-rate of the neighborhood. For example, let us go back to the two 4×4 squares in Figure 6.5.4, of types $+$ and $-$. Instead of dividing the plane into 4×4 squares and placing a type $+$ or type $-$ configuration arbitrarily in each one of them, where the cardinality of distinct configurations is $2^{\mathbb{Z}^2}$, we shall follow a different pattern. We can build a 4-regular infinite tree, *i.e.*, an infinite connected cycle-free graph where every degree is 4. What we get then is an "abstract" or "exotic" polysquare surface, but a perfectly well-defined legitimate surface nonetheless.

More precisely, we start with a 4×4 square of type $+$ or type $-$. For each one of the 4 sides, we attach a new 4×4 square of type $+$ or type $-$, with arbitrary choice. Each one of these new 4×4 squares has 3 free sides, and for each one these, we attach a new 4×4 square of type $+$ or type $-$, again with arbitrary choice, and call them "second-round new". Each one the second-round new 4×4 squares has 3 free sides, and for each of these, we attach a new 4×4 square of type $+$ or type $-$, again with arbitrary choice, and call them "third-round new". And so on, we keep going forever. Then the growth-rate of the n-th neighborhood is exponential in the range of 3^n.

6.6. **Time-quantitative density in a cube-maze.** The concept of square-maze in Section 6.5 has a straightforward generalization to polycubes that we call a cube-maze.

We call an infinite polycube a *cube-maze* if the lengths of the X-streets, Y-streets and Z-streets are uniformly bounded. Let $\ell \geqslant 2$ be any integer. We call a cube-maze an *ℓ-cube-maze* if every X-street, Y-street and Z-street has length at most ℓ, and there is a street that has length equal to ℓ. As usual, we assume that $\mathcal{P}$ consists of unit size cubes which we call *cube atoms*. We choose an arbitrary cube atom of $\mathcal{P}$, choose any of its 8 corner points, and refer to this particular corner point as the origin $\mathbf{0}$.

We study 1-direction geodesic flow, *i.e.*, generalized torus line flow, inside such a cube-maze $\mathcal{P}$. If geodesic flow in the cube-maze is an 8-direction flow, like in the case of billiards, then we can apply an 8-copy construction, analogous to the 4-copy construction in the 2-dimensional case, and convert the original problem to an equivalent problem of geodesic flow on a different cube-maze with 1-direction flow.

Let $k \geqslant 1$ be an integer, and consider the cubic equation

$$x^3 + \ell!kx - 1 = 0. \tag{6.6.1}$$

The cubic polynomial $x^3 + \ell!kx - 1$ is strictly increasing and has precisely one root $\alpha = \alpha(k; \ell)$ satisfying

$$\frac{1}{\ell!k + 1} < \alpha < \frac{1}{\ell!k}. \tag{6.6.2}$$

Analogous to our discussion in Section 6.3, $\mathcal{L}$ denotes the s-L-line starting from the origin with direction vector $\mathbf{v}_0 = (\alpha, \alpha^2, 1)$, $\mathcal{L}^*$ denotes the s-L-line starting from the origin with direction vector $\mathbf{v}_1 = (1, \alpha, \alpha^2)$, and $\mathcal{L}^{**}$ denotes the s-L-line starting from the origin with direction vector $\mathbf{v}_2 = (\alpha^2, 1, \alpha)$. Note that $\mathcal{L}$ consists of *left to right detour crossings* of Z-streets, $\mathcal{L}^*$ consists of *front to back detour crossings* of X-streets, and $\mathcal{L}^{**}$ consists of *bottom to top detour crossings* of Y-streets. Furthermore, $\mathcal{L}^*$ is the shortline of $\mathcal{L}$, $\mathcal{L}^{**}$ is the shortline of $\mathcal{L}^*$, and $\mathcal{L}$ is the shortline of $\mathcal{L}^{**}$. Recall also the X-face hitting property, that $\mathcal{L}$ and $\mathcal{L}^*$ hit every X-face at precisely the same points, the Y-face hitting property, that $\mathcal{L}^*$ and $\mathcal{L}^{**}$ hit every Y-face at precisely the same points, and the Z-face hitting property, that $\mathcal{L}^{**}$ and $\mathcal{L}$ hit every Z-face at precisely the same points.

Our goal is to prove the following density result.

Theorem 6.6.1 ("time-quantitative density in a cube-maze")**.** *For any fixed integer $\ell \geqslant 2$, let $\mathcal{P}$ be a j-cube-maze for some $2 \leqslant j \leqslant \ell$. For any fixed constant $\varepsilon > 0$, there exist infinitely many vectors $\mathbf{v}_0$ such that the half-infinite 1-directional geodesic $\mathcal{L}(\mathbf{v}_0; t)$, $t \geqslant 0$, starting at the origin $\mathbf{0}$, with direction vector $\mathbf{v}_0$ and with arc-length parametrization, exhibits time-quantitative density in $\mathcal{P}$ in the following precise sense. For any cube atom H_0 of $\mathcal{P}$, there is an effectively computable threshold constant $C_0 = C_0(H_0; \varepsilon; \mathbf{v}_0)$ such that for every integer $n \geqslant C_0$ and every point $Q \in H_0$, the initial segment $\mathcal{L}(\mathbf{v}_0; t)$, $0 < t < n^{38+\varepsilon}$, gets $1/n$-close to Q.*

In particular, for any fixed constant $\varepsilon > 0$, there is a threshold $k_0 = k_0(\varepsilon)$ such that for every integer $k \geqslant k_0$, the root $\alpha = \alpha(k; \ell)$ of the cubic equation (6.6.1) *in the interval* (6.6.2) *gives rise to a vector $\mathbf{v}_0 = (\alpha, \alpha^2, 1)$ that satisfies the requirements.*

Proof. Our basic idea is the same as that of the proof of Theorem 6.1.2 in Section 6.3 and the proof of Theorem 6.5.1 in Section 6.5, and involves iterated area magnification of *empty* convex sets, *i.e.*, convex sets that have empty intersection with long initial segments of $\mathcal{L}$, $\mathcal{L}^*$ or $\mathcal{L}^{**}$, using the three X-Y-Z-face hitting properties and the 3-periodicity of the shortline process.

Let $L(0)$ be a "long" initial segment of the s-L-line $\mathcal{L}$ in the given cube-maze $\mathcal{P}$. We then define $L(1), L(2), L(3), \ldots$ iteratively from $L(0)$ in the same way as we define $L_k(1), L_k(2), L_k(3), \ldots$ iteratively from $L_k(0)$ in Section 6.3.

Let S_0 be an $L(0)$-free square on an X-face of a cube atom, *i.e.*, S_0 does not contain any point of $L(0)$. We can apply the Enhanced Magnification Process

$$S_0 \to S_1 \to S_2 \to \ldots \to S_{i_0} \tag{6.6.3}$$

in Section 6.3 *verbatim*, terminating the process with the set S_{i_0}, always observing the Rule for Magnification in a Polycube.

Analogous to (6.3.28), we can write

$$\text{length}(L(i)) = \frac{m_i}{\alpha}(1 + \alpha^2 + \alpha^4)^{1/2}, \quad 0 \leqslant i \leqslant i_0,$$

where m_i is some positive real number. The shortline relation then implies the relation

$$m_{i+1} = \alpha m_i, \quad 0 \leqslant i < i_0,$$

and on iterating, we deduce that

$$m_i = \alpha^i m_0.$$

In particular, we have

$$\text{length}(L(i_0)) = \alpha^{i_0} \,\text{length}(L_k(0)). \tag{6.6.4}$$

From the Enhanced Magnification Process, we can also make the following conclusions:

(1) The convex set S_{i_0} is disjoint from $L(i_0)$.

(2) There is a positive absolute constant c_0 such that the convex set S_{i_0} contains at least one of the c_0^2 standard congruent subsquares of side length c_0^{-1} of the square face containing it.

(3) Analogous to (6.3.54), there are two further positive absolute constant c_0^{***} and c_{11} such that the inequality

$$\left(\frac{3c_0}{\sqrt{\text{area}(S_0)}} \right)^2 > \left(\frac{c_0^{***}}{\alpha} \right)^{i_0-3} \alpha_k^{c_{11}} \tag{6.6.5}$$

holds.

Furthermore, we can make the following assumptions:

(4) The integer i_0 is a multiple of 3. The Enhanced Magnification Process can be modified without much difficulty to accommodate this.

(5) The absolute constant c_0 is not equal to j. This will be handy in Lemma 6.6.2 below.

Let H_0 denote a cube atom of $\mathcal{P}$ that contains the origin $\mathbf{0}$. Let H_1 denote a cube atom of $\mathcal{P}$ that contains the $L(0)$-free square S_0, the first set in the chain (6.6.3), on its right X-face, and let H_2 denote a cube atom of $\mathcal{P}$ that contains the $L(i_0)$-free convex set S_{i_0}, the last set in the chain (6.6.3), on its right X-face.

For $0 \leqslant i, j \leqslant 2$, let $d(i,j)$ denote the $\mathcal{P}$-distance between the cube atoms H_i and H_j.

The upper bound $d(1,2) \leqslant 2i_0$ is a straightforward corollary of the i_0-step construction of the magnification process (6.6.3). Indeed, in each step the $\mathcal{P}$-distance increases by at most 2, as a consequence of the triangle inequality. Combining this with the triangle inequality we deduce that the $\mathcal{P}$-distance $d(0,2)$ between the square faces H_0 and H_2 has the upper bound

$$d(0,2) \leqslant d(0,1) + d(1,2) \leqslant d(0,1) + 2i_0. \tag{6.6.6}$$

Analogous to (6.5.12), we wish to establish the inequality

$$\frac{j_0}{9} < d(0,1) + 2i_0. \tag{6.6.7}$$

We need first of all the following analog of Lemma 6.4.3.

Lemma 6.6.1. *Suppose that $\mathcal{P}$ is a j-cube-maze for some $2 \leqslant j \leqslant \ell$ and with 1-direction geodesic flow $\mathcal{L}$ with direction vector $\mathbf{v}_0$ as given in the statement of Theorem 6.6.1, starting from the origin $\mathbf{0}$. Let H' be a given cube atom of $\mathcal{P}$, and let $\mathcal{V}$ denote the finite geodesic made up of the first 3 detour crossings of the i-generation shortline of $\mathcal{L}$ for some integer $i \geqslant 9$ which is a multiple of 3. Suppose that a Z-unit contained in the first 2 detour crossings of $\mathcal{V}$ intersects the right Z-face of H', at a point closer to the back Y-face of H' than to the front Y-face of H'. Then in every cube atom H'' of $\mathcal{P}$ for which the $\mathcal{P}$-distance between H' and H'' is at most 3, the 9-generation ancestor geodesic of $\mathcal{V}$ gives rise to a Z-unit that intersects the right Z-face of H'', at a point closer to the back Y-face of H'' than to the front Y-face of H''.*

This is clearly not enough, as we want to show that some ancestor geodesic intersects every one of the c_0^2 standard congruent subsquares of side length c_0^{-1} on a square face. To achieve this, we shall do some rescaling.

Corresponding to the j-cube-maze $\mathcal{P}$, we construct a cube-maze $c_0\mathcal{P}$ in a similar way as in Section 6.4 to enable our deduction of Lemma 6.4.5. In view of our assumption (5) earlier that c_0 is not equal to j, as long as $\ell \geqslant c_0$, then $c_0 j$ is a

divisor of $\ell!$, so that we may safely consider the geodesic $\mathcal{L}_{c_0}$ with direction vector $\mathbf{v}_0$ in the $c_0 j$-square-maze $c_0\mathcal{P}$.

We thus have the following analog of Lemma 6.4.5.

Lemma 6.6.2. *Suppose that $\mathcal{P}$ is a j-cube-maze for some $2 \leqslant j \leqslant \ell$ and with 1-direction geodesic flow $\mathcal{L}$ with direction vector $\mathbf{v}_0$ as given in the statement of Theorem 6.6.1, starting from the origin $\mathbf{0}$. Let H_1 be a given cube atom of $\mathcal{P}$, and let $\mathcal{V}$ denote the finite geodesic made up of the first 3 detour crossings of the i-generation shortline of $\mathcal{L}$ for some integer $i \geqslant 9(K+1)$ which is a multiple of 3, where K is a positive integer. Suppose that a Z-unit contained in the first 2 detour crossings of $\mathcal{V}$ intersects the right Z-face of H_1. Then for every cube atom H_2 of $\mathcal{P}$ for which the $\mathcal{P}$-distance between H_1 and H_2 is at most $3K$, the $9(K+1)$-generation ancestor geodesic of $\mathcal{V}$ intersects every one of the c_0^2 standard congruent subsquares of side length c_0^{-1} on the right X-face of H_2.*

We are now in a position to prove the inequality (6.6.7). Suppose on the contrary that

$$\frac{j_0}{9} \geqslant d(0,1) + 2i_0.$$

Then in view of (6.6.6), we have

$$\frac{j_0}{9} \geqslant d(0,2).$$

Applying Lemma 6.6.2 with $9(K+1) = j_0$ now leads to a contradiction.

We now complete the proof of Theorem 6.6.1 as follows.

Recall that $L(0)$ is a "long" initial segment of the s-L-line $\mathcal{L}$.

We start with 2 whole detour crossings of $L(0)$, of total length $2\alpha^{-1}(1+\alpha^2+\alpha^4)^{1/2}$. For any integer multiple j of 9, the j-step shortcut-ancestor process, where at each stage we include fractional units proportionally, now gives rise to an initial segment of $L(0)$ with length

$$2\alpha^{-j-1}(1+\alpha^2+\alpha^4)^{1/2}. \tag{6.6.8}$$

We now specify parameter $j = j_0$ to satisfy the the requirement that this segment is contained in $L(i_0)$, so that

$$\text{length}(L(i_0)) \geqslant 2\alpha^{-j-1}(1+\alpha^2+\alpha^4)^{1/2}. \tag{6.6.9}$$

Comparing (6.6.4) and (6.6.8), we see that a condition like

$$m_0\alpha^{i_0} \geqslant 2\alpha^{-j_0} \tag{6.6.10}$$

implies (6.6.9). We conclude, therefore, that if we specify the length of the initial segment $L(0)$ of $\mathcal{L}$ as

$$\text{length}(L(0)) = C_1(\alpha)\alpha^{-j_0-i_0}, \tag{6.6.11}$$

with the constant $C_1(\alpha)$ sufficiently large, then (6.6.9) and (6.6.10) follow.

Combining (6.6.7) and (6.6.11), we have

$$\text{length}(L(0)) \leqslant C_1(\alpha)\alpha^{-9d(0,1)-19i_0} = C_2(\alpha; d(0,1))\left(\frac{1}{\alpha}\right)^{19i_0}. \tag{6.6.12}$$

Given any $\varepsilon > 0$, let $\varepsilon' = \varepsilon/19$, and take k_0 to be an integer satisfying

$$k_0 \geqslant \frac{1}{\ell! c_0^{***}}\left(\frac{1}{c_0^{***}}\right)^{2/\varepsilon'}.$$

Then for any integer $k > k_0$, we have, in view of (6.3.1),

$$\left(\frac{c_0^{***}}{\alpha}\right)^{\varepsilon'/2} > (\ell! k c_0^{***})^{\varepsilon'/2} \geqslant \frac{1}{c_0^{***}}. \tag{6.6.13}$$

Combining (6.6.5) and (6.6.13), we have

$$\left(\frac{3c_0}{\sqrt{\text{area}(S_0)}}\right)^{2+\varepsilon'} > \left(\frac{c_0^{***}}{\alpha}\right)^{i_0-3} \alpha_k^{c_{11}} \left(\frac{1}{c_0^{***}}\right)^{i_0-3} \alpha_k^{c_{11}\varepsilon'/2}.$$

We may clearly assume that $\varepsilon' \leqslant 2$. Then

$$\left(\frac{3c_0}{\sqrt{\text{area}(S_0)}}\right)^{2+\varepsilon'} > \left(\frac{1}{\alpha}\right)^{i_0-3} \alpha_k^{2c_{11}}. \tag{6.6.14}$$

Combining (6.6.12) and (6.6.14), we conclude that

$$\text{length}(L(0)) \leqslant C_3(\alpha; d(0,1)) \left(\frac{3c_0}{\sqrt{\text{area}(S_0)}}\right)^{38+\varepsilon}.$$

Since $\sqrt{\text{area}(S_0)}$ is the side length of the square S_0, this inequality clearly gives the required time-quantitative density, and completes the proof of Theorem 6.6.1. □

We complete this section by constructing some cube-mazes.

The first example is the 3-dimensional analog of the 3-square-maze in Figure 6.5.3. The building blocks are $3 \times 3 \times 3$ cubes with "holes" in the middle, and these blocks are glued together by $1 \times 1 \times 1$ cubes in such a way to form a 3-dimensional lattice (somewhat like $\mathbb{Z}^3$), creating further "holes". With face identification analogous to the edge identification in Figure 6.5.3, we see that we have a 3-cube-maze.

Finally, we construct an uncountable family of aperiodic cube-mazes. The idea is based on 3-dimensional analogs of Figure 6.5.4.

Let $p > 2$ be a prime, and consider a $p \times p \times p$ block of unit size cubes. For ease of description, suppose that the bottom left vertex is $(0,0,0)$ and the top right vertex is (p,p,p), and that for every $0 \leqslant i,j,k < p$, $H(i,j,k)$ denotes the unit size cube with bottom left vertex (i,j,k). Let $q \neq r$ be primes distinct from p. For every $0 \leqslant i,j < p$, let $0 \leqslant z_{i,j} < p$ be the unique solution of the congruence $z_i \equiv qi + rj \bmod p$. Now consider a building block where each cube $H(i,j,z_i)$, $0 \leqslant i,j < p$, is a unit size gray cube (hole). Then any p successive unit size cubes in the x-, y- or z-direction contain precisely one gray unit size cube. We can call this the type (p,q,r) configuration. On the other hand, we can repeat the same argument with primes $q' \neq r'$ different from p, q and r, and obtain a type (p,q',r') configuration. Divide 3-space into $p \times p \times p$ cubes, and in each one place a type (p,q,r) or a type (p,q',r') configuration arbitrarily. The cardinality of the number of different infinite configurations is $2^{\mathbb{Z}^3}$. Thus we obtain an uncountable family of aperiodic j-cube-mazes where $j \leqslant 2p-2$.

6.7. **Density on aperiodic surfaces with infinite streets (I).** In Section 6.5 we have proved that, given any positive integer ℓ, there are some slopes that give rise to geodesics that are dense in a *universal* way. More precisely, for *every* j-square-maze with $j \leqslant \ell$, a geodesic starting at a corner point with such a slope exhibits time-quantitative density.

In terms of optics, the billiard case of our result is equivalent to the result that, for any $\ell \geqslant 2$, there are slopes α such that every j-square-maze for $j \leqslant \ell$ with reflecting boundary ("mirrors") can be illuminated by a single ray of light with slope α. This represents an uncountable family of infinite billiards.

While this is quite interesting, what can we say about those infinite polysquare surfaces which are very different from a maze? For instance, what can we say about those polysquare surfaces which have infinite streets? The Ehrenfest wind-tree billiard model, mentioned briefly in the remarks after Theorem 6.5.1, is a rich source

of surfaces. In particular, in the periodic Ehrenfest wind-tree model, every rectangle ("scatterer") has the same size $a \times b$ with $0 < a, b < 1$, and they are placed in the usual horizontal/vertical position, with horizontal and vertical periods both equal to 1. So these double-periodic models all have infinitely many infinite horizontal and vertical streets. Figure 6.7.1 illustrates the simplest special case $a = b = 1/2$ of such a model, with square scatterers of side length $1/2$. The symbolic dotted square in the lower-right corner represents a *table-period*.

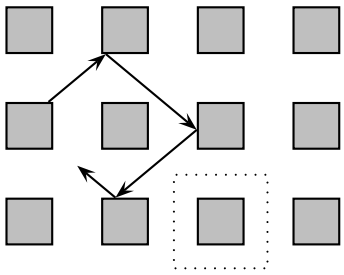

Figure 6.7.1: double-periodic wind-tree billiard model with side length $1/2$

As also mentioned in those earlier remarks, there are many recent results in the *periodic* case with congruent rectangular obstacles centered at all integer lattice points in $\mathbb{Z}^2$, but none of these results guarantee density.

A natural way to make these periodic models *aperiodic* is to drop infinitely many obstacles at some *irregularly chosen* lattice points. We next formulate such a result, which goes back to the original aperiodic form of the Ehrenfest wind-tree model. We cannot prove ergodicity, but we can prove a quantitative form of density of individual orbits. Note that ergodicity and time-quantitative density are not compatible.

The Uncountable Family of f-configurations. The idea of f-configurations is a natural way to produce an uncountable family of explicit aperiodic configurations of obstacles.

We divide the plane into a union of 3×3 squares

$$Q(i,j) = \left[3i - \frac{3}{2}, 3i + \frac{3}{2}\right) \times \left[3j - \frac{3}{2}, 3j + \frac{3}{2}\right), \quad (i,j) \in \mathbb{Z}^2,$$

each centered at the lattice point $(3i, 3j) \in \mathbb{Z}^2$.

Let $\mathcal{F}$ denote the family of all functions $f : \mathbb{Z}^2 \to \{\pm 1\}$. Clearly $\mathcal{F}$ is an uncountable set.

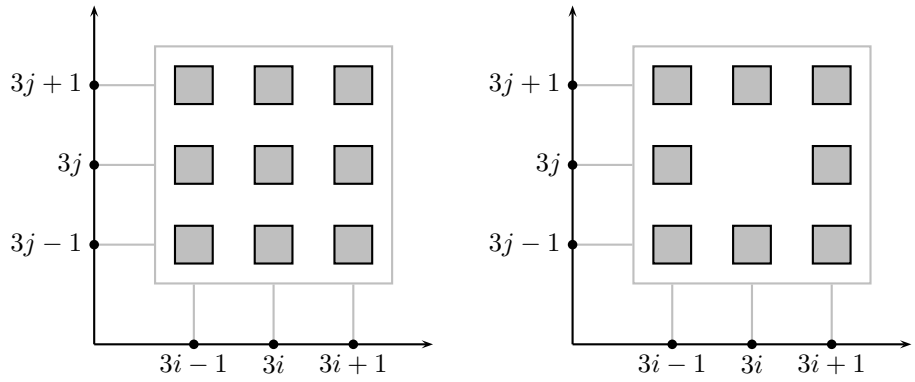

Figure 6.7.2: the 3×3 square $Q(i,j)$ with $f(i,j) = +1$ and with $f(i,j) = -1$

For each $(i,j) \in \mathbb{Z}^2$, we now place an obstacle in the form of an aligned square of side length $1/2$ centered at each of the 8 lattice points in $Q(i,j)$ that is distinct from the lattice point $(3i, 3j)$. For each function $f \in \mathcal{F}$, we place an extra obstacle in

the form of an aligned square of side length $1/2$ centered at the lattice point $(3i, 3j)$ if $f(i, j) = +1$, but do not place such an extra obstacle if $f(i, j) = -1$. We refer to this configuration of obstacles as the f-configuration of $Q(i, j)$, as illustrated in Figure 6.7.2.

Notice that in every f-configuration an "empty" lattice point without obstacle is surrounded by 24 "non-empty" lattice points with obstacles, as illustrated in Figure 6.7.3.

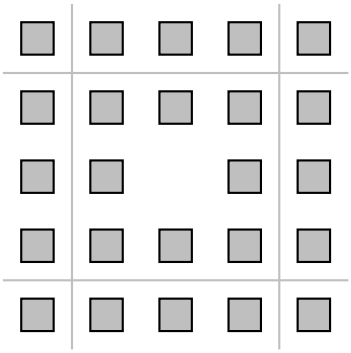

Figure 6.7.3: a lattice point without obstacle in the f-configuration

In fact, all we need in a configuration is that the distance between any two "empty" lattice points is greater than 2.

The set of periodic f-configurations is countable, negligible compared to the uncountable total, implying that the overwhelming majority of f-configurations are aperiodic.

We claim that there are infinitely many explicit starting points and infinitely many explicit quadratic irrational slopes such that the corresponding billiard orbits exhibit time-quantitative density for *all* f-configurations with $f \in \mathcal{F}$.

To prove this, the obvious difficulty is that we cannot directly apply Theorem 6.5.1 in the original "horizontal/vertical" way, since this wind-tree model has infinite horizontal and vertical streets, so it is not a square-maze. The trick is to apply it in an *indirect* way by working with "tilted streets".

In the simpler case when $f(i, j) = +1$, so that there is no missing obstacle, we can consider finite ± 45-degree streets as illustrated in Figure 6.7.4.

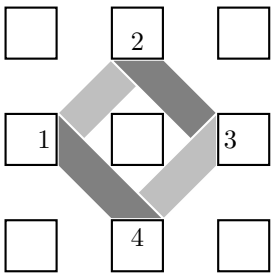

Figure 6.7.4: finite tilted street in the case $f(i, j) = 1$

Note that this tilted street has two orientations: clockwise and counter-clockwise. For example, in the clockwise direction, we go from 1 to 2, illustrated in lighter shade, then from 2 to 3, illustrated in darker shade, then from 3 to 4, illustrated in lighter shade, and finally from 4 back to 1, illustrated in darker shade.

In the other case when $f(i, j) = -1$, so that there is a missing obstacle, we can consider finite ± 45-degree streets as illustrated in Figure 6.7.5.

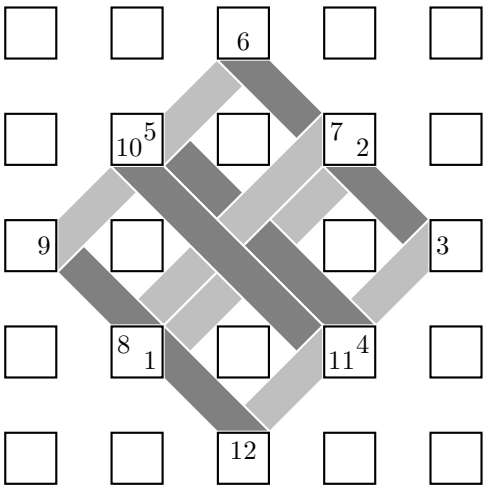

Figure 6.7.5: finite tilted street in the case $f(i,j) = -1$

Note that this tilted street also has two orientations. For example, we can go from 1 to 2, illustrated in lighter shade, then from 2 to 3, illustrated in darker shade, and so on, and finally from 12 back to 1, illustrated in darker shade.

While the basic idea of proving density by combining the finite "tilted streets" with Theorem 6.5.1 is very simple, the technical details are somewhat complicated. We shall therefore first give a detailed discussion in a simpler case where there is only one infinite street. For this case, it is much easier to visualize the corresponding infinite polysquare surface with 1-direction geodesic flow. Hopefully, after that discussion it will be less difficult to understand the more complicated case of wind-tree models such as those illustrated in Figures 6.7.1–6.7.2 that have infinitely many infinite streets.

One of the simplest examples involving a single infinite street is the ∞-L-strip billiard shown in Figure 6.7.6.

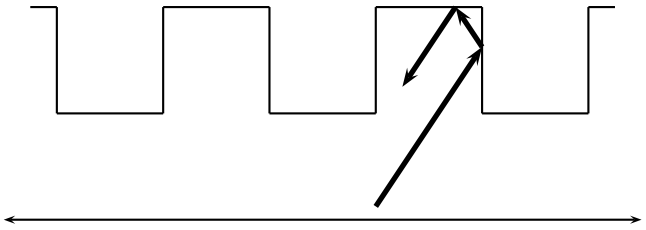

Figure 6.7.6: ∞-L-strip region as an infinite billiard table

For this ∞-L-strip, Figure 6.7.7 shows an explicit slope-2 street. The slope-2 billiard flow, illustrated by the dashed arrows, first maps the interval AB to the interval CD (via reflection on a horizontal edge), illustrated in lighter shade, then onwards to the interval EF (via reflection on a vertical edge), illustrated in darker shade, then to the intervals CB, AG, HI and then back to AB.

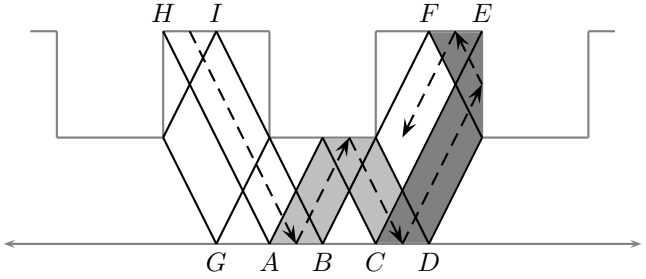

Figure 6.7.7: slope-2 street in the ∞-L-strip billiard

Reversing the orientation, we have a reverse cycle in the same street, the slope-(-2) version of the tilted street.

Next we use the classical trick of "unfolding" that reduces the study of the ∞-L-strip billiard, a 4-direction flow, to a 1-direction geodesic flow on an appropriate infinite polysquare surface. We call this surface the 1-*direction billiard surface of the* ∞-*L-strip*, and denote it by $\mathrm{Bil}(\infty; 1)$. To find this infinite polysquare surface, we glue together 4 reflected copies of the ∞-L-strip region in a suitable way.

Note that the L-shape is the building block of the ∞-L-strip region, as illustrated in Figure 6.7.8. The ∞-L-strip region can be split into a doubly infinite sequence $\ldots, L_{i-1}, L_i, L_{i+1}, \ldots$ of L-shapes.

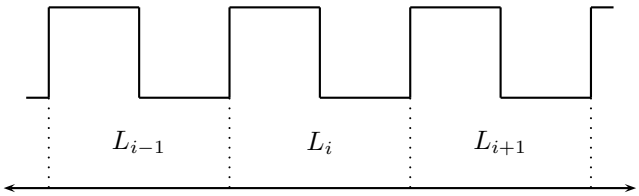

Figure 6.7.8: the L-shape as building blocks of the ∞-L-strip region

To describe $\mathrm{Bil}(\infty; 1)$, we take 4 reflected copies of each of the L-shapes L_i; see Figure 6.7.9. We then obtain $\mathrm{Bil}(\infty; 1)$ by gluing together the infinitely many copies of these 4-copy-L_i.

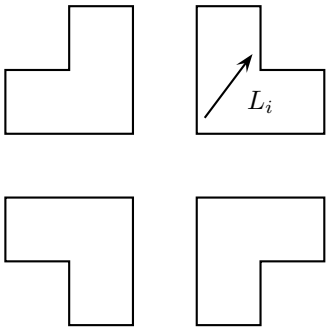

Figure 6.7.9: building the 4-copy version of the L-shape L_i

Clearly there is billiard flow from each L-shape L_i to its two immediate neighbours L_{i-1} and L_{i+1}. We therefore need to identify corresponding edges of these 4-copy versions very carefully. A simple examination will convince the reader that the edge identifications can be as illustrated in Figure 6.7.10.

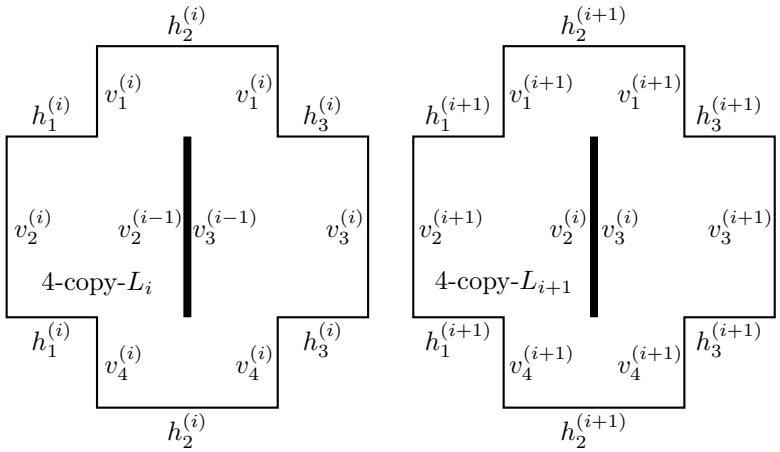

Figure 6.7.10: 4-copy-L_i and 4-copy-L_{i+1} together with edge identifications

Note that a 1-direction geodesic with positive slope on Bil$(\infty; 1)$ that goes from the vertical edge $v_2^{(i)}$ to the vertical edge $v_2^{(i-1)}$ corresponds to a billiard path with negative slope going from L_i to L_{i-1}, whereas a 1-direction geodesic with positive slope on Bil$(\infty; 1)$ that goes from the vertical edge $v_3^{(i-1)}$ to the vertical edge $v_3^{(i)}$ corresponds to a billiard path with positive slope going from L_{i-1} to L_i.

It is much easier to visualize the somewhat messy picture of the slope-2 street and the corresponding slope-(-2) street in Figure 6.7.7 on the surface Bil$(\infty; 1)$. Figure 6.7.11 gives a good visualization of the slope-2 street.

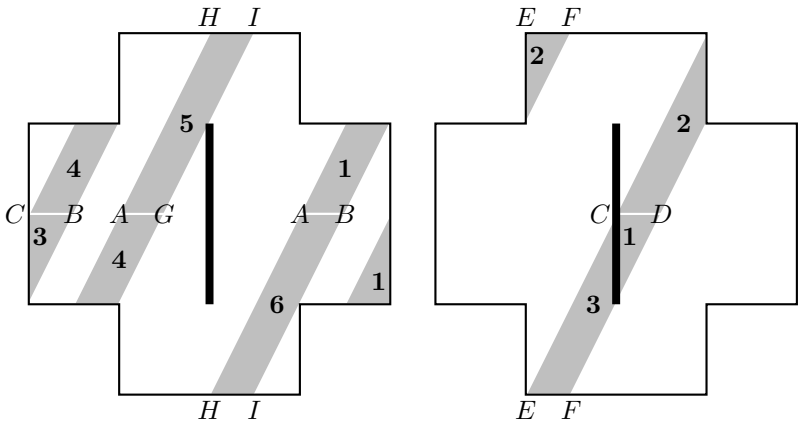

Figure 6.7.11: visualizing the slope-2 street in Figure 6.7.7

Figure 6.7.12 gives a good visualization of the slope-(-2) street.

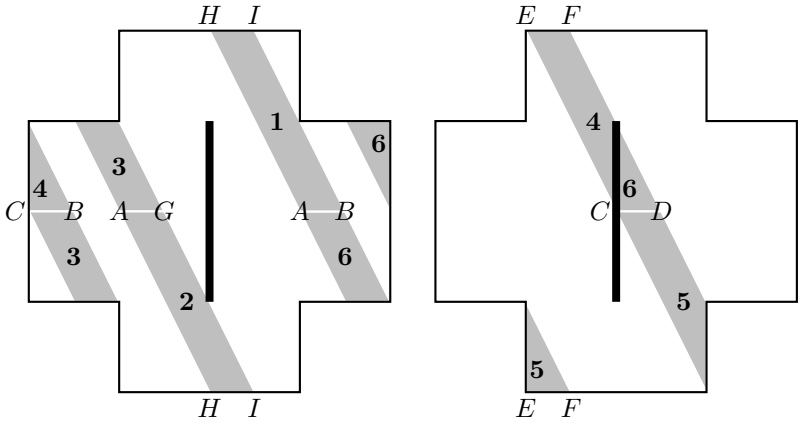

Figure 6.7.12: visualizing the slope-(-2) street in Figure 6.7.7

If we return to Figure 6.7.7 and work out a slope-2 street starting with the interval GA, then the darker shaded region in Figure 6.7.13 gives a good visualization of this new slope-2 street.

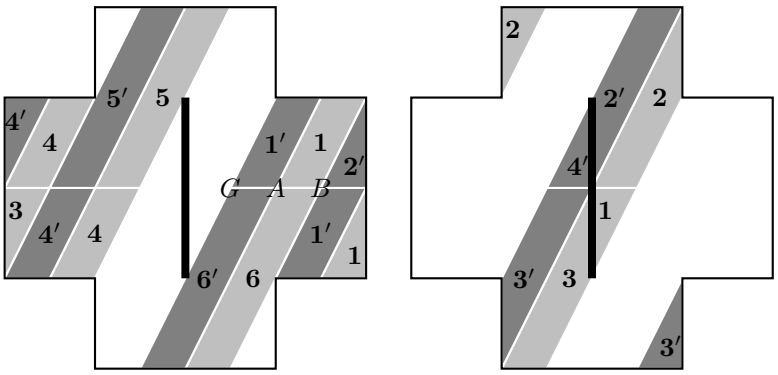

Figure 6.7.13: two slope-2 streets in Figure 6.7.7

Note that the union of the shaded areas in Figure 6.7.13 gives precisely one 4-copy L-shape. For simplicity, we shall refer to NE_i' and NE_i'' as the two slope-2 streets, or north-east streets, in the 4-copy-L_i. Similarly, we can refer to NW_i' and NW_i'' as the slope-(-2) streets, or north-west streets, in the 4-copy-L_i.

Thus the infinite families $\mathrm{NE}_i', \mathrm{NE}_i''$, $i \in \mathbb{Z}$, and $\mathrm{NW}_i', \mathrm{NW}_i''$, $i \in \mathbb{Z}$, of streets, linked together, give a street decomposition of the flat surface $\mathrm{Bil}(\infty; 1)$. These are pairs of congruent finite streets in two directions: slope-2 (north-east) and slope-(-2) (north-west). For convenience, we call them NE-streets and NW-streets respectively.

This setup is very similar to the situation in Theorem 6.5.1, where we have finite streets of bounded length in the horizontal and vertical directions. Indeed, we can use this decomposition to convert the flat surface $\mathrm{Bil}(\infty; 1)$ into a *maze*.

This is, however, not a square-maze, but a *rhombus-maze*. We can clearly split each of the 4-copy-L-shapes into a union of rhombi as illustrated in Figure 6.7.14.

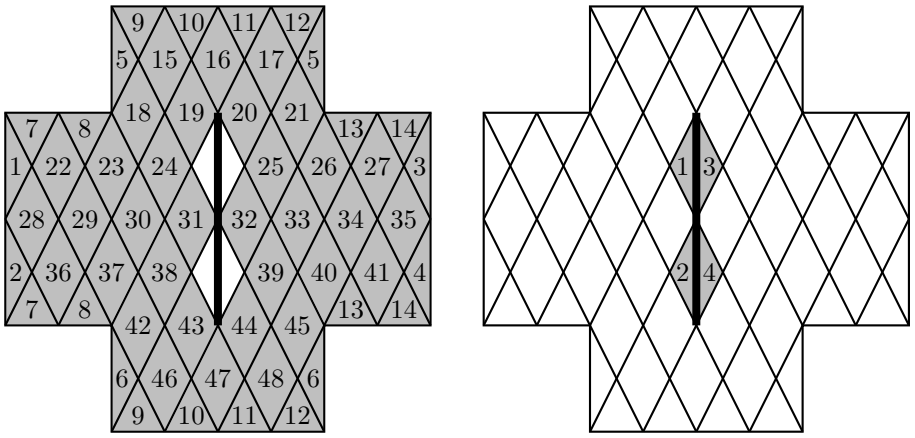

Figure 6.7.14: splitting the 4-copy-L_i into a union of rhombi

Note that edge identification clearly plays a key role in the partitions of the 4-copy-L-shapes.

Let us look at the NE-street that contains the rhombus A, say, in Figure 6.7.15 below.

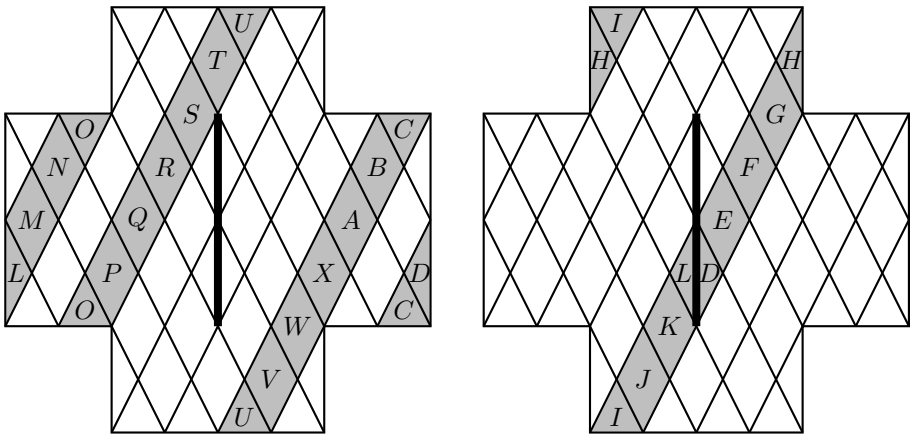

Figure 6.7.15: a street NE_i

If we now move north-east, starting at the rhombus A, then it is easy to see that the NE-street comprises the 24 rhombi $A, B, C, \ldots, X$ as illustrated by the shaded part. Thus the street length of any NE-street is equal to 24.

A similar argument will show that the street length of any NW-street is also equal to 24.

This gives rise to a rhombus-maze where every street has length 24.

We have the following analog of Theorem 6.5.1.

Theorem 6.7.1 ("time-quantitative density in a rhombus-maze"). *Let $\ell \geqslant 2$ be a fixed integer, and let $\mathcal{P}$ be a j-rhombus-maze for some $2 \leqslant j \leqslant \ell$. For any fixed constant $\varepsilon > 0$, there exist infinitely many quadratic irrational numbers α such that the geodesic $V(\alpha; t)$, $t \geqslant 0$, on $\mathcal{P}$, starting at the origin $\mathbf{0}$, with slope α and with arc-length parametrization, exhibits time-quantitative density in the following precise sense. For any rhombus face S_0 of $\mathcal{P}$, there is an effectively computable threshold constant $c_0 = c_0(S_0; \varepsilon; \alpha)$ such that for every integer $n \geqslant c_0$ and every point $Q \in S_0$, the initial segment $V(\alpha; t)$, $0 < t < n^{3+\varepsilon}$, gets $1/n$-close to Q.*

To deduce this from Theorem 6.5.1, we simply need a linear transformation to convert the rhombi to squares. The linear transformation converts geodesics and their shortlines in the corresponding square-maze into their counterparts in the rhombus-maze.

Recall that a 4-direction billiard trajectory in the ∞-L-strip corresponds to a 1-direction geodesic flow in $\mathrm{Bil}(\infty; 1)$ which can be viewed as a rhombus-maze. Theorem 6.7.1 thus leads immediately to the following result.

Theorem 6.7.2. *There are infinitely many explicit quadratic irrational slopes such that every billiard trajectory in the ∞-L-strip starting from a corner and having such a slope exhibits time-quantitative density on the ∞-L-strip.*

We now illustrate the ideas by finding such a quadratic irrational slope given by Theorems 6.7.1 and 6.7.2.

A typical rhombus that we have constructed is illustrated in Figure 6.7.16. It has side length $\sqrt{5}/4$ and area $1/4$.

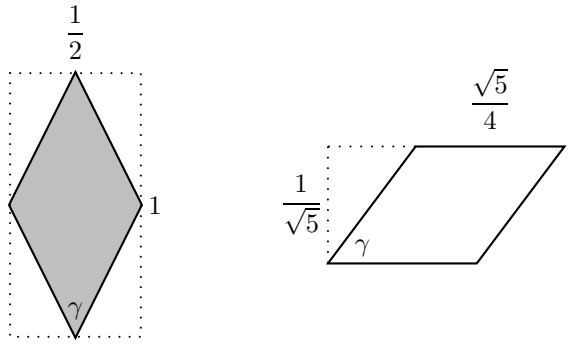

Figure 6.7.16: a typical rhombus

Let γ denote the acute angle in this rhombus. Then $\tan(\gamma/2) = 1/2$, and so

$$\tan \gamma = \frac{4}{3}. \tag{6.7.1}$$

To relate our discussion with Theorem 6.5.1, we consider the illustration in Figure 6.7.17. The bottom half shows a street in the rhombus-maze consisting of precisely 24 successive rhombi.

Recall that in Theorem 6.5.1 in the case of an ℓ-square-maze, we make use of quadratic irrational slopes α given by (6.5.1). More precisely, we have

$$\alpha = a + \frac{1}{\alpha},$$

where the positive integer a is divisible by $\ell!$. If every street is of length ℓ, then we can relax this condition on a to require it to be divisible by ℓ. In particular, if every street is of length 24, then the choice $a = 24$ is permissible. Furthermore, if the geodesic, illustrated by the bold arrow in the top half of Figure 6.7.17, has slope α, then its shortline, illustrated by the long arrow, has slope α^{-1}. Thus the angle that the geodesic makes with the vertical axis is the same as the angle the

shortline makes with the horizontal axis. Indeed, the geodesic and its shortline are mutual shortlines that satisfy the same edge cutting property.

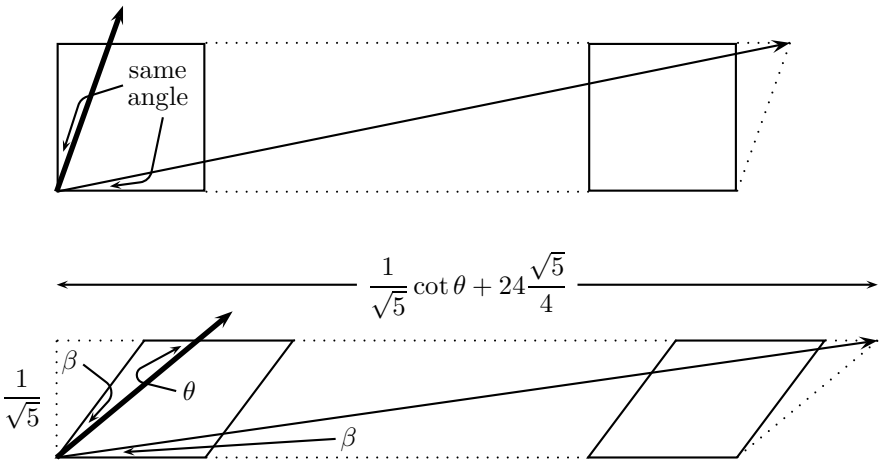

Figure 6.7.17: finding a dense 1-direction flow in $\mathrm{Bil}(\infty; 1)$

We now replicate this situation in the rhombus setup. We require the geodesic and its shortline to be mutual shortlines. Let β be the angle that the shortline, illustrated by the long arrow in the bottom half of Figure 6.7.17, makes with the horizontal side of the rhombus. Then the geodesic, illustrated by the bold arrow, makes the same angle with the other side of the rhombus. If θ is the angle that the geodesic makes with the horizontal side, then we must have $\theta + \beta = \gamma$, and so it follows from (6.7.1) that

$$\tan(\theta + \beta) = \frac{4}{3}, \quad \text{or} \quad \frac{3}{4} = \frac{\cot\theta\cot\beta - 1}{\cot\theta + \cot\beta}. \tag{6.7.2}$$

On the other hand, in view of the same edge cutting property, we must have

$$\frac{\frac{1}{\sqrt{5}}\cot\theta + 24\frac{\sqrt{5}}{4}}{\frac{1}{\sqrt{5}}} = \cot\beta, \quad \text{or} \quad \cot\beta = \cot\theta + 30. \tag{6.7.3}$$

Combining (6.7.2) and (6.7.3), and writing $s = \cot\theta$, we have

$$\frac{3}{4} = \frac{s(s+30) - 1}{2s + 30},$$

which is equivalent to the quadratic equation $4s^2 + 114s - 94 = 0$, with positive root

$$\cot\theta = \frac{-114 + 10\sqrt{145}}{8} = \frac{-57 + 5\sqrt{145}}{4}.$$

Note that θ is the angle relative to a side of the rhombus. The angle relative to the horizontal axis can easily be deduced from this. We omit the details.

6.8. **Density on aperiodic surfaces with infinite streets (II).** The ∞-L-strip happens to be periodic, but periodicity is not necessary for the success of our method. Note that in some periodic cases Hooper [13], Hooper–Hubert–Weiss [14], Hubert–Weiss [16], and Ralston–Troubetzkoy [23] can prove ergodicity for some billiards on infinite surfaces, and ergodicity implies density. They use a completely different approach that reduces the infinite dynamics to the well understood dynamics of the "period", which is a compact system. This reduction method is quite special, and does not work for the infinite periodic case in general. Of course in the aperiodic case this reduction method breaks down.

Our method, on the other hand, does work in both the infinite periodic and aperiodic cases. To illustrate this, we describe next an uncountable family of infinite

aperiodic surfaces for which we can prove density for some billiards. We shall generalize the ∞-L-strip region which, as seen in Figure 6.7.8, is built from congruent L-shapes.

The Uncountable Family of $\{L_i\}_{i\in\mathbf{Z}}$-strips. Given arbitrary integers $v \geqslant 2$ and $h \geqslant 2$, we define the (v, h)-L-shape in a most natural way as follows. It consists of precisely one horizontal street of h unit size square faces and one vertical street of v unit size square faces, with the left square face of the horizontal street identical to the bottom square face of the vertical street.

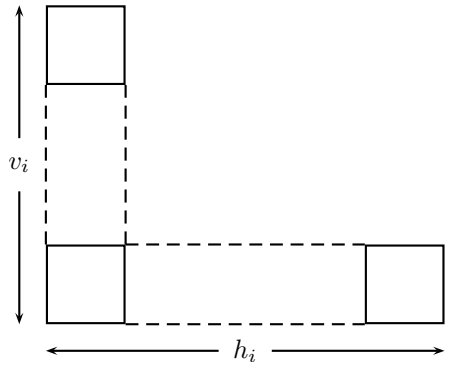

Figure 6.8.1: the L-shape L_i

Thus the special case $v = h = 2$ gives back the usual L-shape. For every $i \in \mathbb{Z}$, let L_i be a (v_i, h_i)-L-shape, and we take the disjoint union of all L_i, $i \in \mathbb{Z}$, such that the horizontal streets of L_i, $i \in \mathbb{Z}$, form a single infinite strip, and L_i and L_{i+1}, $i \in \mathbb{Z}$, are consecutive. We refer to this union as the $\{L_i\}_{i\in\mathbb{Z}}$-strip.

Consider first the $\{L_i\}_{i\in\mathbb{Z}}$-strip in the special case when there is an integer r such that

$$h_i \leqslant r, \quad v_i \in \{2, 4\}, \quad i \in \mathbb{Z}. \tag{6.8.1}$$

Under these conditions we can reduce the billiard problem to a problem of 1-direction geodesic flow on a rhombus-maze and then apply Theorem 6.7.2. This ultimately gives billiard trajectories that exhibit time-quantitative density. To see this, note that under the conditions (6.8.1), the slope-2 street construction similar to that in Figure 6.7.7 can be made, as illustrated in one case by Figure 6.8.2. In this case, the slope-2 billiard flow, illustrated by the dashed arrows, first maps the interval AB to the interval CD (via reflection on a vertical edge), illustrated in lighter shade, then onwards to the interval EB (via multiple reflections on vertical edges), then to the intervals AF, GH, IJ, KH, GF and then back to AB.

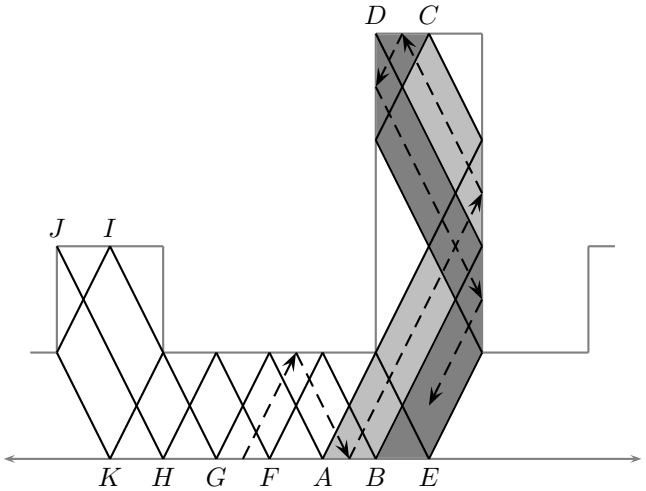

Figure 6.8.2: slope-2 street in the case $v_i = 2$, $h_i = 3$, $v_{i+1} = 4$

Reversing the orientation, we have a reverse cycle in the same street, the slope-(-2) version of the tilted street.

The only irrelevant change is that different horizontal streets may have different lengths, but the lengths are uniformly bounded.

We shall show later that the same method works far beyond the special case (6.8.1). Consider, for instance, the $\{L_i\}_{i\in\mathbb{Z}}$-strip such that there is an integer r such that

$$h_i \leqslant r, \quad v_i \leqslant r, \quad i \in \mathbb{Z}, \tag{6.8.2}$$

and

$$\text{there are at most } r \text{ consecutive } v_i,\ i \in \mathbb{Z}, \text{ that are powers of 2.} \tag{6.8.3}$$

To reduce a billiard trajectory to a 1-direction geodesic flow on a rhombus-maze, the basic idea is essentially the same. We use "finite tilted streets", but the slope is not necessarily equal to 2. We shall show that under the conditions (6.8.2) and (6.8.3), there always exists an integer m so that we can construct a slope-m street decomposition like in Figures 6.7.7 and 6.8.2. Such a street decomposition is based on the following elementary number-theoretic lemma. For any integer $k \geqslant 2$, consider a k-tower of k unit size square faces on top of each other in vertical position with two "gates" that we call g_1, the left gate, and g_2, the right gate, as illustrated in Figure 6.8.3, which also shows the 4 possible types of exits for a point billiard.

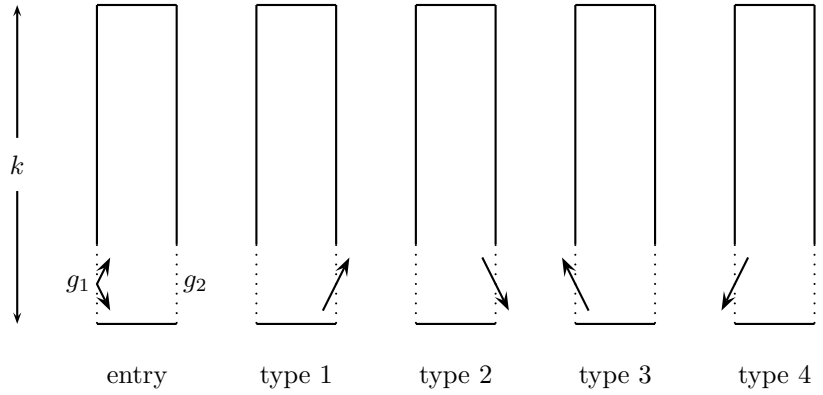

Figure 6.8.3: k-tower with two gates g_1 and g_2

Lemma 6.8.1. *Let $k \geqslant 2$ and m with $|m| \geqslant 2$ be two integers. Suppose that a billiard enters a k-tower through the left gate g_1 with slope m. Let $x_0 = x_0(k,m) \geqslant 1$ denote the smallest positive integer such that*

$$mx_0 \equiv 0 \bmod 2k \quad \textit{or} \quad mx_0 \equiv -1 \bmod 2k.$$

If $m > 0$, then

(i) *if x_0 is odd and $mx_0 \equiv 0 \bmod 2k$, then the billiard has exit type 1;*
(ii) *if x_0 is odd and $mx_0 \equiv -1 \bmod 2k$, then the billiard has exit type 2;*
(iii) *if x_0 is even, then the billiard has exit type 3.*

If $m < 0$, then

(iv) *if x_0 is odd and $mx_0 \equiv 0 \bmod 2k$, then the billiard has exit type 2;*
(v) *if x_0 is odd and $mx_0 \equiv -1 \bmod 2k$, then the billiard has exit type 1;*
(vi) *if x_0 is even, then the billiard has exit type 4.*

Proof. For convenience, assume that the billiard has unit vertical speed.

Suppose first of all that $m > 0$. It is clear that at time mt, $t = 1, 2, 3, \ldots$, following entry to the k-tower, the billiard hits a vertical side of the k-tower, on the right if t is odd, and on the left if t is even. We want to trap the smallest integer value $t = x_0$ when the billiard hits the side of the bottom square face.

If it hits the side of the bottom square face before a final bounce off the bottom edge, then

$$mx_0 + 1 \equiv 0 \bmod 2k, \quad \text{so that} \quad mx_0 \equiv -1 \bmod 2k.$$

If x_0 is odd, then it hits the right side, and (ii) follows. Note that x_0 cannot be even in this case.

If it hits the side of the bottom square face after a final bounce off the bottom edge, then

$$mx_0 \equiv 0 \bmod 2k.$$

If x_0 is odd, then it hits the right side, and (i) follows. If x_0 is even, then it hits the left side, and (iii) follows.

Suppose next that $m < 0$. Then the billiard bounces off the bottom edge before it goes up the k-tower. It is clear that at time $-mt$, $t = 1, 2, 3, \ldots$, the billiard hits the side of the k-tower, on the right if t is odd, and on the left if t is even. We want to trap the smallest integer value $t = x_0$ when the billiard hits the side of the bottom square face.

If it hits the side of the bottom square face after a final bounce off the bottom edge, then

$$-mx_0 - 1 \equiv 0 \bmod 2k, \quad \text{so that} \quad mx_0 \equiv -1 \bmod 2k.$$

If x_0 is odd, then it hits the right side, and (v) follows. Note that x_0 cannot be even in this case.

If it hits the side of the bottom square face before a final bounce off the bottom edge, then

$$-mx_0 \equiv 0 \bmod 2k, \quad \text{so that} \quad mx_0 \equiv 0 \bmod 2k.$$

If x_0 is odd, then it hits the right side, and (iv) follows. If it is even, then it hits the left side, and (vi) follows. □

Using symmetry, we can deduce an analogous result when the billiard enters a k-tower through the right gate g_2.

Note that the case $m \equiv k \bmod 2k$ is particularly simple. Since $k \geqslant 2$, we have $x_0 = x_0(k, m) = 2$, and the billiard bounces back, with exit type 3 or 4.

Exit types 1 and 2 represent *transient states*, and exit types 3 and 4 indicate that the billiard, having come from the left, *bounces back* at this k-tower to the left. To construct a "finite tilted street", it is necessary, and also sufficient, that there are *bounce backs on both sides* along the $\{L_i\}_{i\in\mathbb{Z}}$-strip, as illustrated in Figure 6.8.4.

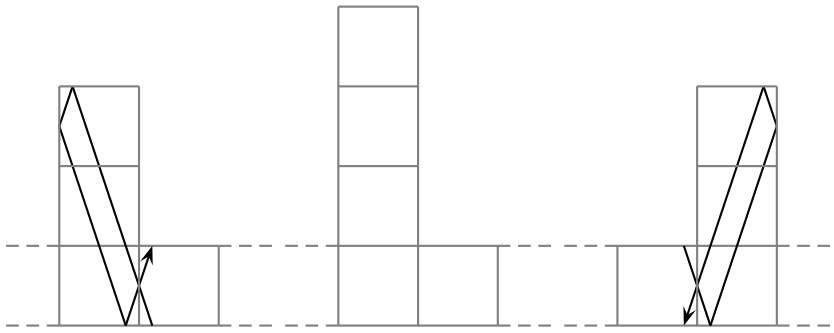

Figure 6.8.4: bounce backs on both sides

Next we apply Lemma 6.8.1 in some special cases of the $\{L_i\}_{i\in\mathbb{Z}}$-strip billiard, where, for each $i \in \mathbb{Z}$, L_i is a (v_i, h_i)-L-shape. Note that every 1-tower leads to a transient state, so the value of h_i is irrelevant, and we only need to study k-towers for $k \geqslant 2$.

Case 1. Suppose that $h_i \geqslant 2$ and $v_i = 2$, $i \in \mathbb{Z}$. We have studied this case when $h_i = 2$, $i \in \mathbb{Z}$, in Section 6.7 with slopes $m = \pm 2$, and the result extends to other values of h_i. Now we consider other integer values of m. To study the effect of the 2-towers, we can use Lemma 6.8.1 with $k = 2$, so that $2k = 4$.

For $m \equiv 2 \bmod 4$, since $k = 2$, the condition $m \equiv k \bmod 2k$ holds automatically, and $x_0 = 2$, so conclusion (iii) or (vi) of Lemma 6.8.1 applies. This means that any billiard with such a slope that enters a 2-tower from the left exits through the left, then later enters the next 2-tower from the right and exits through the right. The billiard path is therefore bounded between these two 2-towers. Since the slope is an integer, the billiard can only hit the bottom edge of the $\{L_i\}_{i\in\mathbb{Z}}$-strip between these two 2-towers at finitely many points, and so must repeat.

For $m \equiv 0 \bmod 4$, it is clear that $x_0 = 1$ and $mx_0 \equiv 0 \bmod 4$, so conclusion (i) or (iv) of Lemma 6.8.1 applies. This means that any billiard with such a slope that enters a 2-tower from the left exits through the right, then enters the next 2-tower from the left exits through the right, and so on, leading to a useless infinite street.

For $m \equiv 1 \bmod 4$, it is clear that $x_0 = 3$ and $mx_0 \equiv -1 \bmod 4$, so conclusion (ii) or (v) of Lemma 6.8.1 applies. This means that any billiard with such a slope that enters a 2-tower from the left exits through the right, leading to a useless infinite street.

For $m \equiv 3 \bmod 4$, it is clear that $x_0 = 1$ and $mx_0 \equiv -1 \bmod 4$, so conclusion (ii) or (v) of Lemma 6.8.1 applies. This means that any billiard with such a slope that enters a 2-tower from the left exits through the right, leading to a useless infinite street.

Case 2. Suppose that $h_i \geqslant 2$ and $v_i = 3$, $i \in \mathbb{Z}$. To study the effect of the 3-towers, we can use Lemma 6.8.1 with $k = 3$, so that $2k = 6$.

For $m \equiv 3 \bmod 6$, since $k = 3$, the condition $m \equiv k \bmod 2k$ holds automatically, and $x_0 = 2$, so conclusion (iii) or (vi) of Lemma 6.8.1 applies. This means that any billiard with such a slope that enters a 3-tower from the left exits through the left, then later enters the next 3-tower from the right and exits through the right. The billiard path is therefore bounded between these two 3-towers. Since the slope is an integer, the billiard can only hit the bottom edge of the $\{L_i\}_{i\in\mathbb{Z}}$-strip between these two 3-towers at finitely many points, and so must repeat.

For $m \equiv 0, 1, 2, 4, 5 \bmod 6$, we have respectively $x_0 = 1, 5, 3, 3, 1$, so conclusions (iii) and (vi) of Lemma 6.8.1 do not apply. This means that any billiard with such a slope that enters a 3-tower from the left exits through the right, leading to a useless infinite street.

Case 3. Suppose that $h_i \geqslant 2$, $i \in \mathbb{Z}$, and $v_i = 2$ for every integer $i < 0$ and $v_i = 3$ for every integer $i \geqslant 0$. To achieve a bounce back at a 2-tower, we note from Case 1 that the integer slope m of the billiard must satisfy $m \equiv 2 \bmod 4$, so that m must be even. On the other hand, to achieve a bounce back at a 3-tower, we note from Case 2 that the integer slope m of the billiard must satisfy $m \equiv 3 \bmod 6$, so that m must be odd. So there cannot be any finite slope-m street.

Case 4. There exist integers $r, s, m \geqslant 2$ such that $v_i \leqslant r$, $h_i \leqslant r$, $i \in \mathbb{Z}$, and for every $i \in \mathbb{Z}$, there exists $i \leqslant j < i + s$ such that $m \equiv v_j \bmod 2v_j$. In this case, we have $x_0 = x_0(v_j, m) = 2$. This means that for any $2s$ successive L_i, there are two bounce backs, guaranteeing finite slope-m streets in between.

Finally, we establish the following far reaching generalization of Theorem 6.7.2.

Theorem 6.8.1. *Consider an arbitrary $\{L_i\}_{i\in\mathbb{Z}}$-strip such that there exists an integer $r \geqslant 2$ such that* (6.8.2) *and* (6.8.3) *hold. Then there are infinitely many explicit quadratic slopes such that every billiard trajectory in the $\{L_i\}_{i\in\mathbb{Z}}$-strip starting from*

a corner and having such a slope exhibits time-quantitative density on the $\{L_i\}_{i\in\mathbb{Z}}$*-strip.*

Proof. The conditions (6.8.2) and (6.8.3) imply that among $r+1$ consecutive v_i, there exists v_j which is not a power of 2, so that v_j has an odd prime factor p. We shall study the v_j-tower in L_j, and show that this gives rise to a bounce back. To ensure a bounce back, we must make sure that exit types 1 and 2 do not take place. It follows from Lemma 6.8.1 that both conditions

$$x_0 \text{ is odd} \quad \text{and} \quad mx_0 \equiv 0 \bmod 2v_j \tag{6.8.4}$$

and

$$x_0 \text{ is odd} \quad \text{and} \quad mx_0 \equiv -1 \bmod 2v_j \tag{6.8.5}$$

must fail.

To ensure that (6.8.4) fails, it is sufficient that (i) the multiplicity of 2 in the prime factorization of m is less than the multiplicity of 2 in the prime factorization of $2v_j$. On the other hand, to ensure that (6.8.5) fails, it is sufficient that (ii) the numbers m and $2v_j$ are not relatively prime.

Let $m = p$. Then both m and $2v_j$ are multiples of p, so they are not relatively prime. On the other hand, the multiplicity of 2 in the prime factorization of m is 0, while the multiplicity of 2 in the prime factorization of $2k$ is at least 1. So both (i) and (ii) hold, ensuring that both (6.8.4) and (6.8.5) fail. □

6.9. **Density on aperiodic surfaces with infinite streets (III).** We now return to the wind-tree billiard models discussed at the beginning of Section 6.7; in particular, to the billiard models illustrated by Figures 6.7.1–6.7.5, where the side length of the square obstacles is equal to 1/2. We shall use our study of the ∞-L-strip billiard to guide us to a better understanding of these more complicated wind-tree models.

Figures 6.7.4 and 6.7.5 illustrate that tilted streets of slopes ± 1 lead to finite streets for billiards in f-configurations. Thus the corresponding problem of 1-direction geodesic flow in the 4-copy versions of these f-configurations can be viewed as a problem of 1-direction geodesic flow in a rhombus-maze, where the rhombi are squares tilted at 45 degrees.

Let us rescale appropriately so that all square obstacles have side length equal to 1. Any f-configuration is made up of building blocks as illustrated in Figure 6.9.1.

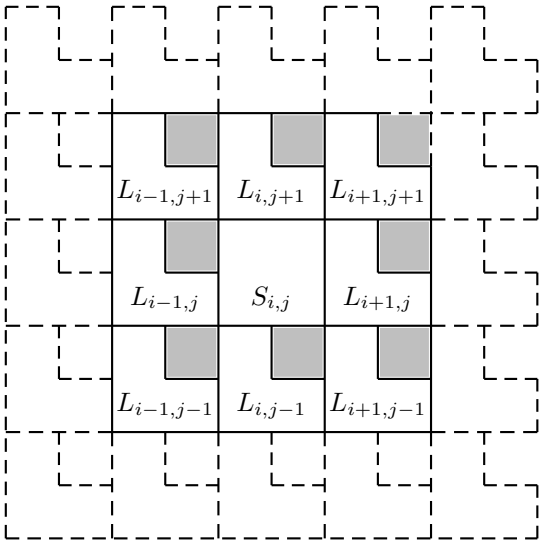

Figure 6.9.1: L-shapes with replacement square corresponding to missing obstacle

Each building block contains 8 L-shapes together with a square $S_{i,j}$ in the middle, or where the middle square $S_{i,j}$ is replaced by yet another L-shape $L_{i,j}$. The building block is surrounded by 15 L-shapes from neighboring building blocks.

To construct the 4-copy versions of these f-configurations, we construct the 4-copy version of each of the L-shapes and squares. As there is symmetry between the problem of horizontal edge pairing and the problem of vertical edge pairing, we shall only discuss the latter. Figure 6.9.2 illustrates the typical situation, with reference to j omitted.

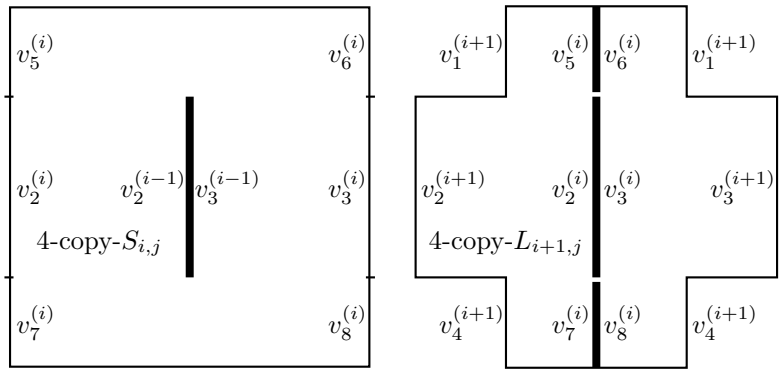

Figure 6.9.2: pairing of vertical edges in 4-copy versions of $S_{i,j}$ and $L_{i+1,j}$

Viewed this way, these f-configurations share some of the features of the ∞-L-strip. For instance, we observe that the edge pairings on the double vertical edges in the middle of the square and the L-shape are precisely the same as in Figure 6.7.10. The presence of the square $S_{i,j}$ instead of an L-shape $L_{i,j}$ leads to new vertical edge pairings in $S_{i,j}$ and $L_{i+1,j}$. However, these new edge pairings do not involve any edges of the the 4-copy versions of any other squares or L-shapes.

We thus establish part (i) of the following result which is a generalization of Theorem 6.7.2.

Theorem 6.9.1. (i) *There are infinitely many explicit quadratic irrational slopes such that every billiard trajectory in any f-configuration starting from a corner and having such a slope exhibits time-quantitative density on the f-configuration.*

(ii) *Furthermore, the collection of such slopes gives rise to a dense set on the unit circle.*

Figure 6.9.3 below is an alternative to Figure 6.7.4, and shows a finite street of slope 1/3 in the same model.

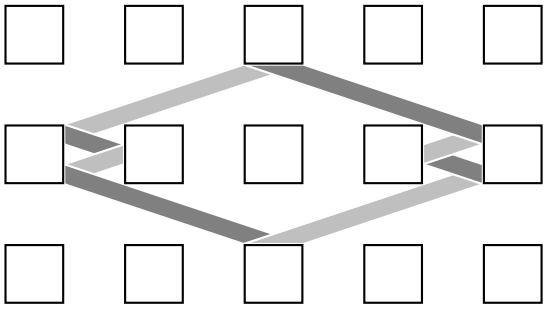

Figure 6.9.3: finite street of slope 1/3

Together, they show that the slopes 1 and 1/3 are *completely periodic* rational directions in the same periodic wind-tree model. Here *completely periodic* refers to the property that every billiard having this slope is periodic and so finite.

To study part (ii) of Theorem 6.9.1, we need a result of Hubert, Lelièvre and Trubetzkoy [15].

Lemma 6.9.1. *In the 2-dimensional Ehrenfest periodic wind-tree billiard model with $a = b = 1/2$, a rational slope k/ℓ, given in lowest terms, is completely periodic if and only if both k and ℓ are odd.*

Proof of Theorem 6.9.1(ii). Since the set of rational slopes k/ℓ, given in lowest terms, with both k and ℓ odd is dense on the unit circle, Theorem 6.9.1(ii) follows on combining Lemma 6.9.1 with the proof of Theorem 6.9.1(i). □

For the Ehrenfest periodic wind-tree billiard model with $a = b = 3/4$, Figure 6.9.4 shows a finite periodic street of slope 3.

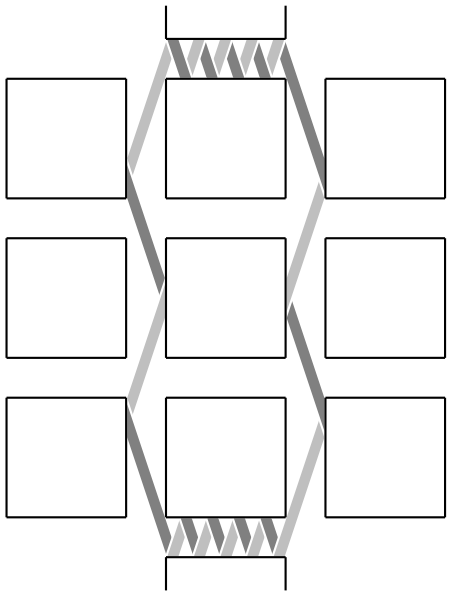

Figure 6.9.4: finite street of slope 3 in wind-tree billiard mode with $a = b = 3/4$

Thus this model can be reduced to a problem of 1-direction geodesic flow in a rhombus-maze.

Figure 6.9.4 is an analog of Figure 6.7.4, and we leave it to the reader to draw an analog of Figure 6.7.5. With that, it is straightforward to prove a perfect analog of Theorem 6.9.1 in this new case.

Indeed, there are infinitely many cases of the Ehrenfest periodic wind-tree billiard model and their aperiodic f-configuration analogs of the for which we can establish analogs of Theorem 6.9.1. It is based on the following result of Hubert, Lelièvre and Trubetzkoy [15].

Lemma 6.9.2. *Consider the 2-dimensional periodic wind-tree billiard model with rectangle size $a \times b$, and assume that both $0 < a < 1$ and $0 < b < 1$ are rational. Suppose that $a = p/q$ and $b = r/s$ in lowest terms.*

(i) *If both p, r are odd and both q, s are even, then there exists a completely periodic rational direction.*

(ii) *If both p, r are even and both q, s are odd, then there is no completely periodic rational direction.*

In the case (i), the three authors give an explicit algorithm for finding these perfectly periodic rational directions. It is based on the work of McMullen [21] concerning the so-called Weierstrass points on L-surfaces, a subject beyond the scope of our present paper.

We can establish analogs of Theorem 6.9.1 for those Ehrenfest periodic wind-tree billiard models and their aperiodic f-configuration-like billiard models for those a and b satisfying the conditions of Lemma 6.9.2(i).

If $a = p/q$ and $b = r/s$, in lowest terms, are such that both p, r are even and both q, s are odd, then our method breaks down, in view of Lemma 6.9.2(ii), and we are not able to prove density. This leads to the following interesting question.

Open Problem 4. *Is there an analog of Theorem 6.9.1 for the Ehrenfest periodic wind-tree billiard model or its aperiodic f-configuration analog for those values of $a = p/q$ and $b = r/s$, in lowest terms, such that p, r are even and both q, s are odd?*

In Sections 6.7–6.9, we have established that there are many polysquare surfaces $\mathcal{P}$ with infinite streets for which we can establish time-quantitative density for certain billiard trajectories. There, through the use of tilted streets, we can view $\mathcal{P}$ as a 2-dimensional maze, and this allows us to apply Theorem 6.5.1 to the 4-copy version of $\mathcal{P}$. Now, for any such polysquare surface $\mathcal{P}$, it is clear that $\mathcal{P}' = \mathcal{P} \times [0, 1]$ is a polycube. Since $\mathcal{P}$ can be viewed as a 2-dimensional maze, $\mathcal{P}'$ can be viewed as a 3-dimensional maze. In this 3-dimensional maze, there are 2 types of streets each of which is simply the cartesian product of a tilted street in $\mathcal{P}$ with $[0, 1]$, while a third type of streets all have length 1 in the new direction. This allows us to establish time-quantitative density for certain billiard trajectories in $\mathcal{P}'$ by applying Theorem 6.6.1 to the 8-copy version of $\mathcal{P}'$.

Note, however, that these are all degenerate examples, as we have got rid of perhaps the key difficulty by "essentially" removing one of the directions and turning the problem of finding finite tilted streets in $\mathcal{P}'$ into a de-facto 2-dimensional one.

We do not know any polycube with infinite streets in all three directions for which we can establish time-quantitative density for any billiard trajectory.

A particularly interesting question in this direction is the following.

Open Problem 5. *Can one prove a 3-dimensional analog of Theorem 6.9.1(i), i.e., a density result in the 3-dimensional Ehrenfest periodic wind-tree billiard model?*

Our primary interest in this paper is to study infinite aperiodic systems. Nevertheless, for the sake of completeness, we conclude with a brief summary of what is known about the general double-periodic wind-tree model. These models are *recurrent i.e.*, for almost every direction, the billiard returns arbitrarily close to every point of the infinite trajectory; see [1, 15].

Note that recurrence does not imply density, but of course density implies recurrence.

On the other hand, Delecroix [5] has given an explicit set of initial slopes with positive Hausdorff dimension for which the orbit fails recurrence. In fact, the orbit goes to infinity, *i.e.*, the distance of the billiard from the starting point tends to infinity as the time $t \to \infty$. What is more, these orbits are self-avoiding!

The doubly-periodic wind-tree models have an absence of ergodicity in almost every direction; see [8]. Moreover, these models exhibit surprisingly large "super-random" escape rate to infinity for almost every direction. Actually, the *super-random* escape rate to infinity means order of magnitude $T^{2/3}$; see [6]. More precisely, for a typical direction, a billiard orbit of length T can go as far as $T^{2/3}$ from the starting point. This is in sharp contrast to our results! Indeed, whenever our shortline method proves density on an infinite surface, then the orbit exhibits much smaller escape rate $\log T$ to infinity. See the Remark after the proof of Theorem 6.5.1 in Section 6.5.

The escape rate $T^{2/3}$ is called *super-random*, because the symmetric random walk has escape rate $T^{1/2}$ ("square-root size fluctuation"), so the escape rate is greater than random.

References

[1] A. Avila, P. Hubert. Recurrence for the wind-tree model. *Ann. Inst. H. Poincaré Anal. Non Linéaire* **37** (2020), 1–11.

[2] J. Beck, M. Donders, Y. Yang. Quantitative behavior of non-integrable systems (I). *Acta Math. Hungar.* **161** (2020), 66–184.

[3] J. Beck, M. Donders, Y. Yang. Quantitative behavior of non-integrable systems (II). *Acta Math. Hungar.* **162** (2020), 220–324.

[4] J.W.S. Cassels. *An Introduction to Diophantine Approximation* (Cambridge University Press, 1957).

[5] V. Delecroix. Divergent directions in some periodic wind-tree models. *J. Mod. Dynam.* **7** (2013), 1–29.

[6] V. Delecroix, P. Hubert, S. Lelièvre. Diffusion for the periodic wind-tree model. *Ann. Sci. École Norm. Sup.* **47** (2014), 1085–1110.

[7] P. Ehrenfest, T. Ehrenfest. *The Conceptual Foundations of Statistical Approach in Mechanics* (Dover, 1990).

[8] K. Fraczek, C.Ulcigrai. Non-ergodic Z-periodic billiards and infinite translation surfaces. *Invent. Math.* **197** (2014), 241–298.

[9] G.H. Hardy, J.E. Littlewood. Some problems of diophantine approximation: the lattice points of a right-angled triangle I. *Proc. London Math. Soc.* **3** (1920), 15–36.

[10] G.H. Hardy, J.E. Littlewood. Some problems of diophantine approximation: the lattice points of a right-angled triangle II. *Abh. Math. Sem. Univ. Hamburg* **1** (1922), 212–249.

[11] J. Hardy, J. Weber. Diffusion in a periodic wind-tree model. *J. Math. Phys.* **21** (1980), 1802–1808.

[12] E. Hlawka. Zur Theorie des Figurengitters. *Math. Ann.* **125** (1952), 183–207.

[13] P. Hooper. The invariant measures of some infinite interval exchange maps. *Geom. Topol.* **19** (2015), 1895–2038.

[14] P. Hooper, P. Hubert, B. Weiss. Dynamics on the infinite staircase. *Discrete Contin. Dyn. Syst.* **33** (2013), 4342–4347.

[15] P. Hubert, S. Lelièvre, S. Troubetzkoy. The Ehrenfest wind-tree model: periodic directions, recurrence, diffusion. *J. Reine Angew. Math.* **656** (2011), 223–244.

[16] P. Hubert, B. Weiss. Ergodicity for infinite periodic translation surfaces. *Compos. Math.* **149** (2013), 1364–1380.

[17] A. Katok, A. Zemlyakov. Topological transitivity of billiards in polygons. *Math. Notes* **18** (1975), 760–764.

[18] A.Ya. Khinchin. Einige Sätze über Kettenbruche, mit Anwendungen auf die Theorie der Diophantischen Approximationen. *Math. Ann.* **92** (1924), 115–125.

[19] A.Ya. Khinchin. *Continued Fractions* (Dover, 1997).

[20] K. Mahler. Ein Übertragungsprinzip für lineare Ungleichungen. *Časopis Pěst. Math. Fys.* **68** (1939), 85–92.

[21] C. McMullen. Teichmüller curves in genus two: discriminant and spin. *Math. Ann.* **333** (2005), 87–130.

[22] A. Ostrowski. Bemerkungen zur Theorie der Diophantischen Approximationen. *Abh. Math. Sem. Univ. Hamburg* **1** (1922), 77–98.

[23] D. Ralston, S. Troubetzkoy. Ergodic infinite group extension of geodesic flows on translation surfaces. *J. Mod. Dynam.* **6** (2012), 477–497.

[24] A.M. Sabogal, S. Troubetzkoy. Ergodicity of the Ehrenfest wind-tree model. *C. R. Acad. Sci. Paris* **354** (2016), 1032–1036.

[25] H. Weyl. Über die Gleichverteilung von Zahlen mod. Eins. *Math. Ann.* **77** (1916), 313–352.

Department of Mathematics, Rutgers University, Hill Center for the Mathematical Sciences, Piscataway NJ 08854, USA

E-mail address: jbeck@math.rutgers.edu

Department of Mathematics and Statistics, Macquarie University, Sydney NSW 2109, Australia

E-mail address: william.chen@mq.edu.au

Department of Mathematics, Rutgers University, Hill Center for the Mathematical Sciences, Piscataway NJ 08854, USA

E-mail address: yy458@math.rutgers.edu